

# An efficient model of cosmology dependence in the covariance matrix of the matter power spectrum

Theodore Steele,<sup>1,\*</sup> Robert E. Smith,<sup>1,†</sup> and Roisin O'Connor<sup>1</sup>

<sup>1</sup>*Astronomy Centre, Department of Physics and Astronomy, University of Sussex, BN1 9RH, UK*

(Dated: January 21, 2026)

Covariance matrices are essential cosmological probes of fundamental physics, providing information on numerous fundamental physical parameters and varying with any change in the underlying cosmology. However, this cosmology dependence, while providing excellent information, also makes them computationally intensive to compute, as a new covariance matrix must explicitly be calculated for every variation in cosmology before comparisons to observational data can be made.

In this paper, we develop an efficient model for estimating the parameter dependence of the covariance matrix of the matter power spectrum by Taylor expanding around a known value of the parameter space. This method allows us to use a relatively small number of input cosmologies, specifically one fiducial cosmology and two further cosmologies for each parameter. We explicitly calculate the covariance matrices for these cosmologies and then develop a new model that allows us to interpolate from these the form of the covariance matrix with a cosmology that is located elsewhere in that given parameter space without explicit perturbation theory calculations. This method speeds up covariance matrix calculations in new cosmologies by orders of magnitude compared to explicit perturbation theory calculations at each point in a given parameter space.

Using different approximations, we develop three versions of our interpolated covariance matrix and validate the model by recreating all of our input cosmologies using all three forms, both with and without super-sample covariance corrections in each case, and show that the models provide robust recreations of the original results, with the different approximations being valid in certain regimes.

## CONTENTS

I. Introduction	2
II. Perturbatively Modeling the covariance matrix	3
A. Band Averaging	4
III. Modeling the parameter dependencies of the covariance matrix	5
A. Developing the response matrix $\mathbf{R}$	6
IV. Reconstructing Simulation Covariance Matrices	7
V. Discussion	8
A. Standard Perturbation Theory	45
1. The Power Spectrum	46
2. The Bispectrum	47
3. The Trispectrum	47
B. Simulation Parameters	48
C. Response Matrices	48
D. Reconstructed Matrix Accuracy	48
References	48

\* [T.W.Steele@sussex.ac.uk](mailto:T.W.Steele@sussex.ac.uk)

† [r.e.smith@sussex.ac.uk](mailto:r.e.smith@sussex.ac.uk)

## I. INTRODUCTION

Modern cosmology is concerned to a large extent with constraining the vast parameter spaces of fundamental physics using cosmological probes. Current and near future large scale structure (LSS) surveys such as Euclid [1], LSST [2], SPHEREx [3], SKA [4], DESI [5], WFIRST [6], 4MOST [7], PFS [8], KiDS [9], BOSS [10], and eBOSS [11] will provide an unprecedented amount of data with which we may constrain various physical parameters, such as  $\sigma_8$ ,  $\Omega_m$ ,  $\Omega_b$ ,  $h$ , and  $n_s$ , among many others.

LSS surveys measure the deviation of matter densities from the cosmic average and formulate statistical measures of the correlation between density peaks in Fourier space to study the impacts of physical phenomena at different scales. The power spectrum is the fundamental object of study, defined as being the Fourier transform of the two-point correlation function of density fields normalised to the average cosmic density. The bispectrum is the Fourier transform of the three-point correlation function and the trispectrum is the Fourier transform of the four-point correlator. Both the bispectrum and trispectrum vanish in the case of Gaussian density fields as described by Wick's theorem and therefore provide quantisations of non-Gaussian effects. Further statistics, such as the covariance matrices of these correlators, are also widely studied in their own right for their ability to combine both the power spectrum and higher order correlators into a simple and convenient mathematical object. All of these statistics can be calculated analytically [12–18] as functions of fundamental physical parameters [19–23] and compared to observations [24–30] to place constraints on those parameters. The most commonly used such analytic model is Standard Perturbation Theory (SPT) [12], which takes the linear power spectrum of a given cosmology and uses recursion relations to derive a set of analytic estimates for higher order statistics of that same cosmology.

The covariance matrix of the power spectrum is given, in the Gaussian case, by a diagonal matrix of variance terms entirely derived from the power spectrum and, in the non-Gaussian case, by a non-diagonal matrix with off-diagonal terms sourced from the trispectrum. SPT calculations are usually done in the context of a smooth, continuous matter field in which the only force taken into account is gravity. In order to accommodate the granulation of dark matter into halos, shot noise terms must be introduced which, in the case of the covariance matrix, introduce new off-diagonal terms derived from the bispectrum and power spectrum as well as a constant term. Furthermore, as any SPT calculation or simulation or observational measurement will divide the space being studied into bins and there will inevitably be unbinned regions of momentum space which exceed in wavelength the lowest frequency bin, and since longer wavelength modes can couple to those in higher wavelength bins and affect the results of the analyses contained within them, a phenomenon referred to as super-sample covariance (SSC)[31, 32], terms may be added into both SPT and measured covariance matrices to account for feedback on studied modes from those beyond the limit of the study. To accommodate baryonic matter, additional terms must be introduced which are referred to as biasing parameters. However, for the purposes of this paper we focus entirely upon granulated dark matter and leave the incorporation of biasing into our results for a future paper.

Traditionally, covariance matrices would be calculated individually for any given set of physical parameters. This is computationally intensive and becomes unfeasible for mapping multi-dimensional parameter spaces with any degree of precision, as each point in parameter space will need a new simulation to be run to generate linear and non-linear spectra at that point followed by intensive perturbative calculations.

In this paper, we develop an efficient method for estimating the parameter dependence of the covariance matrix which requires explicit calculations only at a single point in the parameter space. This method is based upon a Taylor expansion of the covariance matrix around that point for small variations of the parameters in question. By defining new expressions from the ensuing expanded matrix which quantify sensitivity to parameter variations, we are able to derive an expression for the covariance matrix as a function of input parameters which may be analytically calculated from a pre-existing set of covariance matrices, negating the need for additional computations of the full matrix with new simulation data. This permits parameter spaces to be explored with trivial computational time and no need for additional simulations beyond those that were used to establish the model.

To demonstrate the method, we employ the QUIJOTE simulation results [33] to generate both non-linear and SPT covariance matrices that map the parameter space with dimensions  $\{\sigma_8, \Omega_m, \Omega_b, h, n_s\}$ . We then use these matrices to generate new matrices at sample points in parameter space that were not explicitly run in the simulations to demonstrate the abilities of the model.

This model serves to permit mapping of the parameter space of the covariance matrix of large scale structure in both greater depth and shorter times than would be possible before, by allowing only a relatively small number of simulations to be used to generate continuous matrix functions that take a trivial amount of time to compute at any given point in parameter space.

## II. PERTURBATIVELY MODELING THE COVARIANCE MATRIX

In this section we will review the standard form for the theoretical covariance matrix as modeled with SPT (itself summarised in App. A) in both the Gaussian and non-Gaussian cases before incorporating shot-noise terms and SSC corrections. We will then band average the matrix, permitting studies in discrete bins, as is standard in both theoretical and observational analyses of LSS.

In a purely Gaussian case, the covariance matrix is simply given by [34]

$$C^G(\mathbf{k}_1, \mathbf{k}_2) = P(k_1)P(k_2) (\delta_{\mathbf{k}_1, \mathbf{k}_2}^K + \delta_{\mathbf{k}_1, -\mathbf{k}_2}^K) . \quad (1)$$

Incorporating non-Gaussianity necessitates including the connected trispectrum in configurations corresponding to pairs of coupled power spectra [35], providing off-diagonal elements as well as modifying the diagonals:

$$C(\mathbf{k}_1, \mathbf{k}_2) = \frac{1}{V_\mu} T(\mathbf{k}_1, \mathbf{k}_2, -\mathbf{k}_1, -\mathbf{k}_2) + P(k_1)P(k_2) (\delta_{\mathbf{k}_1, \mathbf{k}_2}^K + \delta_{\mathbf{k}_1, -\mathbf{k}_2}^K) \quad (2)$$

When dealing with discrete tracers such as halos, shot noise terms become relevant [36], as the above estimators treat matter as being a continuous field and do not model discretised clumping. Shot noise terms primarily come in three forms: a constant addition that accounts for Poissonian variance from random point sampling, a bispectrum term that accounts for non-Gaussianity introduced by gravitational collapse, and an additional power spectrum term that relates to the scale dependence of discrete tracer formation that arises from the scale dependent distribution of matter in the continuous matter field.

Incorporating these three shot noise terms, we arrive at the Gaussian and non-Gaussian covariance matrix for discretised tracers:

$$C^G(\mathbf{k}_1, \mathbf{k}_2) = \left[ P(k_1) + \frac{1}{\bar{n}} \right] \left[ P(k_2) + \frac{1}{\bar{n}} \right] (\delta_{\mathbf{k}_1 + \mathbf{k}_2, 0}^K + \delta_{\mathbf{k}_1 - \mathbf{k}_2, 0}^K) + \frac{1}{\bar{n}^2 V_\mu} [P(\mathbf{k}_1) + P(\mathbf{k}_2) + P(-\mathbf{k}_1) + P(-\mathbf{k}_2)] + \frac{1}{\bar{n}^3 V_\mu} \quad (3)$$

$$C(\mathbf{k}_1, \mathbf{k}_2) = \frac{T^c(\mathbf{k}_1, \mathbf{k}_2, -\mathbf{k}_1, -\mathbf{k}_2)}{V_\mu} + \left[ P(k_1) + \frac{1}{\bar{n}} \right] \left[ P(k_2) + \frac{1}{\bar{n}} \right] (\delta_{\mathbf{k}_1 + \mathbf{k}_2, 0}^K + \delta_{\mathbf{k}_1 - \mathbf{k}_2, 0}^K) + \frac{1}{\bar{n} V_\mu} [B(\mathbf{k}_1, \mathbf{k}_2, -\mathbf{k}_1 - \mathbf{k}_2) + B(\mathbf{k}_1, -\mathbf{k}_2, \mathbf{k}_2 - \mathbf{k}_1) + B(-\mathbf{k}_1, \mathbf{k}_2, \mathbf{k}_1 - \mathbf{k}_2) + B(-\mathbf{k}_1, -\mathbf{k}_2, \mathbf{k}_1 + \mathbf{k}_2)] + \frac{1}{\bar{n}^2 V_\mu} [P(\mathbf{k}_1 + \mathbf{k}_2) + P(\mathbf{k}_1 - \mathbf{k}_2)] + \frac{1}{\bar{n}^2 V_\mu} [P(\mathbf{k}_1) + P(\mathbf{k}_2) + P(-\mathbf{k}_1) + P(-\mathbf{k}_2)] + \frac{1}{\bar{n}^3 V_\mu} , \quad (4)$$

Of course, structure on scales larger than those measured in a given survey or simulation will have gravitational effects on those within those measured volumes. These effects can become significant and are accounted for by incorporating super-sample covariance (SSC) corrections to our models as were originally derived in [31]. This takes the form of an integral over the power spectrum on all scales physically larger than the cell volume coupled at each point in momentum space to the power spectra at those points:

$$\text{SSC}(\mathbf{k}_1, \mathbf{k}_2) = P(k_1)P(k_2) \int_0^{k_{\min}} \frac{dk}{2\pi^2} k^2 P_{11}(k) , \quad (5)$$

which is added directly to the covariance matrix to correct for coupling between the modes being sampled and those beyond the sample limits.

From the covariance matrix, the correlation matrix can be defined as

$$r(\mathbf{k}_1, \mathbf{k}_2) = \frac{C(\mathbf{k}_1, \mathbf{k}_2)}{\sqrt{C(\mathbf{k}_1, \mathbf{k}_1)C(\mathbf{k}_2, \mathbf{k}_2)}} \quad (6)$$

and the reduced covariance matrix can be defined as

$$C^R(\mathbf{k}_1, \mathbf{k}_2) = \frac{C(\mathbf{k}_1, \mathbf{k}_2)}{\sqrt{C^G(\mathbf{k}_1, \mathbf{k}_1)C^G(\mathbf{k}_2, \mathbf{k}_2)}} . \quad (7)$$

Furthermore, we note that the correlation matrix and the diagonal matrix of the standard deviations of individual modes,  $\mathbf{D}$ , can be combined to return the covariance matrix as

$$\mathbf{C} = \mathbf{D} \mathbf{r} \mathbf{D} . \quad (8)$$

### A. Band Averaging

The covariance and correlation matrices discussed so far have applied to individual pairs of wavenumbers. In practice, it is not practical to correlate every mode individually and they are instead band averaged, with those averages then being correlated to generate a band averaged set of correlators. We can define the band averaged spectra as

$$\bar{P}(k_i) \equiv \int_{V_{s,i}} \frac{d\mathbf{k}_1}{V_{s,i}} P(\mathbf{k}_1) , \quad (9)$$

$$\bar{P}(k_i, k_j) \equiv \int_{V_{s,i}} \frac{d\mathbf{k}_1}{V_{s,i}} \int_{V_{s,j}} \frac{d\mathbf{k}_2}{V_{s,j}} P(\mathbf{k}_1 + \mathbf{k}_2) , \quad (10)$$

$$\bar{B}(k_i, k_j) \equiv \int_{V_{s,i}} \frac{d\mathbf{k}_1}{V_{s,i}} \int_{V_{s,j}} \frac{d\mathbf{k}_2}{V_{s,j}} B(\mathbf{k}_1, \mathbf{k}_2, -\mathbf{k}_1 - \mathbf{k}_2) , \quad (11)$$

$$\bar{T}^c(k_i, k_j) \equiv \int_{V_{s,i}} \frac{d\mathbf{k}_1}{V_{s,i}} \int_{V_{s,j}} \frac{d\mathbf{k}_2}{V_{s,j}} T^c(\mathbf{k}_1, \mathbf{k}_2, -\mathbf{k}_1, -\mathbf{k}_2) , \quad (12)$$

where  $V_{s,i}$  is the volume of band  $i$ . The covariance matrix of the band averaged power spectrum is given simply given by the band average of the covariance matrix itself:

$$\bar{C}(k_i, k_j) \equiv \int_{V_{s,i}} \frac{d\mathbf{k}_1}{V_{s,i}} \int_{V_{s,j}} \frac{d\mathbf{k}_2}{V_{s,j}} C(\mathbf{k}_1, \mathbf{k}_2) , \quad (13)$$

Upon inserting Eq. (1) into Eq. (13), we obtain an expression for the band averaged Gaussian covariance matrix of a continuous matter field:

$$\bar{C}(k_i, k_j) = \frac{2}{N_i} \left( \bar{P}(k_i) + \frac{1}{\bar{n}} \right)^2 \delta_{k_i, k_j}^K , \quad (14)$$

where  $N_i$  is the number of modes in the  $i$ th  $k$ -space shell<sup>1</sup>. In the case of a Gaussian field with discretised tracers, this becomes

$$\bar{C}(k_i, k_j) = \frac{2}{N_{k_i}} \left( \bar{P}(k_i) + \frac{1}{\bar{n}} \right)^2 \delta_{k_i, k_j}^K + \frac{2}{\bar{n}^2 V_\mu} [\bar{P}(k_i, k_j) + \bar{P}(k_i) + \bar{P}(k_j)] + \frac{1}{\bar{n}^3 V_\mu} . \quad (15)$$

The band averaged non-Gaussian covariance matrix can likewise be obtained by inserting Eq. (4) into Eq. (13) to obtain

$$\begin{aligned} \bar{C}(k_i, k_j) &= \frac{\bar{T}^c(k_i, k_j)}{V_\mu} + \frac{2}{N_i} \left[ \bar{P}(k_i) + \frac{1}{\bar{n}} \right]^2 \delta_{k_i, k_j}^K + \frac{4}{\bar{n} V_\mu} \bar{B}(k_i, k_j) \\ &+ \frac{2}{\bar{n}^2 V_\mu} [\bar{P}(k_i, k_j) + \bar{P}(k_i) + \bar{P}(k_j)] + \frac{1}{\bar{n}^3 V_\mu} , \end{aligned} \quad (16)$$

where  $\bar{n}$  is the particle number density<sup>2</sup>, and  $V_\mu$  is the cell volume<sup>3</sup>. To incorporate super-sample covariance, we would likewise band average over the power spectra in Eq. (5) to obtain

$$\overline{\text{SSC}}(k_i, k_j) = \bar{P}(k_i) \bar{P}(k_j) \int_0^{k_{\min}} \frac{dk}{2\pi^2} k^2 P(k) , \quad (17)$$

which can be added directly to Eqs. (15) and (16) to incorporate super-sample covariance effects. Given the dominance of the linear power spectrum on super-sample scales, we calculate Eq. (17) with only the linear power spectrum in all of our subsequent analysis.

<sup>1</sup> This is given by  $(V_{i+1} - V_i)/(2\pi/L)^3$  and in our analysis we are using simulations for which the cell length  $L = 1\text{h}^{-1} \text{Gpc}$

<sup>2</sup> In the case of the simulations we are using, this is given by  $(512/1000)^3$

<sup>3</sup> In our case given by  $1000^3 \text{Mpc}^3$

### III. MODELING THE PARAMETER DEPENDENCIES OF THE COVARIANCE MATRIX

We wish to develop a model which will allow us to estimate the covariance matrix at a chosen set of parameters without explicitly calculating it. We propose doing this by Taylor expanding around a fiducial covariance matrix in an appropriately dimensioned parameter space and estimating the new covariance matrix by tuning a simple parametrisation of the expansion parameters.

We begin with a set of non-linear covariance matrices as well as corresponding models. For example, we might run a set of simulations and measure both the linear and non-linear power spectra from their final states. We could then use the linear power spectrum to establish a model covariance matrix using Standard Perturbation Theory (SPT) or one of its variants. We hereafter refer to the non-linear covariance matrices measured directly as true covariance matrices and label them  $\mathbf{C}_t$  and label model covariance matrices  $\mathbf{C}_m$ .

To provide a natural measure of the accuracy of a given model, we may define

$$\mathbf{Y}(\boldsymbol{\theta}) \equiv \mathbf{C}_m^{-1}(\boldsymbol{\theta})\mathbf{C}_t(\boldsymbol{\theta}), \quad (18)$$

which would be an identity matrix in the case of a perfect model.

Now, it naturally follows that

$$\mathbf{C}_t(\boldsymbol{\theta}) = \mathbf{C}_m(\boldsymbol{\theta})\mathbf{C}_m^{-1}(\boldsymbol{\theta})\mathbf{C}_t(\boldsymbol{\theta}) = \mathbf{C}_m(\boldsymbol{\theta})\mathbf{Y}(\boldsymbol{\theta}). \quad (19)$$

This gives us an estimator of the true covariance matrix in terms of a given model and a measure of that model's accuracy. Naturally, the equation as given above would rely upon taking the non-linear matrix *a priori* in order to calculate  $\mathbf{Y}$ . However, in the analysis that follows, we will demonstrate how an approximate form may be derived that will permit the reconstruction of true covariance matrices from models derived from the results of simulations with different parameters. Ultimately, this will serve to provide us with an estimator of the true covariance matrix at one set of parameters without having to explicitly measure either the linear or non-linear power spectrum at those parameters, relying instead upon a pre-existing set of results at a different point in parameter space.

To begin, we note that  $\mathbf{Y}(\boldsymbol{\theta})$ , which measures the effectiveness of the SPT model, will be parameter dependent and can be Taylor expanded around some fiducial point in parameter space  $\boldsymbol{\theta}_0$  to give:

$$\begin{aligned} \mathbf{Y}(\boldsymbol{\theta}) &\approx \mathbf{Y}(\boldsymbol{\theta}_0) \left[ \mathbf{I} + \mathbf{Y}^{-1}(\boldsymbol{\theta}_0) \sum_{\alpha} \left. \frac{\partial \mathbf{Y}(\boldsymbol{\theta})}{\partial \theta_{\alpha}} \right|_{\boldsymbol{\theta}_0} \Delta \theta_{\alpha} \right] \\ &= \mathbf{Y}(\boldsymbol{\theta}_0) \left[ \mathbf{I} + \sum_{\alpha} \mathbf{R}_{\alpha}(\boldsymbol{\theta}_0) \Delta \theta_{\alpha} \right], \end{aligned} \quad (20)$$

where we have truncated the expansion at first order and defined a constant matrix that controls the strength of the response to a variation in parameter space, which we call the response matrix:

$$\mathbf{R}_{\alpha}(\boldsymbol{\theta}_0) \equiv \mathbf{Y}^{-1}(\boldsymbol{\theta}_0) \left. \frac{\partial \mathbf{Y}(\boldsymbol{\theta})}{\partial \theta_{\alpha}} \right|_{\boldsymbol{\theta}_0}. \quad (21)$$

This provides us with a measure of the parameter dependence of the disparity between perturbation theory and non-linear simulation results which we use to estimate  $Y$  at a given point in parameter space without having any simulation results at that point.

Due to the fact that these results stem from a Taylor expansion, they will be viable within local regions around those fiducial points that have been sampled from simulations, permitting continuous explorations of those regions without explicit simulations at every point as would traditionally be required.

We now note that the Taylor expansion may introduce asymmetry into the  $\mathbf{Y}$  matrix, which would be unphysical but potentially non-zero due to inherent inaccuracies in any model. In order to provide a symmetric estimator for the true covariance matrix, we therefore define

$$\mathbf{C}_{t\parallel}(\boldsymbol{\theta}) = \frac{1}{2} \left[ \mathbf{C}_m(\boldsymbol{\theta})\mathbf{Y}(\boldsymbol{\theta}) + \mathbf{Y}^T(\boldsymbol{\theta})\mathbf{C}_m(\boldsymbol{\theta}) \right]. \quad (22)$$

as well as an estimator of the accuracy of the method

$$\mathbf{C}_{t\perp}(\boldsymbol{\theta}) \equiv \frac{1}{2} \left[ \mathbf{C}_m(\boldsymbol{\theta})\mathbf{Y}(\boldsymbol{\theta}) - \mathbf{Y}^T(\boldsymbol{\theta})\mathbf{C}_m(\boldsymbol{\theta}) \right], \quad (23)$$

which should vanish and so any non-zero contributions should be an indication of the failure of the method.

Inserting Eq. (20) into Eqs. (19) and (25), we have

$$\mathbf{C}_{t\parallel}(\boldsymbol{\theta}) = \frac{1}{2} \left[ \mathbf{C}_m(\boldsymbol{\theta}) \mathbf{Y}(\boldsymbol{\theta}_0) \left( \mathbf{I} + \sum_{\alpha} \mathbf{R}_{\alpha} \Delta \theta_{\alpha} \right) + \left( \mathbf{I} + \sum_{\alpha} \mathbf{R}_{\alpha} \Delta \theta_{\alpha} \right)^T \mathbf{Y}^T(\boldsymbol{\theta}_0) \mathbf{C}_m(\boldsymbol{\theta}) \right] \quad (24)$$

$$\mathbf{C}_{t\perp}(\boldsymbol{\theta}) = \frac{1}{2} \left[ \mathbf{C}_m(\boldsymbol{\theta}) \mathbf{Y}(\boldsymbol{\theta}_0) \left( \mathbf{I} + \sum_{\alpha} \mathbf{R}_{\alpha} \Delta \theta_{\alpha} \right) - \left( \mathbf{I} + \sum_{\alpha} \mathbf{R}_{\alpha} \Delta \theta_{\alpha} \right)^T \mathbf{Y}^T(\boldsymbol{\theta}_0) \mathbf{C}_m(\boldsymbol{\theta}) \right], \quad (25)$$

with the response matrix being as given in Eqs. (29) or (30). We note that the only remaining dependence on the evaluated point in parameter space  $\boldsymbol{\theta}$  on the right hand side is in the model covariance matrix. In order to negate the requirement of explicit computation of a model from a linear power spectrum at that point, we note that we may interpolate a model across parameter space from the same input matrices that are used to calculate the response matrix.

Eq. (24) is an estimator for the covariance matrix at point in parameter space  $\boldsymbol{\theta}$ , obtainable without explicit SPT calculations once the response matrix and fiducial SPT covariance matrix have been provided by interpolating existing SPT matrices to generate a model for  $\mathbf{C}_m(\boldsymbol{\theta})$  that does not require explicit computation at  $\boldsymbol{\theta}$ . This permits rapid explorations of parameter space that would, until this paper, have required explicit SPT calculations for every point in parameter space. Eq. (25) provides a test for the accuracy of this model, vanishing in the unrealistic case of a perfect model and measuring the deviations of the model from what has been measured in simulations in realistic, imperfect models.

In the analyses that follow, we develop two estimators for the response matrix as well as using an approximation in which we set it to zero, such that the reconstructed matrix  $\mathbf{C}_{t\parallel}$  is entirely derived from the interpolated model covariance matrix at  $\boldsymbol{\theta}$  and the ratio of the model and non-linear matrices at the fiducial point  $\boldsymbol{\theta}_0$ .

### A. Developing the response matrix $\mathbf{R}$

We now wish to consider the response matrix given in Eq. (21) and find a convenient estimator for it that can be calculated with a small selection of input cosmologies to permit explorations of the spaces between and around those cosmologies.

Taking the derivative of Eq. (18), we have

$$\frac{\partial \mathbf{Y}(\boldsymbol{\theta})}{\partial \theta_{\alpha}} = \frac{\partial \mathbf{C}_m^{-1}(\boldsymbol{\theta})}{\partial \theta_{\alpha}} \mathbf{C}_t(\boldsymbol{\theta}) + \mathbf{C}_m^{-1}(\boldsymbol{\theta}) \frac{\partial \mathbf{C}_t(\boldsymbol{\theta})}{\partial \theta_{\alpha}}. \quad (26)$$

However, we wish to avoid taking the derivative of the inverse of the SPT matrix, as this could amplify disparities between the model and the simulations.

We avoid this by reparametrising the derivative in question to give

$$\frac{\partial \mathbf{Y}(\boldsymbol{\theta})}{\partial \theta_{\alpha}} = -\mathbf{C}_m^{-1}(\boldsymbol{\theta}) \frac{\partial \mathbf{C}_m(\boldsymbol{\theta})}{\partial \theta_{\alpha}} \mathbf{C}_m^{-1}(\boldsymbol{\theta}) \mathbf{C}_t(\boldsymbol{\theta}) + \mathbf{C}_m^{-1}(\boldsymbol{\theta}) \frac{\partial \mathbf{C}_t(\boldsymbol{\theta})}{\partial \theta_{\alpha}}. \quad (27)$$

On evaluating this at the fiducial point  $\boldsymbol{\theta}_0$  and multiplying by  $\mathbf{Y}^{-1}(\boldsymbol{\theta}_0)$ , we find the response matrix:

$$\begin{aligned} \mathbf{R}_{\alpha}(\boldsymbol{\theta}_0) &= (\mathbf{C}_m^{-1}(\boldsymbol{\theta}_0) \mathbf{C}_t(\boldsymbol{\theta}_0))^{-1} \left[ -\mathbf{C}_m^{-1}(\boldsymbol{\theta}) \frac{\partial \mathbf{C}_m(\boldsymbol{\theta})}{\partial \theta_{\alpha}} \mathbf{C}_m^{-1}(\boldsymbol{\theta}) \mathbf{C}_t(\boldsymbol{\theta}) + \mathbf{C}_m^{-1}(\boldsymbol{\theta}) \frac{\partial \mathbf{C}_t(\boldsymbol{\theta})}{\partial \theta_{\alpha}} \right]_{\boldsymbol{\theta}_0} \\ &= \mathbf{C}_t^{-1}(\boldsymbol{\theta}_0) \left[ \frac{\partial \mathbf{C}_t(\boldsymbol{\theta})}{\partial \theta_{\alpha}} - \frac{\partial \mathbf{C}_m(\boldsymbol{\theta})}{\partial \theta_{\alpha}} \mathbf{C}_m^{-1}(\boldsymbol{\theta}) \mathbf{C}_t(\boldsymbol{\theta}) \right]_{\boldsymbol{\theta}_0}, \end{aligned} \quad (28)$$

where the right-hand-side of the above expression is to be evaluated at  $\boldsymbol{\theta}_0$ . Thus to model the matrix  $\mathbf{R}_{\alpha}$  at the fiducial point, we need to be able to compute the measured and modeled covariance matrices, their inverses, and their derivatives with respect to all relevant parameters at the fiducial point  $\boldsymbol{\theta}_0$ .

Decomposing the measured covariance matrix into a correlation matrix and diagonal standard deviation matrices, the final expression for our response matrix becomes

$$\widehat{\mathbf{R}}_{\alpha} = \widehat{\mathbf{C}_t^{-1}} \left[ \frac{\partial \widehat{\mathbf{D}_t}}{\partial \theta_{\alpha}} \widehat{\mathbf{r}_t} \widehat{\mathbf{D}_t} + \widehat{\mathbf{D}_t} \frac{\partial \widehat{\mathbf{r}_t}}{\partial \theta_{\alpha}} \widehat{\mathbf{D}_t} + \widehat{\mathbf{D}_t} \widehat{\mathbf{r}} \frac{\partial \widehat{\mathbf{D}_t}}{\partial \theta_{\alpha}} - \frac{\partial \mathbf{C}_m}{\partial \theta_{\alpha}} \mathbf{C}_m^{-1} \widehat{\mathbf{C}_t} \right]. \quad (29)$$

In what follows we will also consider the case where the correlation matrix is roughly constant and only slowly varies with cosmology, such that  $\partial \mathbf{r} / \partial \theta_\alpha \approx 0$ . In this case we can approximate the response matrix as:

$$\widehat{\mathbf{R}}_\alpha^{\text{approx}} = \widehat{\mathbf{C}}_t^{-1} \left[ \widehat{\frac{\partial \mathbf{D}_t}{\partial \alpha}} \widehat{\mathbf{r}_t} \widehat{\mathbf{D}_t} + \widehat{\mathbf{D}_t} \widehat{\mathbf{r}} \widehat{\frac{\partial \mathbf{D}_t}{\partial \alpha}} - \frac{\partial \mathbf{C}_m}{\partial \theta_\alpha} \mathbf{C}_m^{-1} \widehat{\mathbf{C}}_t \right]. \quad (30)$$

The motivation for this is to remove what we would expect to be the primary source of noise from the measured covariance matrix while retaining most of the parameter dependence.

Furthermore, we note that the inverse covariance matrix, even for a measured matrix with good signal to noise, may be extremely noisy. As such, we define the reduced response matrix as

$$\widehat{\mathbf{R}}_{\alpha, \text{red}} = \widehat{\frac{\partial \mathbf{D}_t}{\partial \theta_\alpha}} \widehat{\mathbf{r}_t} \widehat{\mathbf{D}_t} + \widehat{\mathbf{D}_t} \widehat{\frac{\partial \mathbf{r}_t}{\partial \theta_\alpha}} \widehat{\mathbf{D}_t} + \widehat{\mathbf{D}_t} \widehat{\mathbf{r}} \widehat{\frac{\partial \mathbf{D}_t}{\partial \theta_\alpha}} - \frac{\partial \mathbf{C}_m}{\partial \theta_\alpha} \mathbf{C}_m^{-1} \widehat{\mathbf{C}}_t, \quad (31)$$

and its approximation

$$\widehat{\mathbf{R}}_{\alpha, \text{red}}^{\text{approx}} = \widehat{\frac{\partial \mathbf{D}_t}{\partial \alpha}} \widehat{\mathbf{r}_t} \widehat{\mathbf{D}_t} + \widehat{\mathbf{D}_t} \widehat{\mathbf{r}} \widehat{\frac{\partial \mathbf{D}_t}{\partial \alpha}} - \frac{\partial \mathbf{C}_m}{\partial \theta_\alpha} \mathbf{C}_m^{-1} \widehat{\mathbf{C}}_t, \quad (32)$$

in order to study the response matrix in the context of a comparatively noiseless environment.

The full and reduced response matrices in both their complete and approximate forms for our various cosmologies are shown in App. C. We note that we used both regular matrix inversion techniques and the Moore-Penrose pseudo-inverse technique and found that both gave the same results to a high degree of precision, indicating that the noise contribution from the inverse covariance matrix is relatively small and can be ignored in the remainder of our analysis.

Having defined these two forms for the response, we now define three estimators for the reconstructed non-linear covariance matrix. Firstly, we define  $C_{\parallel}$  with the full response matrix, found by inserting Eq. (29) into Eq. (24). This is the most complete estimator of the covariance matrix, but risks including sources of noise that contribute minimally to the results through the derivative of the correlation matrix.

Secondly, we define  $C_{\parallel, a}$  which is found by inserting the approximate response matrix as given in Eq. (30) into Eq. (24). This is less complete than the full  $C_{\parallel}$ , but avoids a potential source of noise in the derivative of the correlation matrix and is valid under the assumption that the correlation matrix does not vary significantly with cosmological parameters.

Finally, we define  $C_{\parallel, R=0}$ , found by setting the response matrix to zero in Eq. (24). It provides the simplest and fastest estimator for the non-linear covariance matrix and remove all sources of noise from the derivatives of the measured and modeled matrices with respect to their parameters, but is only valid under the assumption that the accuracy of the model is not in of itself a function of cosmological parameters to any great degree, as that dependence is precisely what the response matrix measures.

#### IV. RECONSTRUCTING SIMULATION COVARIANCE MATRICES

In order to validate our model and compare the accuracies of the different forms of the reconstructed covariance matrix, we begin by taking the linear and non-linear power spectra from each simulation in the QUIJOTE suite (see App. B for details), developing an SPT covariance matrix from the linear spectrum, and then reconstructing each non-linear matrix using our assorted definitions of  $C_{\parallel}$ .

In the event that a given definition of  $C_{\parallel}$  is perfect, it would recreate the non-linear covariance matrix exactly. In practice, we expect it to contain small errors due to a combination of numerical errors and the use of a first order Taylor expansion as an approximation for the  $Y$  matrix. However, we hope to demonstrate that our model yields accurate recreations of non-linear covariance matrices to percent level on all momenta under study. Due to the limitations of SPT, we have limited ourselves to studying the covariance matrices up to  $k \sim 0.3 h \text{ Mpc}^{-1}$ .

In Figures. 1-11 we show the covariance matrices for all cosmologies studied, using non-linear perturbation theory, the simulation results, and the results of Eq. (24) in the context of both the full and approximate response matrices as well as the cases where the response is set to zero, both with and without SSC corrections.

As can be seen in all cases, the SSC corrections dominate the covariance when included; this is expected on the scales under study. As can also be seen, the reconstructed matrices with the response matrix set to zero perform reasonably well in the cases that lack SSC corrections but are noticeably inaccurate, particularly at low momenta, when such corrections are included, indicating a strong parameter dependent disparity between SPT and non-linear covariances on large scales.

In Figs. 12-16, we show the factors  $Y = C_m^{-1}C_t$  with the model covariance matrix being the SPT matrix, the reconstructed matrix with the full response matrix, the reconstructed matrix with the approximate response matrix, and the reconstructed matrix with the response matrix set to zero, for all cosmologies under study. This constitutes an effective test of the accuracy of each model, as in the case that they perfectly recreated the non-linear matrix, they would simply be identity matrices and all deviations from an identity matrix constitute error in the model.

As can be seen, the full response matrix provides the most accurate reconstruction of the original non-linear covariance matrix, with almost all off-diagonal terms being sub-percent level except in one corner. The observation made from the previous set of figures is also shown clearly, with the reconstructed matrices that have the response set to zero being accurate in the case that SSC corrections are not included but becoming highly off-diagonal in the case that they are included, showing that the model is far less accurate without response when SSC corrections are included in both the model and the non-linear matrix, as was also shown in Figs. 1-11.

In Fig. 17-21 we show the reduced covariance matrix for all cosmologies under study in the context of SPT, non-linear simulation results, and both the full and approximate forms of the reconstructed covariance matrix. Since the Gaussian terms dominate the diagonal, this serves primarily to highlight the shape of the off-diagonal terms and to permit comparison of these shapes between the various models and the non-linear results. As can clearly be seen in all cases, the reconstructed matrices are substantially more accurate to the non-linear data than the SPT matrix, both with and without SSC corrections. Indeed, the SPT model fails to capture a substantial amount of the off-diagonal terms at  $k \sim 0.15 h \text{ Mpc}^{-1}$  which are captured most accurately with the full response matrix and to a lesser extent, at least in some cases, with the approximate response matrix.

In Fig. 22 we show the residual of the ratios of the diagonal values of the covariance matrices obtained from Eq. (24) in the context of both the full and approximate response matrices with the non-linear simulation results. In contrast to the previous set of figures, this highlights the primary expected source of deviation, given that we have assumed a comparatively small parameter dependence for the correlation matrix. As can be seen, the residual is sub-percent to percent level in all cases for all  $k$  values studied, indicating a high level of accuracy in our model. Furthermore, we see in the cases of the parameters  $\Omega_m$ ,  $\Omega_b$ , and  $n_s$ , the full response matrix consistently gives more accurate results than the approximate response matrix, though both achieve percent level accuracy up to the limit of our studied momenta. This indicates that the correlation matrix has a non-negligible rate of change with respect to these parameters. In the cases of  $\sigma_8$  and  $h$ , there is not such a clear disparity between the full and approximate response matrix results, indicating that the correlation matrix has a minimal dependence on those parameters compared to the rate of change of the diagonal.

In Figs. 23-32, we show the results of Eq. (25) for our various cosmologies.

In Figs. 37-42 we show the elementwise ratio of  $C_{\perp}(k_1, k_2)/C_{\parallel}(k_1, k_2)$  for our assorted cosmologies.

Given all of these results, we conclude that the full response matrix is necessary for the most accurate model of the non-linear covariance matrix. This indicates that the correlation matrix exhibits a greater parameter dependence than previously assumed, since the only difference between the full and approximate response matrices is the presence of the derivative of the correlation matrix with respect to the parameter under study.

We note that we developed the approximate response matrix to remove the risk of noise without signal from the derivative of the correlation matrix. However, we have found that our model exhibits minimal noise even with these terms present. Thus, given that they improve accuracy without substantially increasing noise, we conclude that the correct way to model future covariance matrices is using the full response matrix.

## V. DISCUSSION

Explorations of the covariance matrix of the power spectrum of large scale structure are integral to the analysis of current and near future survey results. By studying the covariance of the matter power spectrum as a function of physical parameters, we can use upcoming cosmological surveys to place constraints on those parameters, turning cosmological observables into probes of fundamental physics.

Conventionally, theoretical modeling of covariance matrices for a given choice of parameters can be done either using only the linear power spectrum, which is effective only at very low  $k$ , or using full SPT, which is highly computationally intensive.

In this paper, we have presented a new method which permits the rapid evaluation of the covariance matrix at previously unexplored points in parameter space without explicit computation of the matrix at those spaces and without a linear power spectrum from a simulation with those parameters. This method begins by Taylor expanding a fiducial covariance matrix, appropriately parametrising the first order expansion terms, and defining a new estimator from these terms. This results in us developing what we call a response matrix, which describes the extent to which the accuracy of a model varies as a function of the parameters being considered. This method allows us to create an estimate of the non-linear covariance matrix of an unexplored region of parameter space without any simulations or

explicit calculations for that region of parameter space. Applying the method to recreate the covariance matrices we used as inputs for our model, we were able to show that they recreated them to percent level precision out to at least  $k \approx 0.3 \text{ h Mpc}^{-1}$ .

We have used this method with three different variants: one in which we employ the full response matrix, one in which we employ a simplified approximate response matrix, and one in which the response matrix is set to zero and all parameter dependence comes from an interpolation over SPT models. We found that, in all cosmologies considered, all three methods worked well in the case that SSC corrections were omitted, with the full response matrix generally being the most effective, while the inclusion of SSC corrections resulted in the reconstructions with the response set to zero becoming more inaccurate, indicating that the SSC corrections substantially alter the accuracy of the model.

This work has been done in the context of dark matter halos, treated as a discretised matter model with shot noise terms incorporated into both the Gaussian and non-Gaussian SPT models of the covariance matrix, as well as incorporating super-sample covariance corrections. We leave it to a future work to explore the incorporation of biasing and alternative formulations for the incorporation of shot noise.

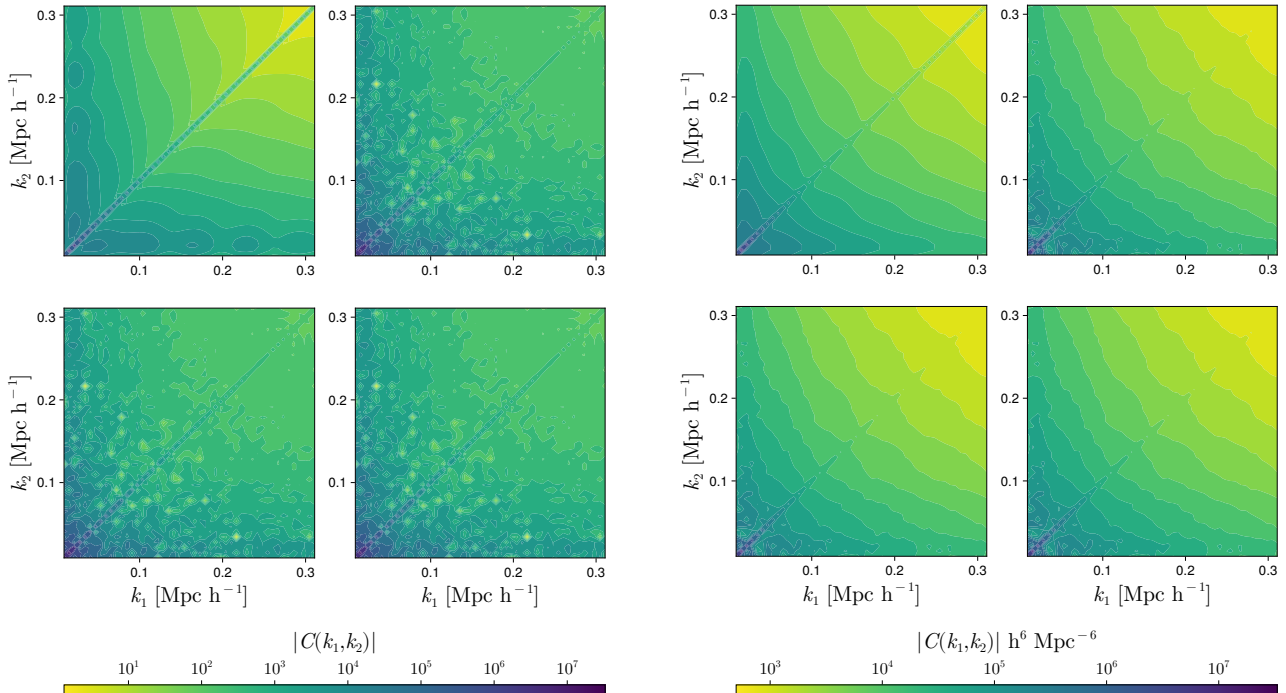


FIG. 1: The covariance matrices for the fiducial cosmology. The left hand pair of columns omit SSC corrections, while the right hand pair of columns include them. In each pair of columns, the top left panel shows the SPT model covariance matrix, the top right panel shows the non-linear covariance matrix from the simulations, the bottom left panel shows the reconstructed covariance matrix from Eq. (24) with the full response matrix as given in Eq. (29), and the bottom right panel shows the reconstructed covariance matrix with the approximated response matrix as given in Eq. (30).

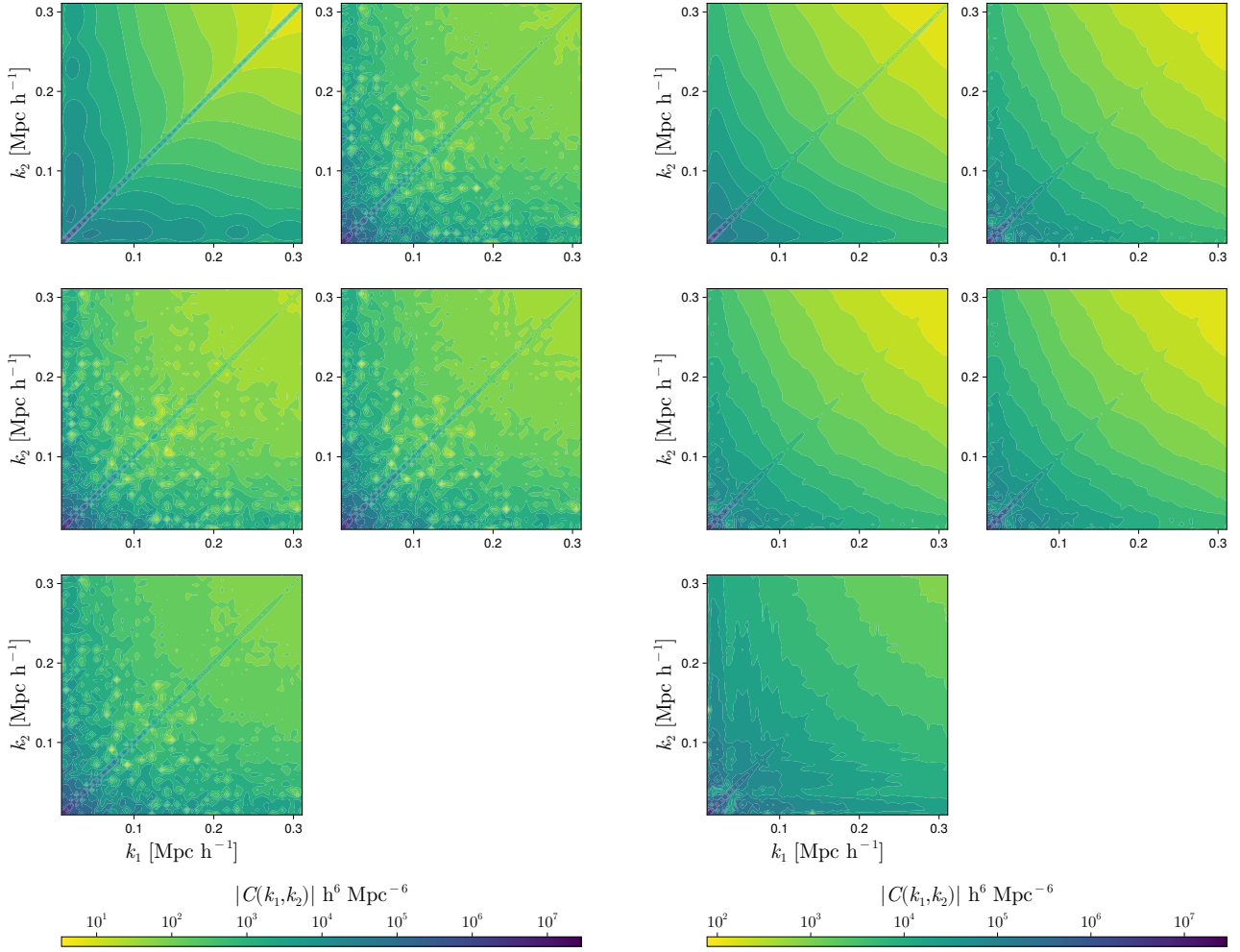


FIG. 2: The covariance matrices for cosmologies with the increased value of the parameter  $\Omega_m$  and other parameters kept as in the fiducial case. The left hand pair of columns omit SSC corrections, while the right hand pair of columns include them. In each set of five panels, the top left panel shows the SPT model covariance matrix, the top right panel shows the non-linear covariance matrix from the simulations, the centre left panel shows the reconstructed covariance matrix from Eq. (24) with the full response matrix as given in Eq. (29), the centre right panel shows the reconstructed covariance matrix with the approximated response matrix as given in Eq. (30), and the bottom panel shows the results of Eq. (24) with the response matrix set to zero.

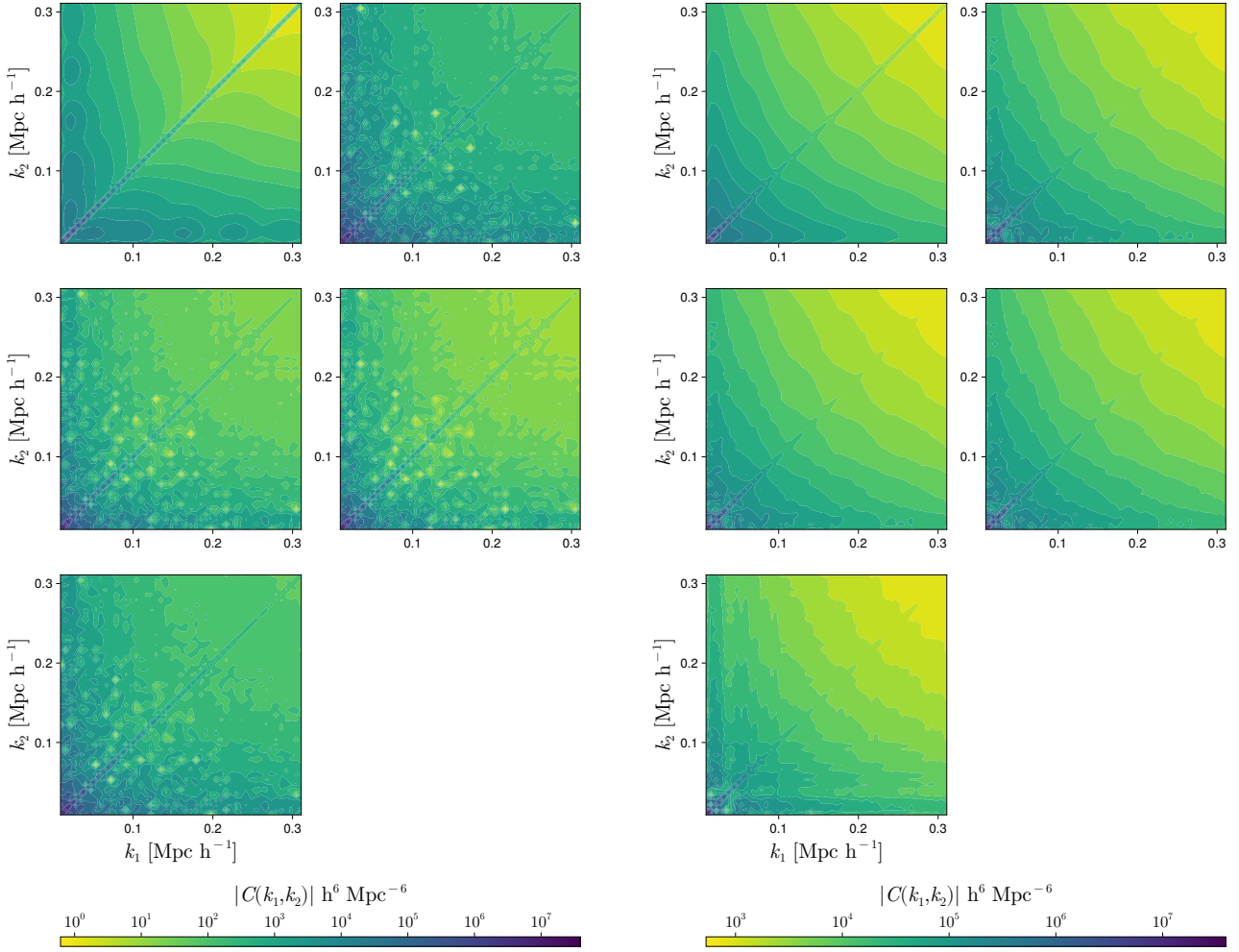


FIG. 3: The covariance matrices for cosmologies with the decreased value of the parameter  $\Omega_m$  and other parameters kept as in the fiducial case. The left hand pair of columns omit SSC corrections, while the right hand pair of columns include them. In each set of five panels, the top left panel shows the SPT model covariance matrix, the top right panel shows the non-linear covariance matrix from the simulations, the centre left panel shows the reconstructed covariance matrix from Eq. (24) with the full response matrix as given in Eq. (29), the centre right panel shows the reconstructed covariance matrix with the approximated response matrix as given in Eq. (30), and the bottom panel shows the results of Eq. (24) with the response matrix set to zero.

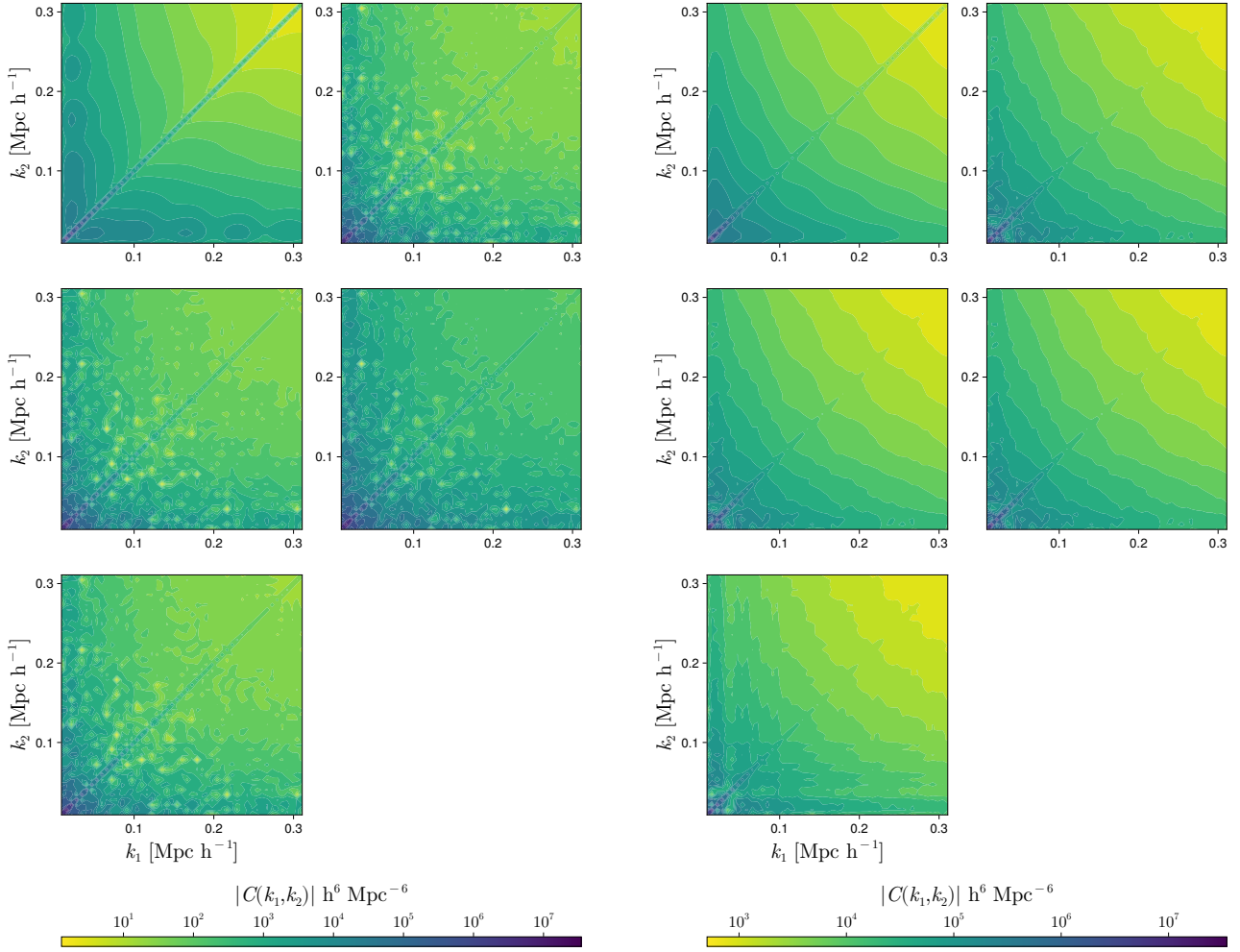


FIG. 4: The covariance matrices for cosmologies with the increased value of the parameter  $\Omega_b$  and other parameters kept as in the fiducial case. The left hand pair of columns omit SSC corrections, while the right hand pair of columns include them. In each set of five panels, the top left panel shows the SPT model covariance matrix, the top right panel shows the non-linear covariance matrix from the simulations, the centre left panel shows the reconstructed covariance matrix from Eq. (24) with the full response matrix as given in Eq. (29), the centre right panel shows the reconstructed covariance matrix with the approximated response matrix as given in Eq. (30), and the bottom panel shows the results of Eq. (24) with the response matrix set to zero.

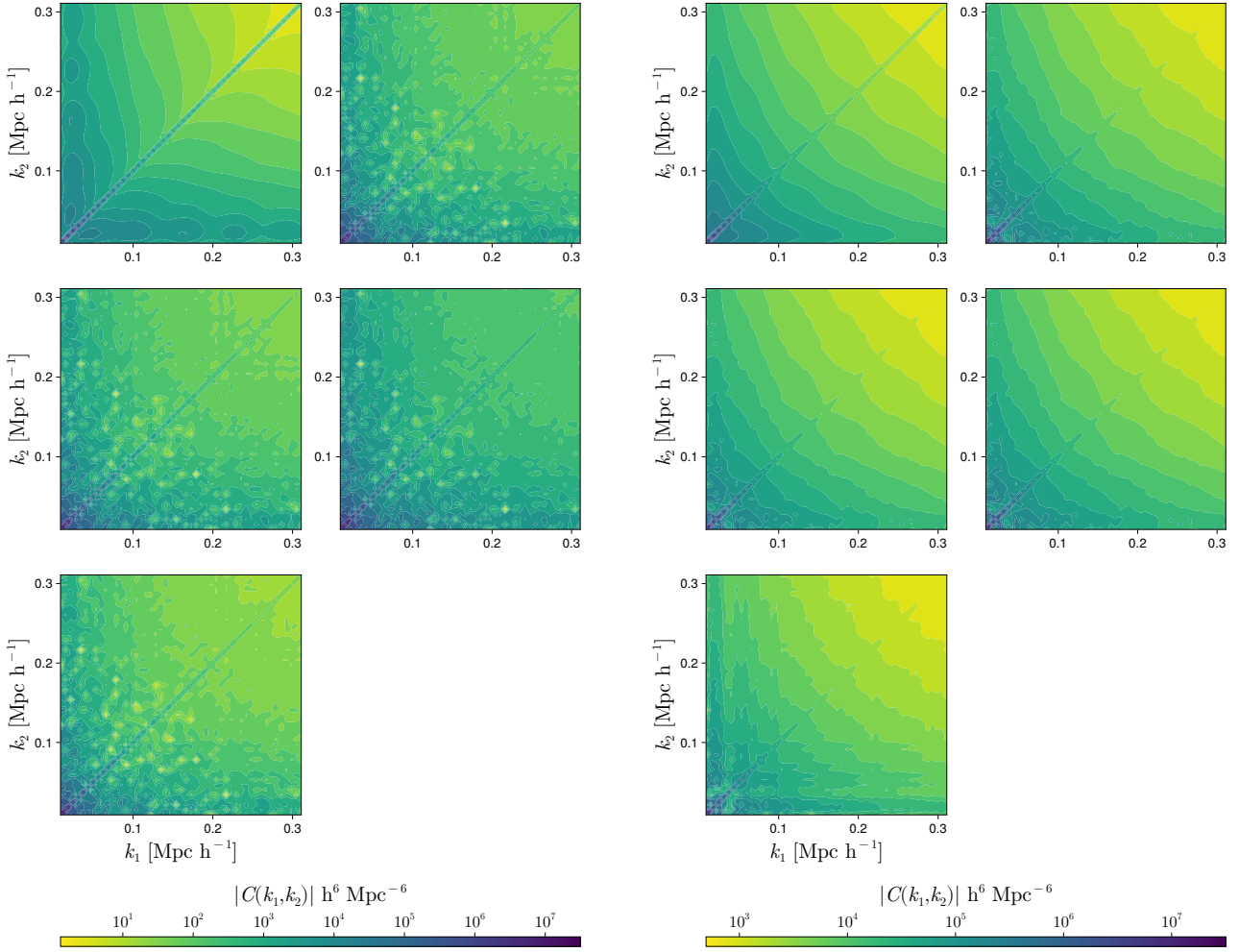


FIG. 5: The covariance matrices for cosmologies with the decreased value of the parameter  $\Omega_b$  and other parameters kept as in the fiducial case. The left hand pair of columns omit SSC corrections, while the right hand pair of columns include them. In each set of five panels, the top left panel shows the SPT model covariance matrix, the top right panel shows the non-linear covariance matrix from the simulations, the centre left panel shows the reconstructed covariance matrix from Eq. (24) with the full response matrix as given in Eq. (29), the centre right panel shows the reconstructed covariance matrix with the approximated response matrix as given in Eq. (30), and the bottom panel shows the results of Eq. (24) with the response matrix set to zero.

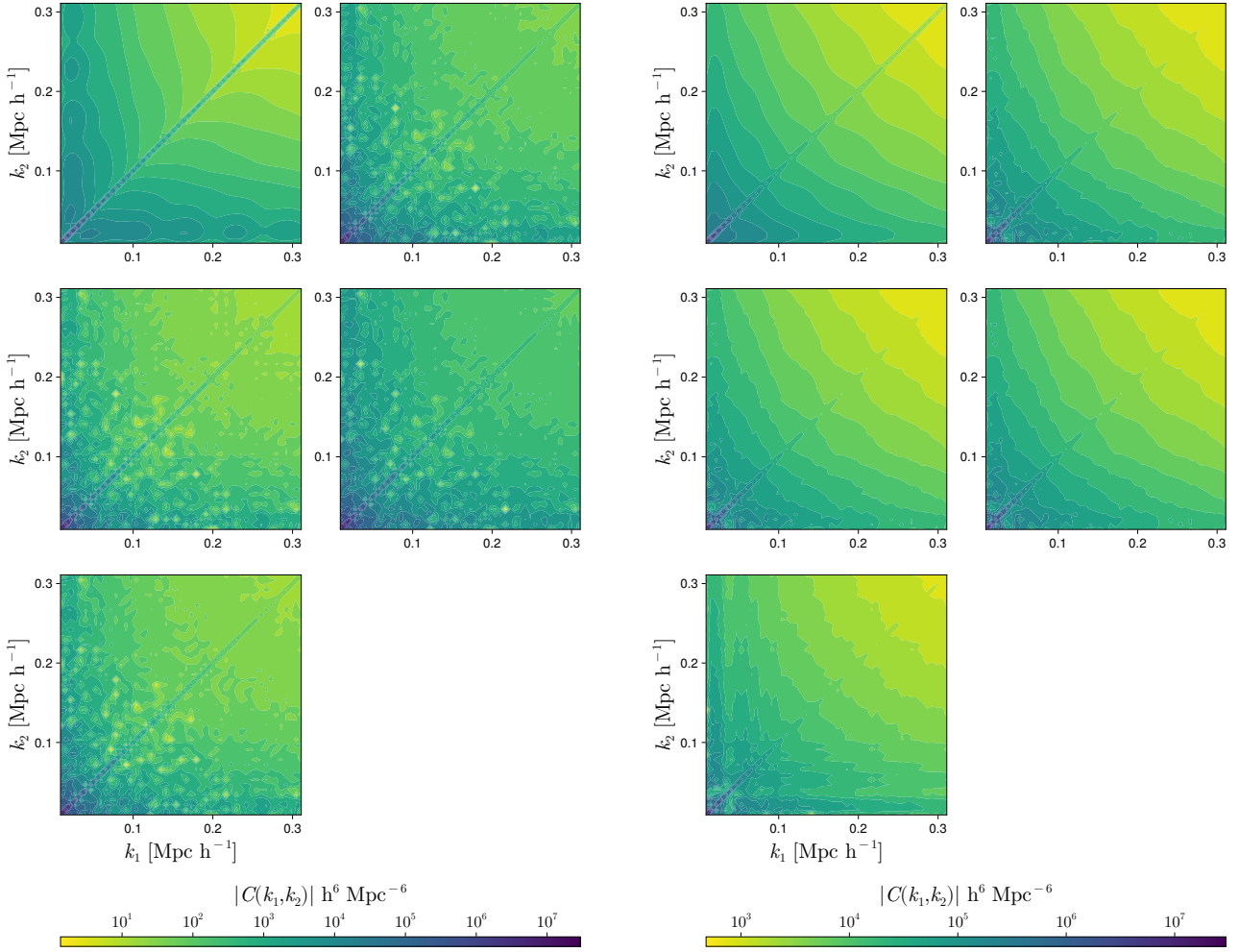


FIG. 6: The covariance matrices for cosmologies with the increased value of the parameter  $n_s$  and other parameters kept as in the fiducial case. The left hand pair of columns omit SSC corrections, while the right hand pair of columns include them. In each set of five panels, the top left panel shows the SPT model covariance matrix, the top right panel shows the non-linear covariance matrix from the simulations, the centre left panel shows the reconstructed covariance matrix from Eq. (24) with the full response matrix as given in Eq. (29), the centre right panel shows the reconstructed covariance matrix with the approximated response matrix as given in Eq. (30), and the bottom panel shows the results of Eq. (24) with the response matrix set to zero.

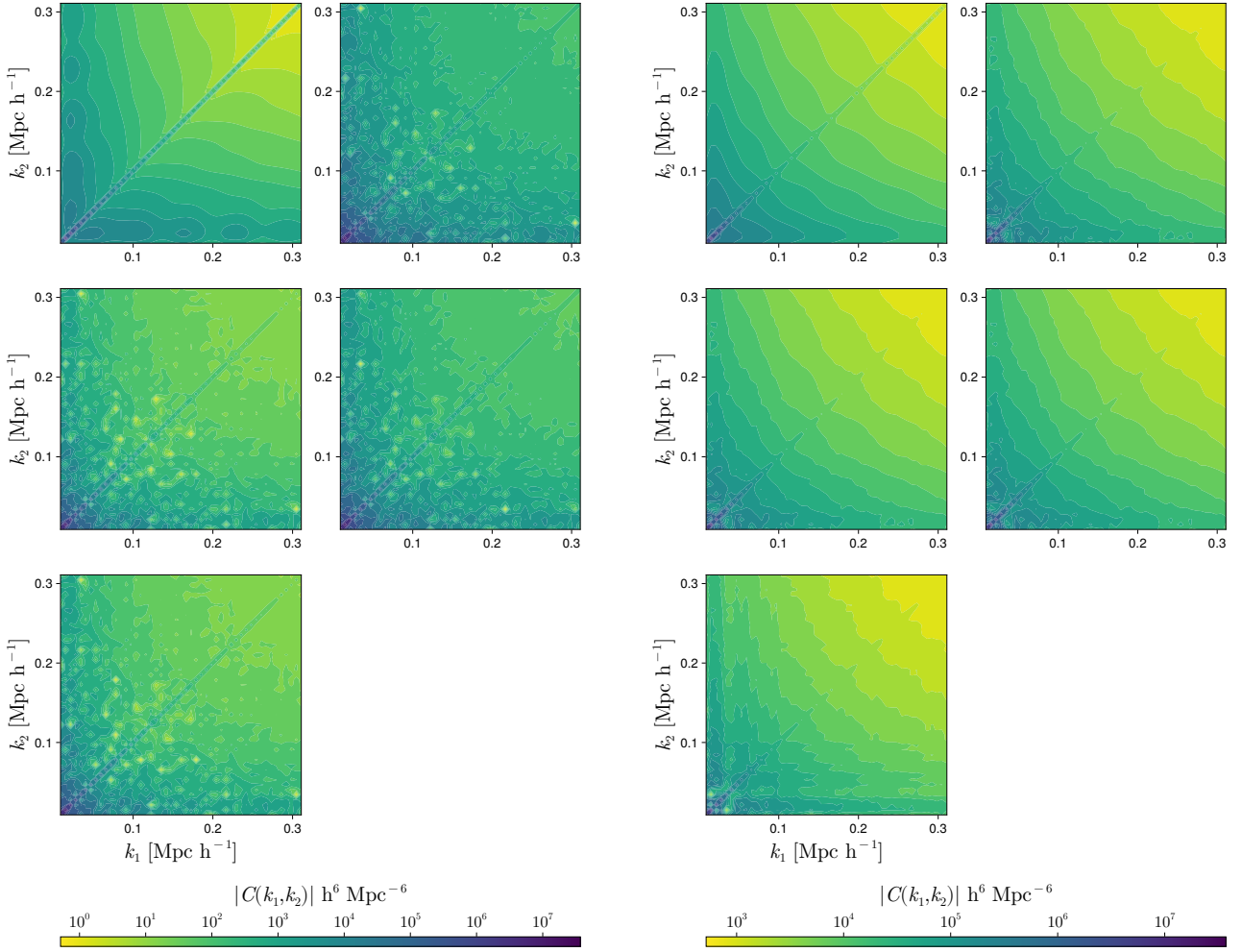


FIG. 7: The covariance matrices for cosmologies with the decreased value of the parameter  $n_s$  and other parameters kept as in the fiducial case. The left hand pair of columns omit SSC corrections, while the right hand pair of columns include them. In each set of five panels, the top left panel shows the SPT model covariance matrix, the top right panel shows the non-linear covariance matrix from the simulations, the centre left panel shows the reconstructed covariance matrix from Eq. (24) with the full response matrix as given in Eq. (29), the centre right panel shows the reconstructed covariance matrix with the approximated response matrix as given in Eq. (30), and the bottom panel shows the results of Eq. (24) with the response matrix set to zero.

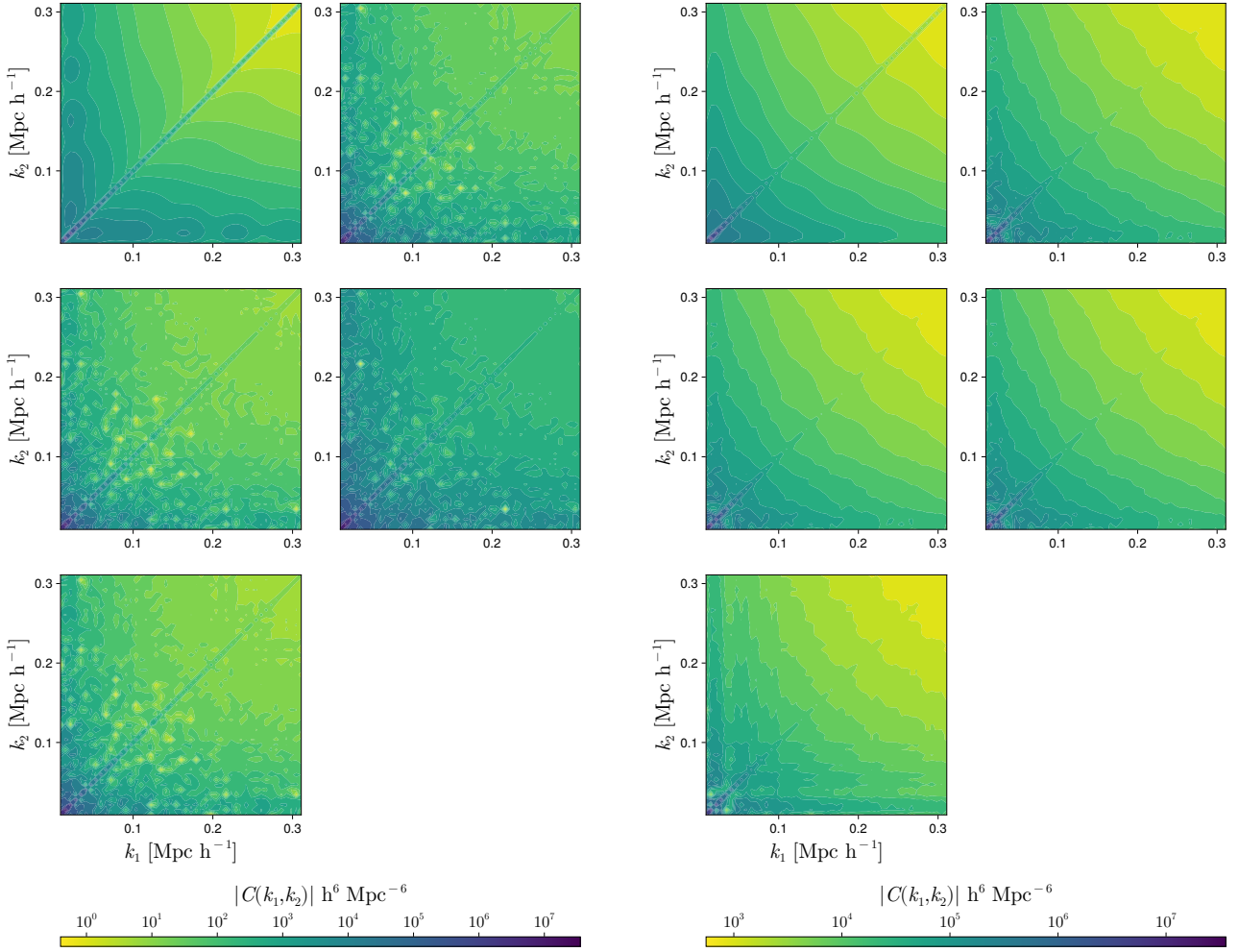


FIG. 8: The covariance matrices for cosmologies with the increased value of the parameter  $\sigma_8$  and other parameters kept as in the fiducial case. The left hand pair of columns omit SSC corrections, while the right hand pair of columns include them. In each set of five panels, the top left panel shows the SPT model covariance matrix, the top right panel shows the non-linear covariance matrix from the simulations, the centre left panel shows the reconstructed covariance matrix from Eq. (24) with the full response matrix as given in Eq. (29), the centre right panel shows the reconstructed covariance matrix with the approximated response matrix as given in Eq. (30), and the bottom panel shows the results of Eq. (24) with the response matrix set to zero.

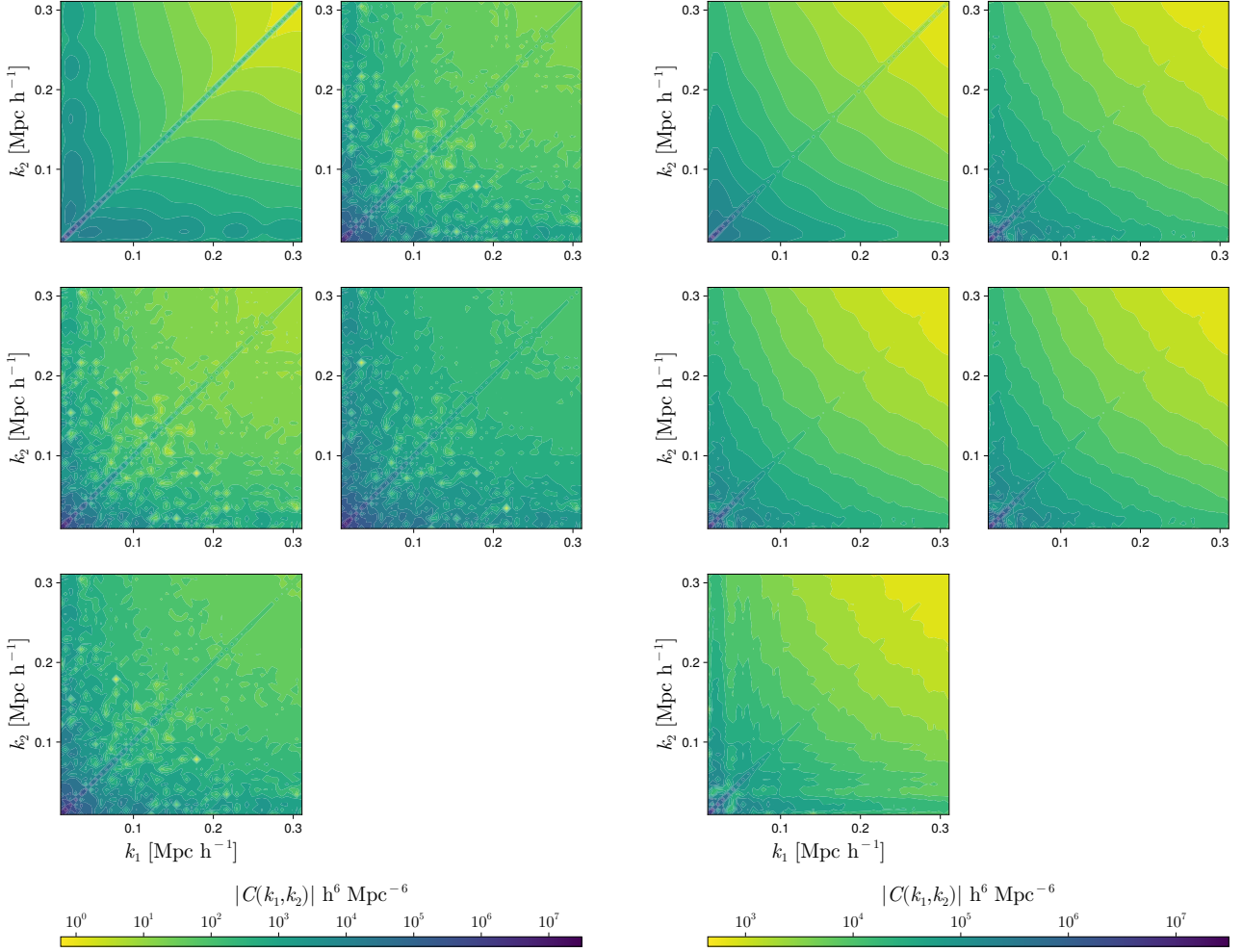


FIG. 9: The covariance matrices for cosmologies with the decreased value of the parameter  $\sigma_8$  and other parameters kept as in the fiducial case. The left hand pair of columns omit SSC corrections, while the right hand pair of columns include them. In each set of five panels, the top left panel shows the SPT model covariance matrix, the top right panel shows the non-linear covariance matrix from the simulations, the centre left panel shows the reconstructed covariance matrix from Eq. (24) with the full response matrix as given in Eq. (29), the centre right panel shows the reconstructed covariance matrix with the approximated response matrix as given in Eq. (30), and the bottom panel shows the results of Eq. (24) with the response matrix set to zero.

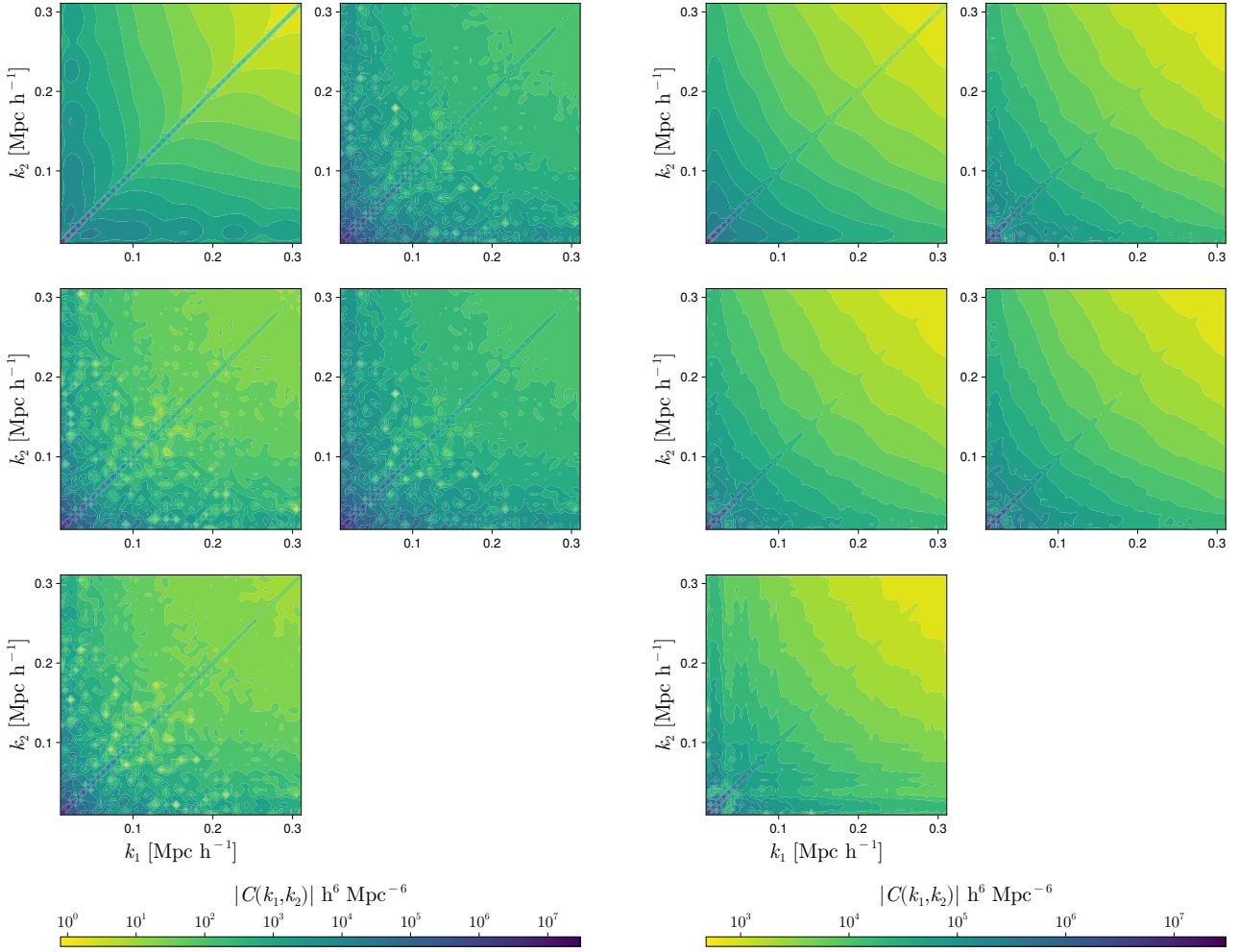


FIG. 10: The covariance matrices for cosmologies with the increased value of the parameter  $h$  and other parameters kept as in the fiducial case. The left hand pair of columns omit SSC corrections, while the right hand pair of columns include them. In each set of five panels, the top left panel shows the SPT model covariance matrix, the top right panel shows the non-linear covariance matrix from the simulations, the centre left panel shows the reconstructed covariance matrix from Eq. (24) with the full response matrix as given in Eq. (29), the centre right panel shows the reconstructed covariance matrix with the approximated response matrix as given in Eq. (30), and the bottom panel shows the results of Eq. (24) with the response matrix set to zero.

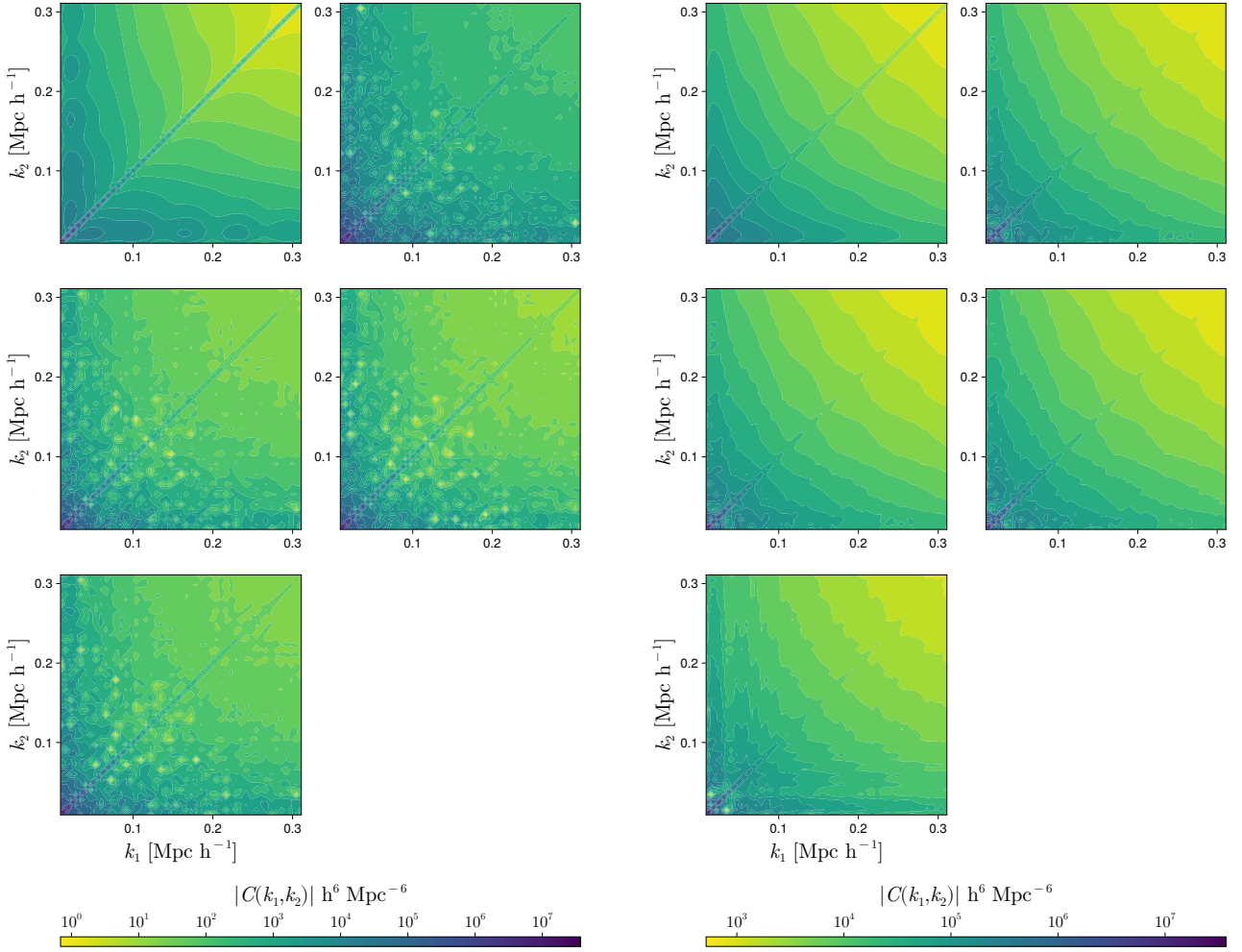


FIG. 11: The covariance matrices for cosmologies with the decreased value of the parameter  $h$  and other parameters kept as in the fiducial case. The left hand pair of columns omit SSC corrections, while the right hand pair of columns include them. In each set of five panels, the top left panel shows the SPT model covariance matrix, the top right panel shows the non-linear covariance matrix from the simulations, the centre left panel shows the reconstructed covariance matrix from Eq. (24) with the full response matrix as given in Eq. (29), the centre right panel shows the reconstructed covariance matrix with the approximated response matrix as given in Eq. (30), and the bottom panel shows the results of Eq. (24) with the response matrix set to zero.

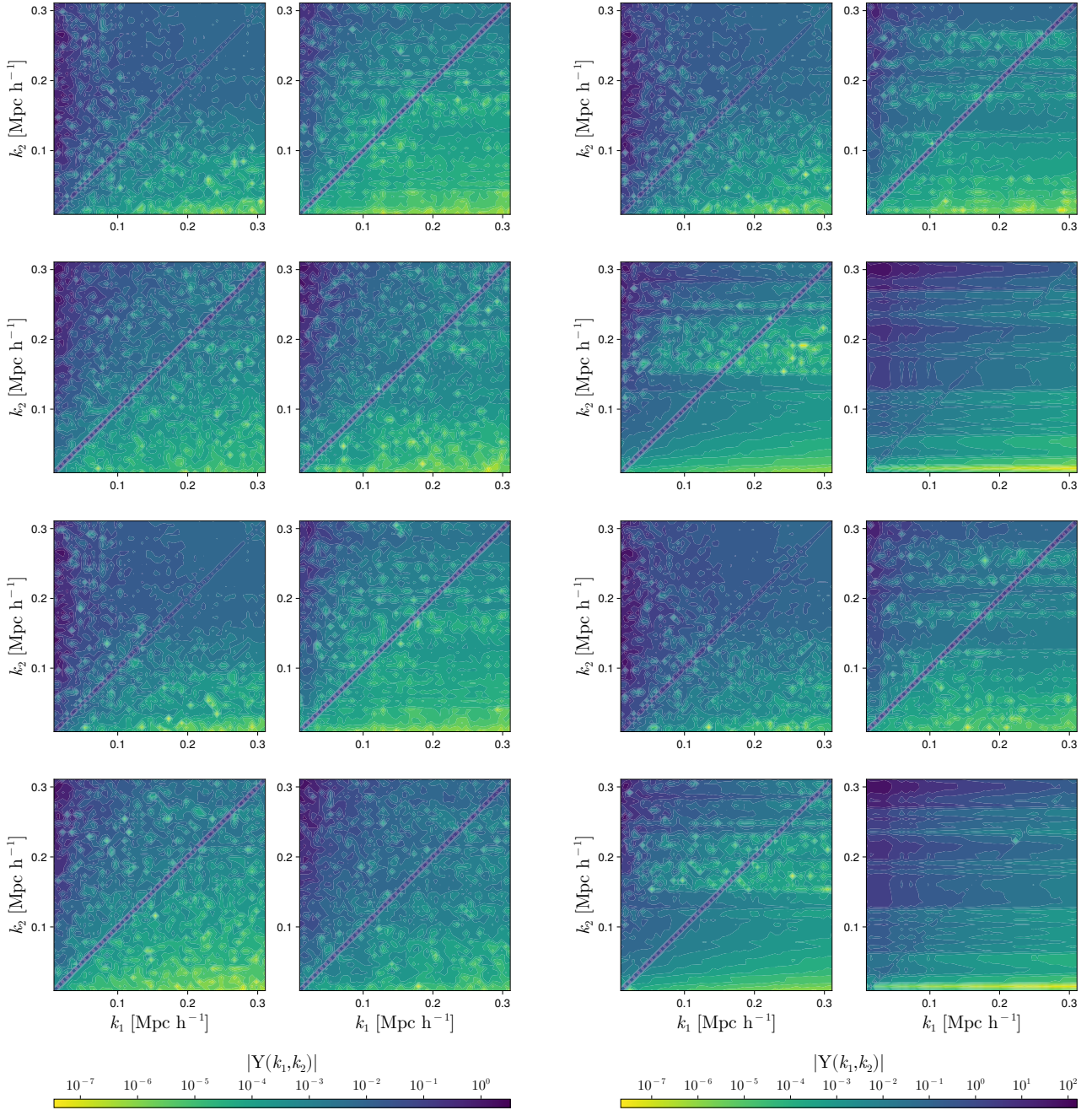


FIG. 12: The factors  $Y = C_m^{-1} C_{nl}$  for the permutation of  $\Omega_m$ . The top two rows show the results with the increased value and the bottom two rows with the decreased value. The left hand pair of columns show the results without SSC corrections and the right hand pair of columns include SSC corrections. The top left panel shows the  $Y$  for the SPT model, the top right panel shows  $Y$  with the full response matrix  $C_{\parallel}$ , the bottom left panel shows  $Y$  with the approximate response matrix  $C_{\parallel,a}$ , and the bottom right panel shows  $Y$  with  $C_{\parallel,R=0}$  in which the response matrix is set to zero.

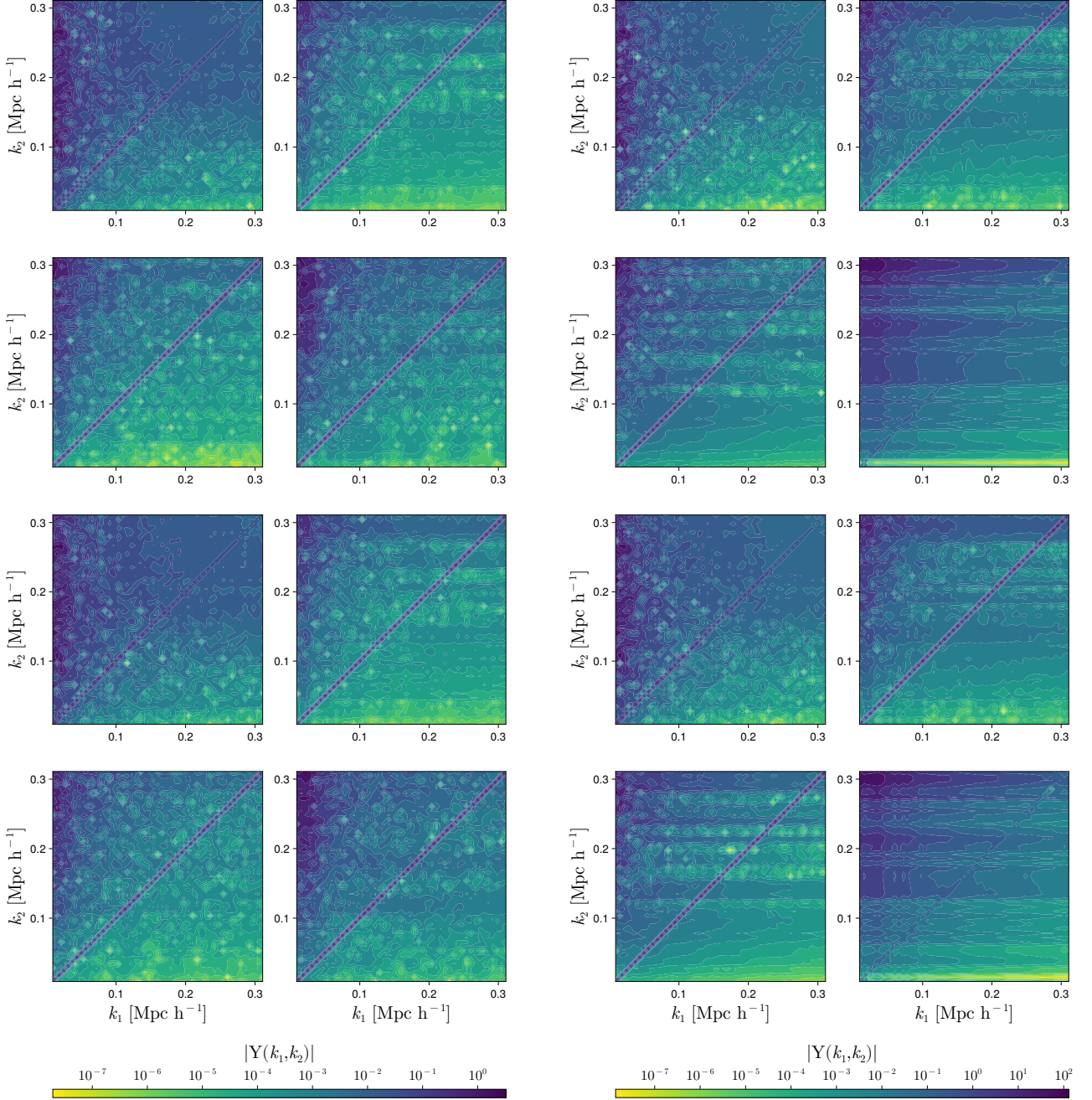


FIG. 13: The factors  $Y = C_m^{-1} C_{nl}$  for the permutation of  $\Omega_b$ . The top two rows show the results with the increased value and the bottom two rows with the decreased value. The left hand pair of columns show the results without SSC corrections and the right hand pair of columns include SSC corrections. The top left panel shows the  $Y$  for the SPT model, the top right panel shows  $Y$  with the full response matrix  $C_{\parallel}$ , the bottom left panel shows  $Y$  with the approximate response matrix estimator  $C_{\parallel,a}$ , and the bottom right panel shows  $Y$  with  $C_{\parallel,R=0}$  in which the response matrix is set to zero.

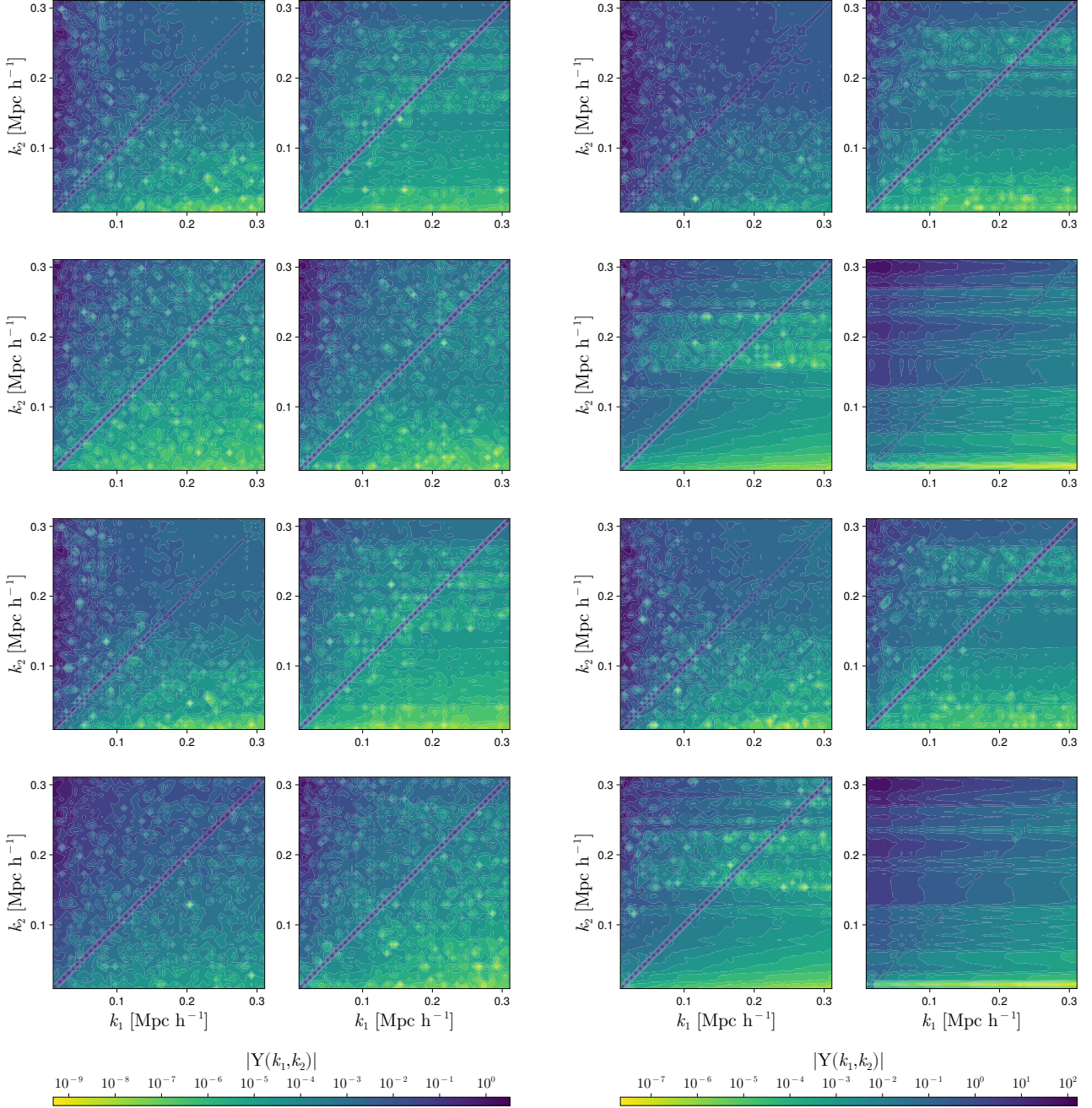


FIG. 14: The factors  $Y = C_m^{-1} C_{nl}$  for the permutation of  $n_s$ . The top two rows show the results with the increased value and the bottom two rows with the decreased value. The left hand pair of columns show the results without SSC corrections and the right hand pair of columns include SSC corrections. The top left panel shows the  $Y$  for the SPT model, the top right panel shows  $Y$  with the full response matrix  $C_{\parallel}$ , the bottom left panel shows  $Y$  with the approximate response matrix  $C_{\parallel,a}$ , and the bottom right panel shows  $Y$  with  $C_{\parallel,R=0}$  in which the response matrix is set to zero.

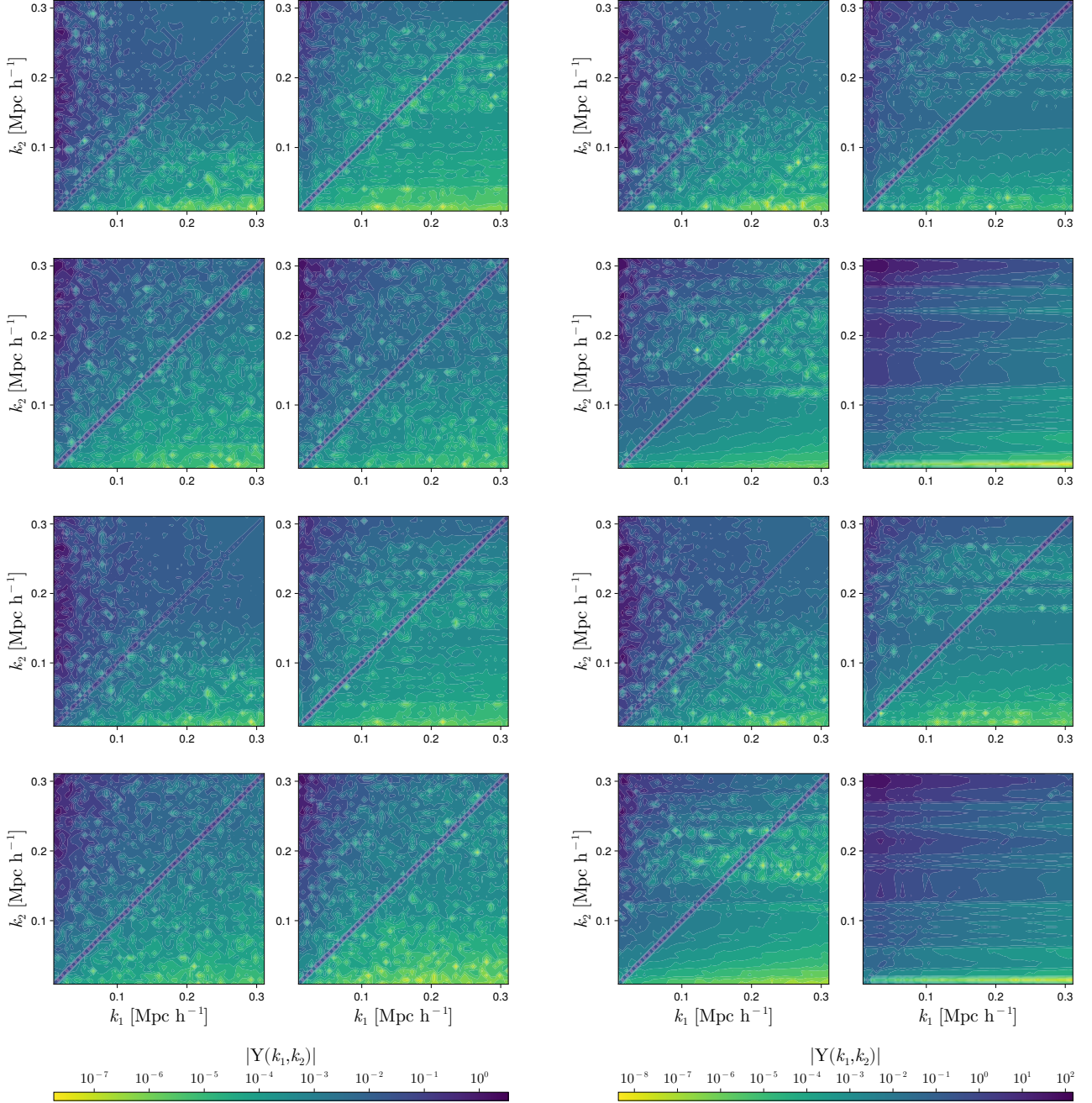


FIG. 15: The factors  $Y = C_m^{-1} C_{nl}$  for the permutation of  $\sigma_8$ . The top two rows show the results with the increased value and the bottom two rows with the decreased value. The left hand pair of columns show the results without SSC corrections and the right hand pair of columns include SSC corrections. The top left panel shows the  $Y$  for the SPT model, the top right panel shows  $Y$  with the full response matrix  $C_{\parallel}$ , the bottom left panel shows  $Y$  with the approximate response matrix  $C_{\parallel,a}$ , and the bottom right panel shows  $Y$  with  $C_{\parallel,R=0}$  in which the response matrix is set to zero.

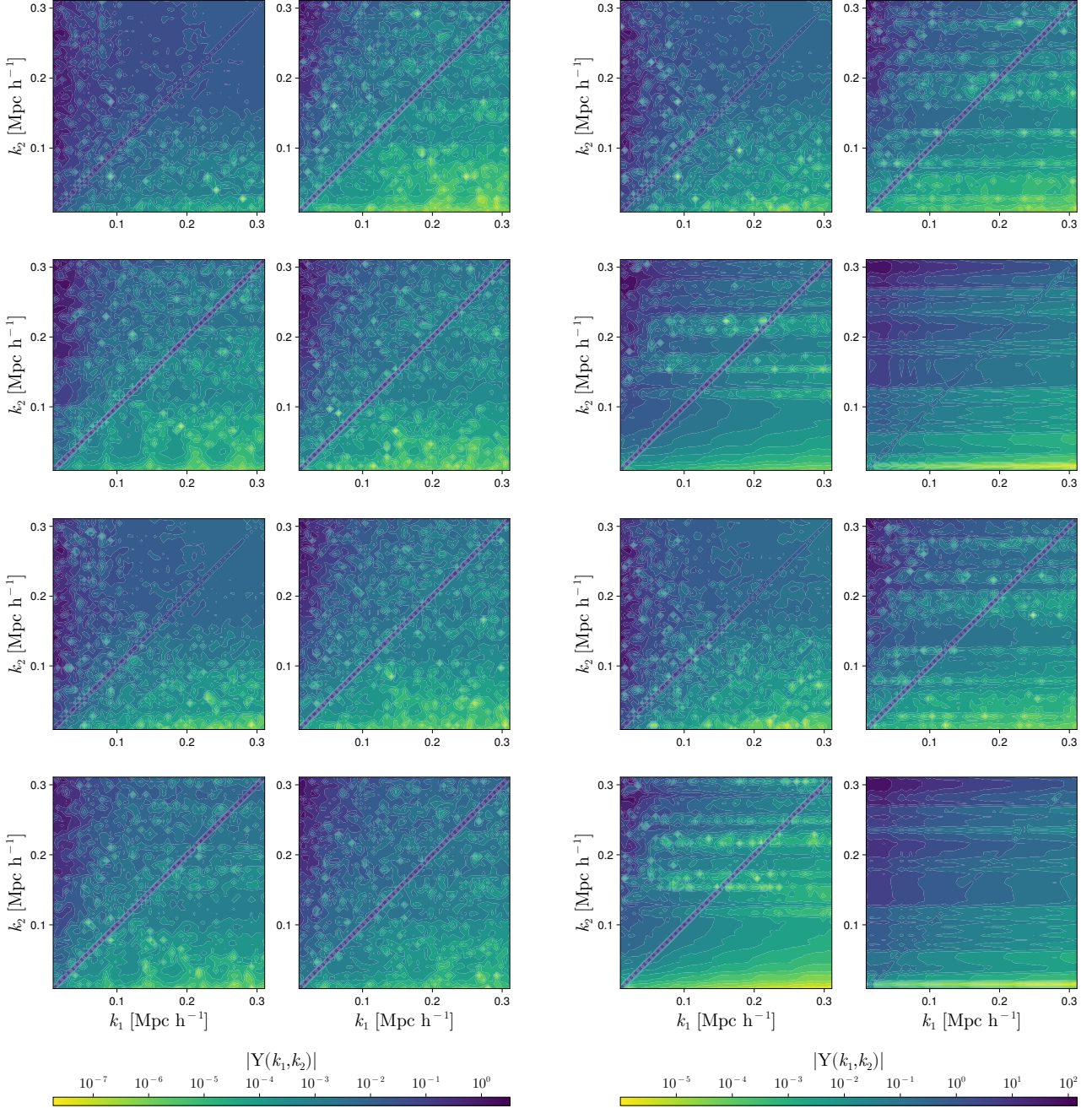


FIG. 16: The factors  $Y = C_m^{-1} C_{nl}$  for the permutation of  $h$ . The top two rows show the results with the increased value and the bottom two rows with the decreased value. The left hand pair of columns show the results without SSC corrections and the right hand pair of columns include SSC corrections. The top left panel shows the  $Y$  for the SPT model, the top right panel shows  $Y$  with the full response matrix  $C_{\parallel}$ , the bottom left panel shows  $Y$  with the approximate response matrix  $C_{\parallel,a}$ , and the bottom right panel shows  $Y$  with  $C_{\parallel,R=0}$  in which the response matrix is set to zero.

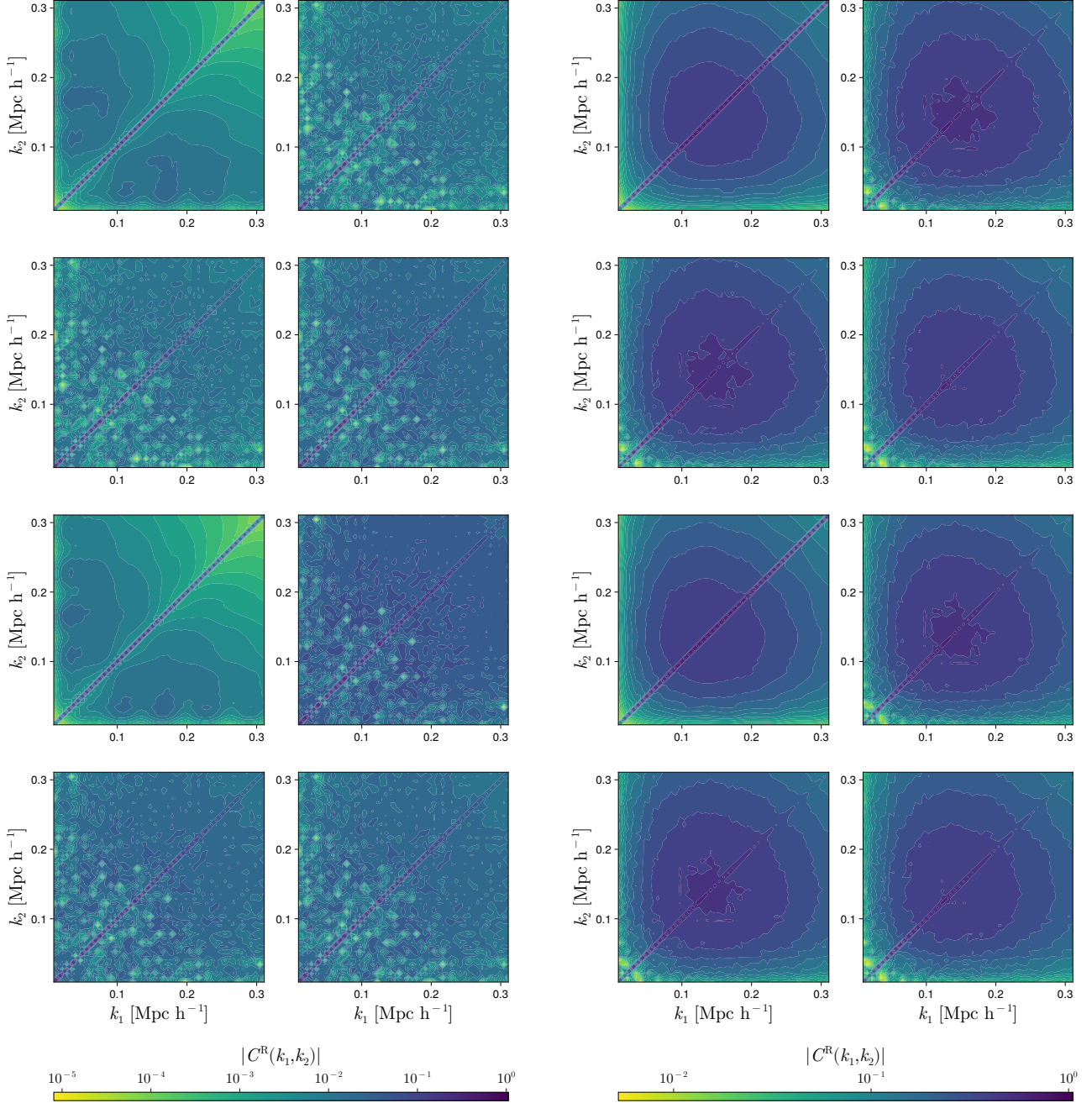


FIG. 17: The reduced covariance matrices for cosmologies with the increased (top two rows) and decreased (bottom two rows) values of the parameter  $\Omega_m$  and other parameters kept at their fiducial values. The left hand pair of columns omit SSC corrections, while the right hand pair of columns include them. In each pair of columns, the top left panel shows the SPT model covariance matrix, the top right panel shows the non-linear covariance matrix from the simulations, the bottom left panel shows the reconstructed covariance matrix from Eq. (24) with the full response matrix as given in Eq. (29), and the bottom right panel shows the reconstructed covariance matrix with the approximated response matrix as given in Eq. (30).

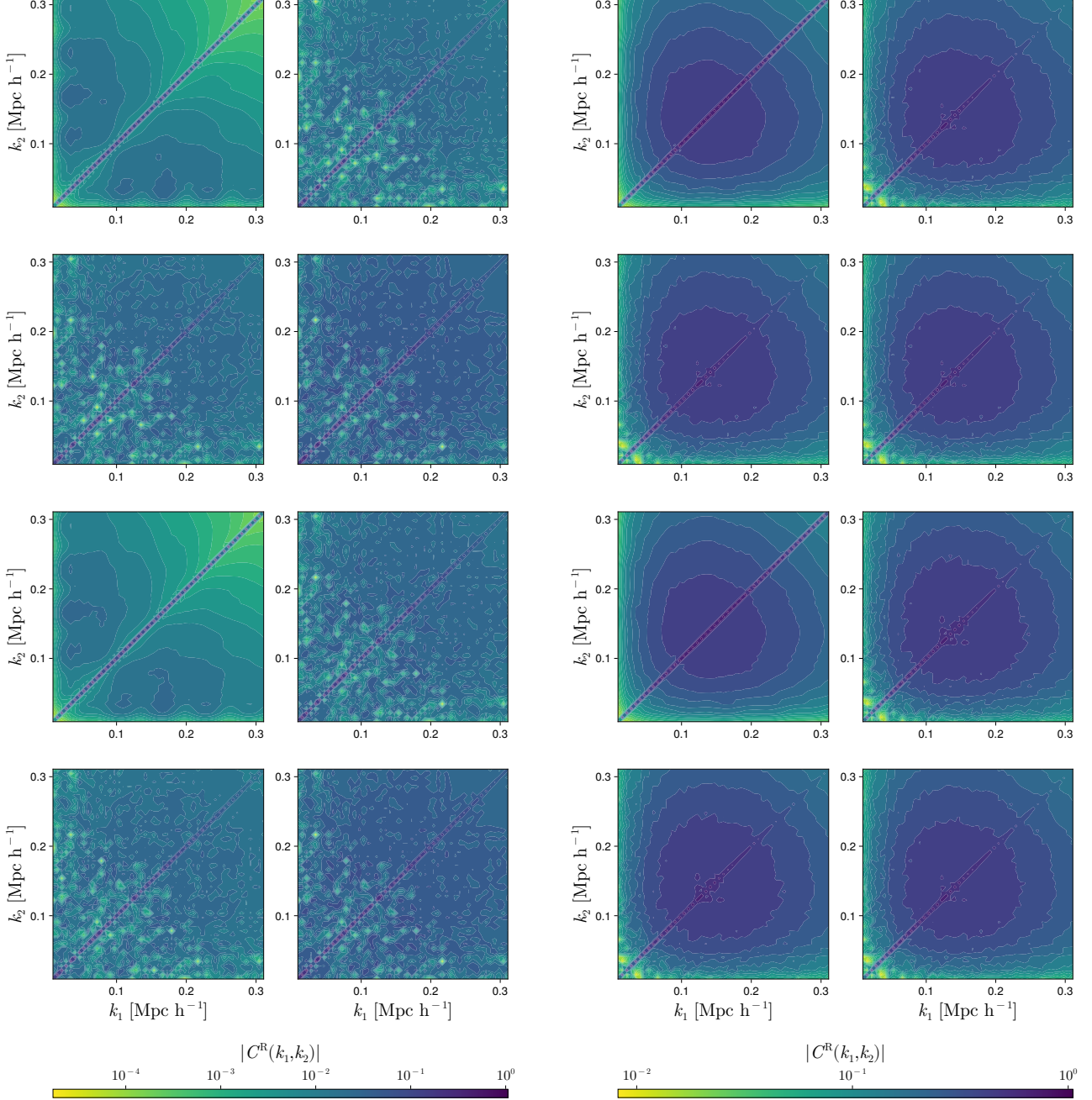


FIG. 18: The reduced covariance matrices for cosmologies with the increased (top two rows) and decreased (bottom two rows) values of the parameter  $\Omega_b$  and other parameters kept at their fiducial values. The left hand pair of columns omit SSC corrections, while the right hand pair of columns include them. In each pair of columns, the top left panel shows the SPT model covariance matrix, the top right panel shows the non-linear covariance matrix from the simulations, the bottom left panel shows the reconstructed covariance matrix from Eq. (24) with the full response matrix as given in Eq. (29), and the bottom right panel shows the reconstructed covariance matrix with the approximated response matrix as given in Eq. (30).

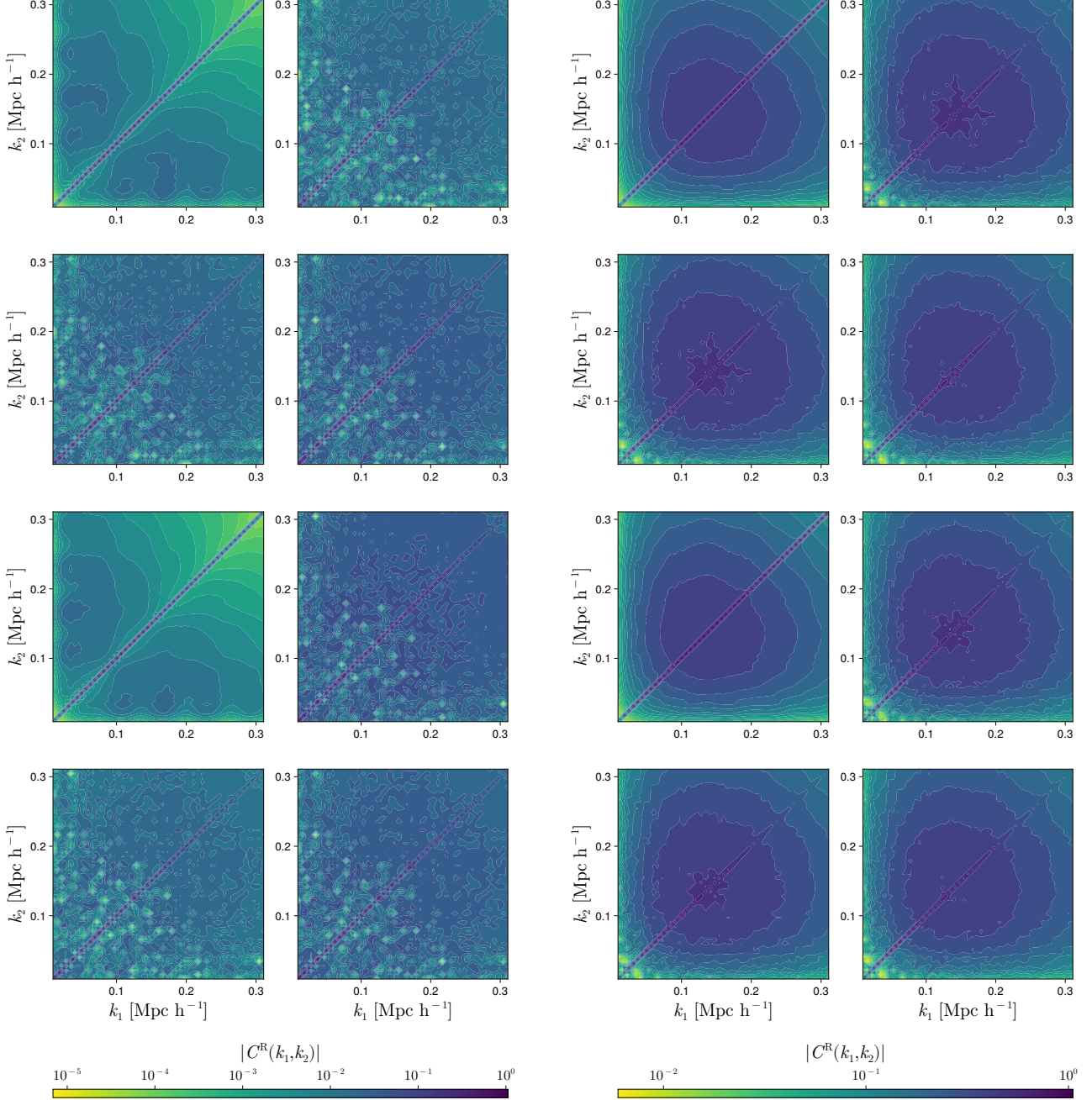


FIG. 19: The reduced covariance matrices for cosmologies with the increased (top two rows) and decreased (bottom two rows) values of the parameter  $n_s$  and other parameters kept at their fiducial values. The left hand pair of columns omit SSC corrections, while the right hand pair of columns include them. In each pair of columns, the top left panel shows the SPT model covariance matrix, the top right panel shows the non-linear covariance matrix from the simulations, the bottom left panel shows the reconstructed covariance matrix from Eq. (24) with the full response matrix as given in Eq. (29), and the bottom right panel shows the reconstructed covariance matrix with the approximated response matrix as given in Eq. (30).

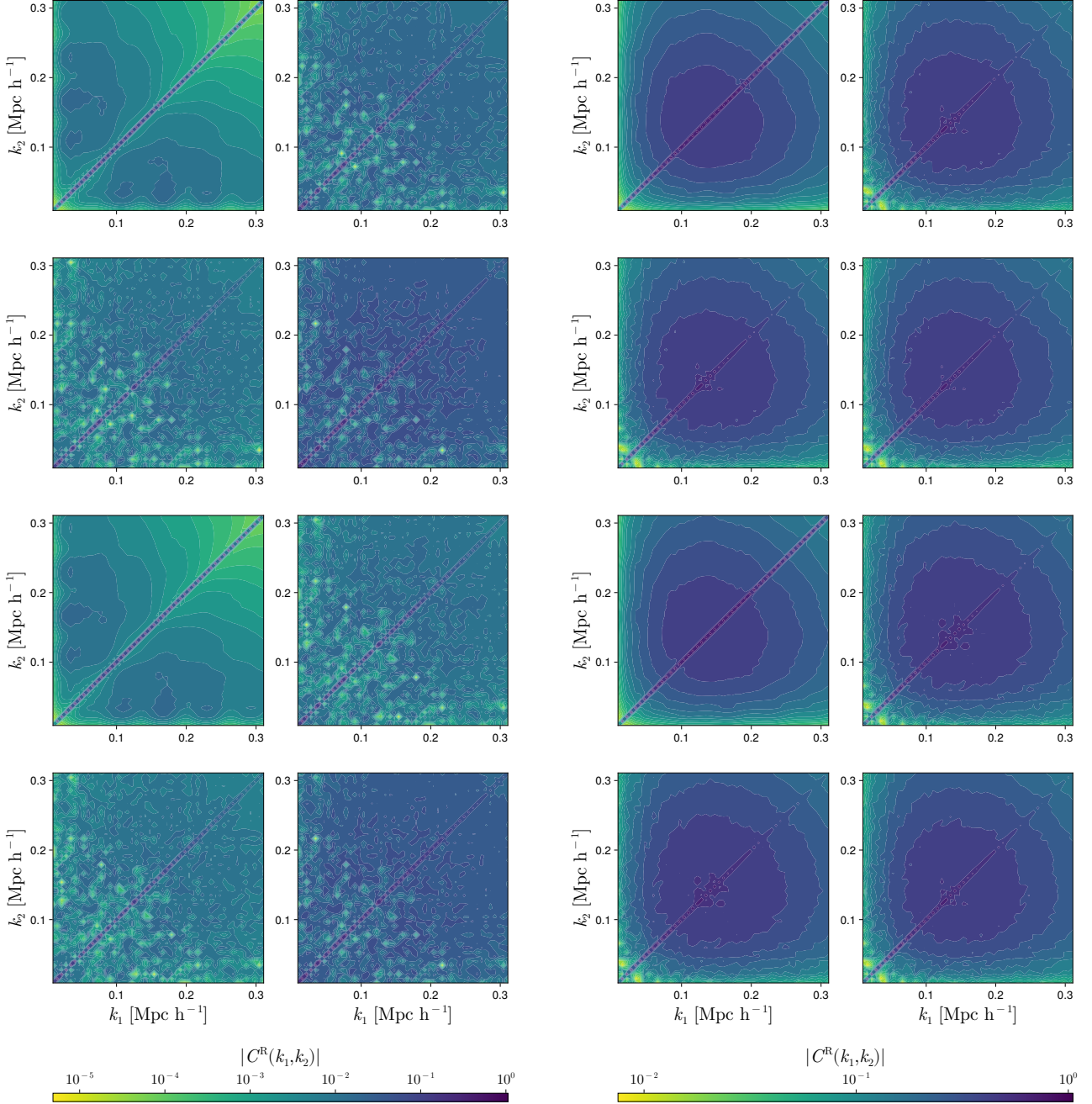


FIG. 20: The reduced covariance matrices for cosmologies with the increased (top two rows) and decreased (bottom two rows) values of the parameter  $\sigma_8$  and other parameters kept at their fiducial values. The left hand pair of columns omit SSC corrections, while the right hand pair of columns include them. In each pair of columns, the top left panel shows the SPT model covariance matrix, the top right panel shows the non-linear covariance matrix from the simulations, the bottom left panel shows the reconstructed covariance matrix from Eq. (24) with the full response matrix as given in Eq. (29), and the bottom right panel shows the reconstructed covariance matrix with the approximated response matrix as given in Eq. (30).

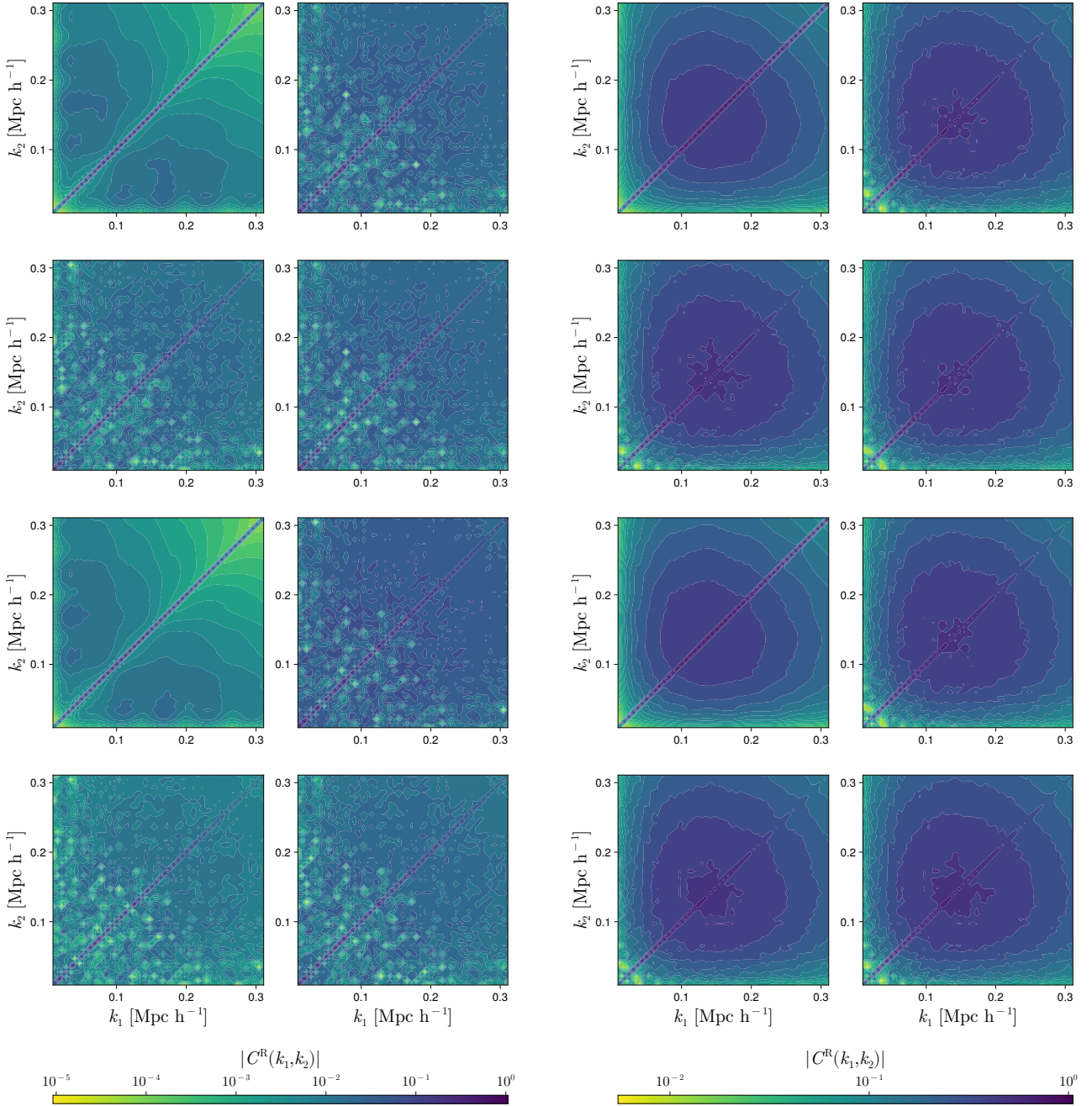


FIG. 21: The reduced covariance matrices for cosmologies with the increased (top two rows) and decreased (bottom two rows) values of the parameter  $h$  and other parameters kept at their fiducial values. The left hand pair of columns omit SSC corrections, while the right hand pair of columns include them. In each pair of columns, the top left panel shows the SPT model covariance matrix, the top right panel shows the non-linear covariance matrix from the simulations, the bottom left panel shows the reconstructed covariance matrix from Eq. (24) with the full response matrix as given in Eq. (29), and the bottom right panel shows the reconstructed covariance matrix with the approximated response matrix as given in Eq. (30).

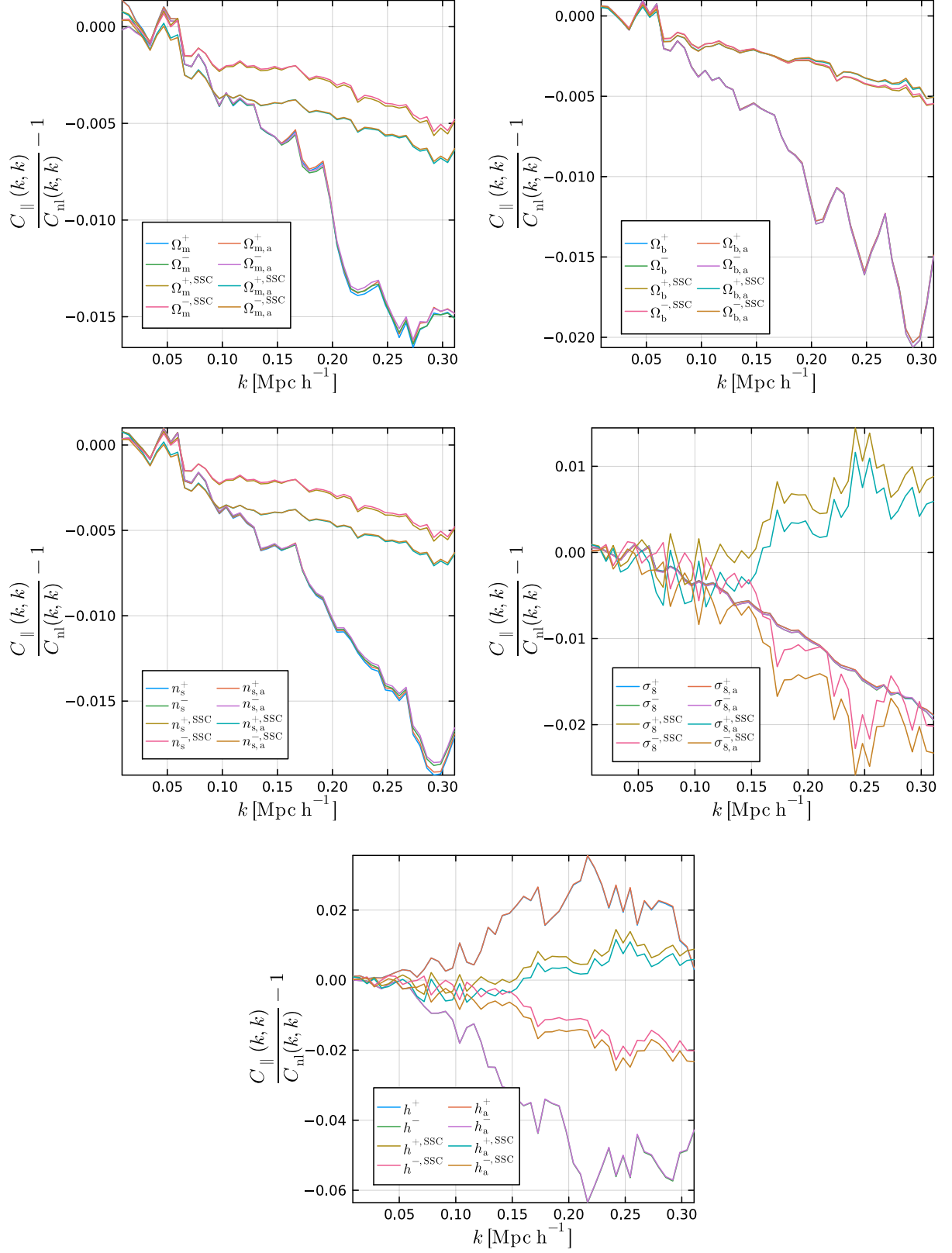


FIG. 22: The residuals of the ratios of the diagonals of the reconstructed and non-linear covariance matrices for all parameter variations with both the full and approximate response matrices, both with and without SSC corrections.

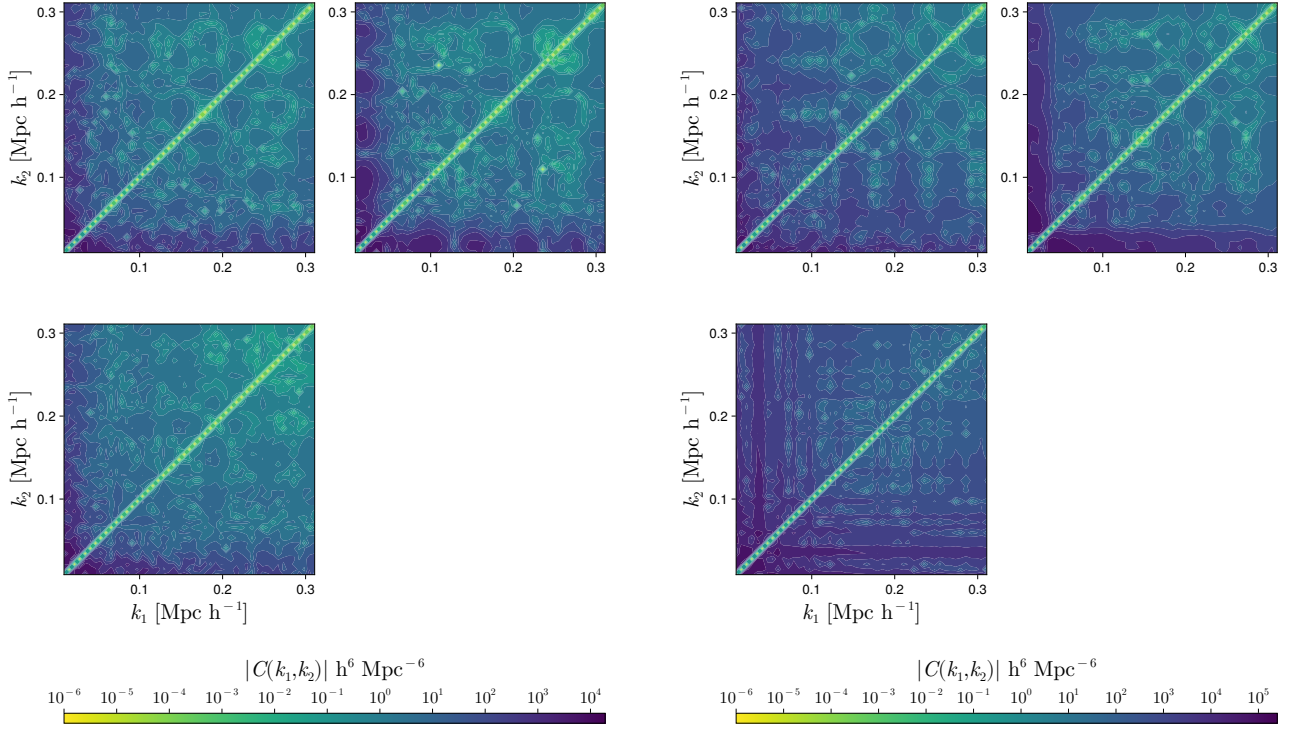


FIG. 23: The asymmetry matrix as given in Eq. (25) for  $\Omega_m$  in the reduced parameter case, without SSC corrections (left hand pair of columns) and with them (right hand pair of columns). In both cases, the top left panel shows the value with the full response matrix, the top right panel shows the result with the approximate response matrix, and the bottom panel shows the result with the response matrix set to zero.

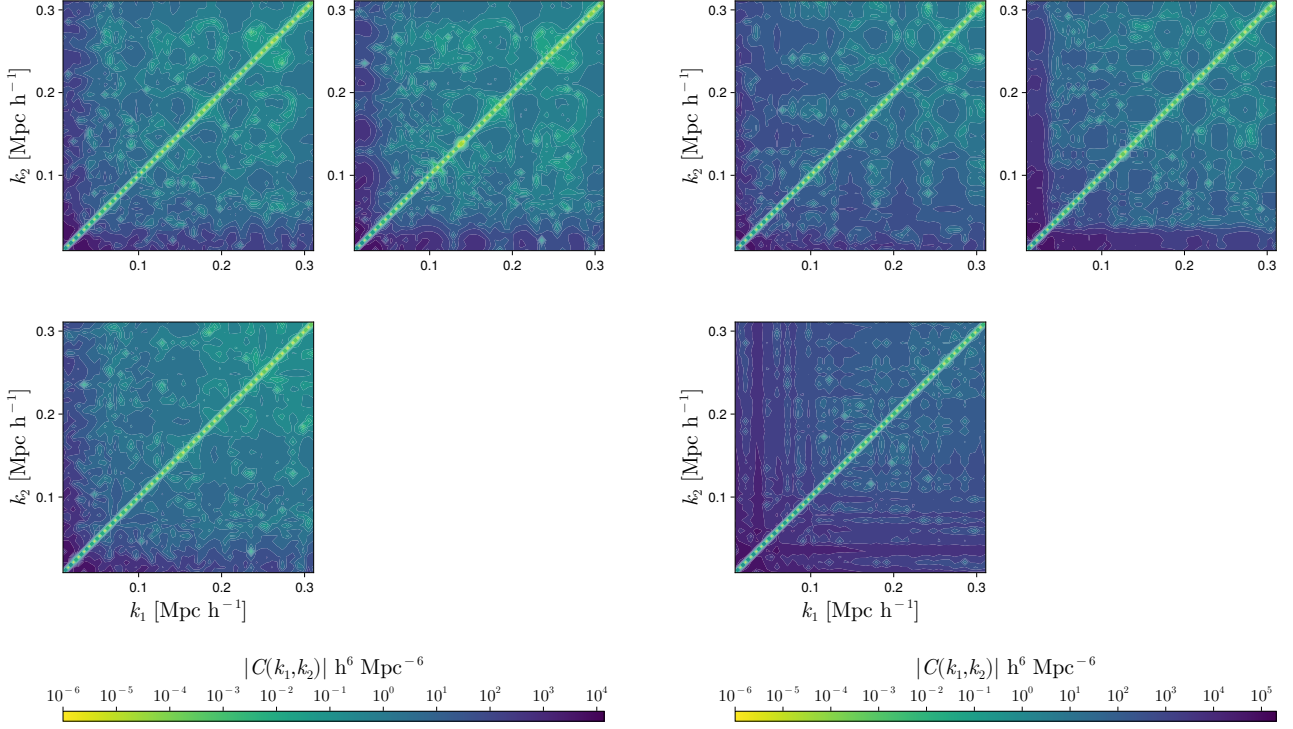


FIG. 24: The asymmetry matrix as given in Eq. (25) for  $\Omega_m$  in the increased parameter case, without SSC corrections (left hand pair of columns) and with them (right hand pair of columns). In both cases, the top left panel shows the value with the full response matrix, the top right panel shows the result with the approximate response matrix, and the bottom panel shows the result with the response matrix set to zero.

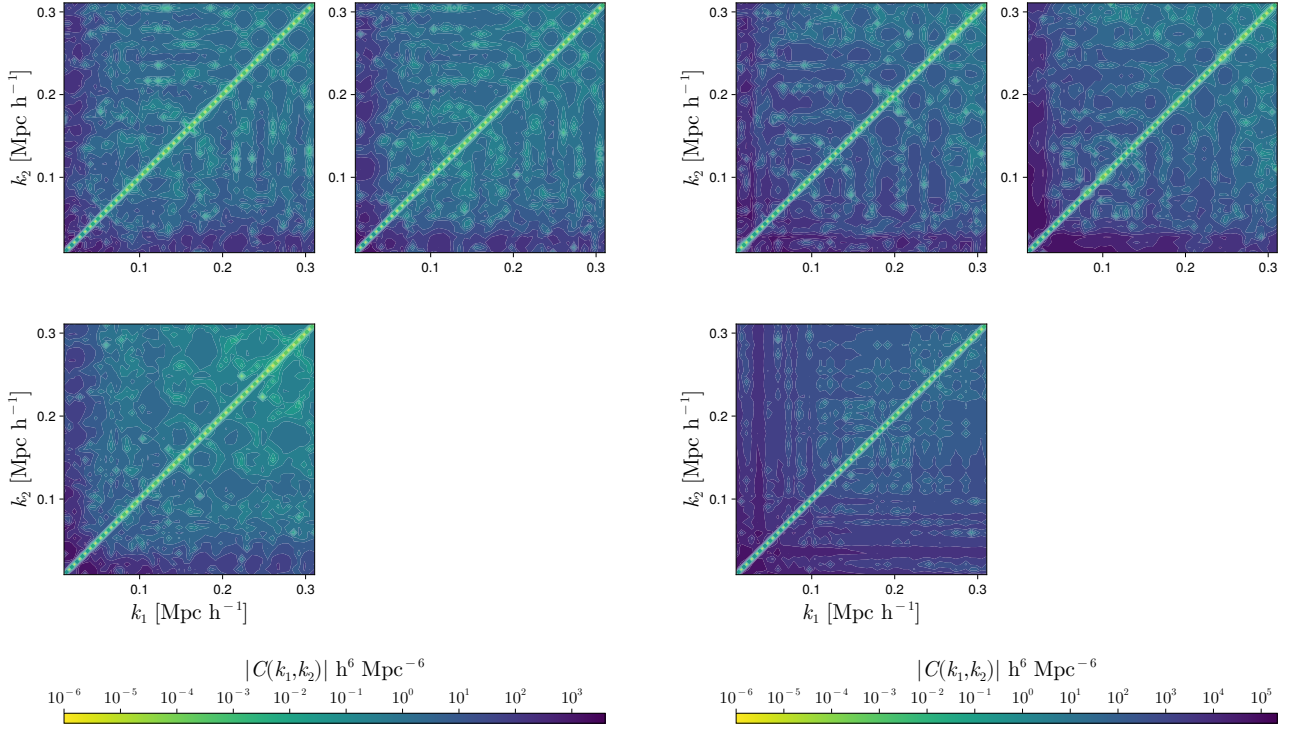


FIG. 25: The asymmetry matrix as given in Eq. (25) for  $\Omega_{\text{bm}}$  in the reduced parameter case, without SSC corrections (left hand pair of columns) and with them (right hand pair of columns). In both cases, the top left panel shows the value with the full response matrix, the top right panel shows the result with the approximate response matrix, and the bottom panel shows the result with the response matrix set to zero.

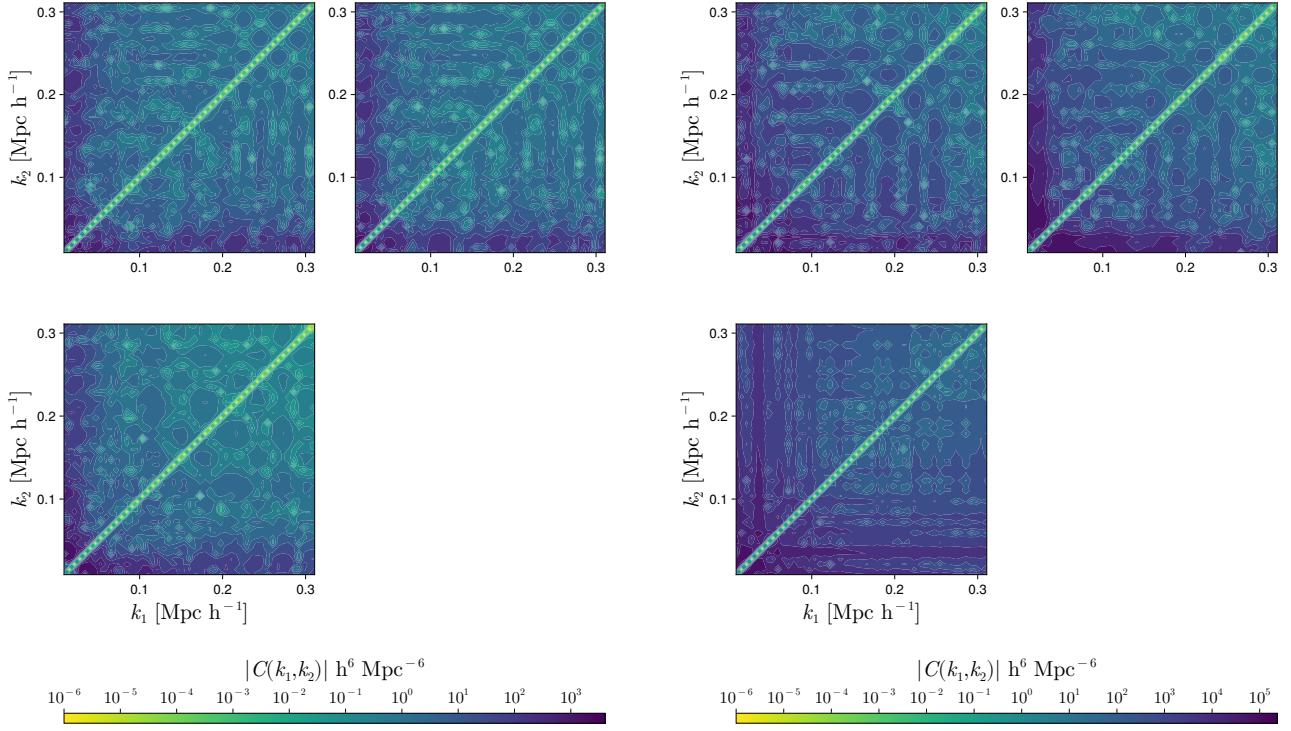


FIG. 26: The asymmetry matrix as given in Eq. (25) for  $\Omega_b$  in the increased parameter case, without SSC corrections (left hand pair of columns) and with them (right hand pair of columns). In both cases, the top left panel shows the value with the full response matrix, the top right panel shows the result with the approximate response matrix, and the bottom panel shows the result with the response matrix set to zero.

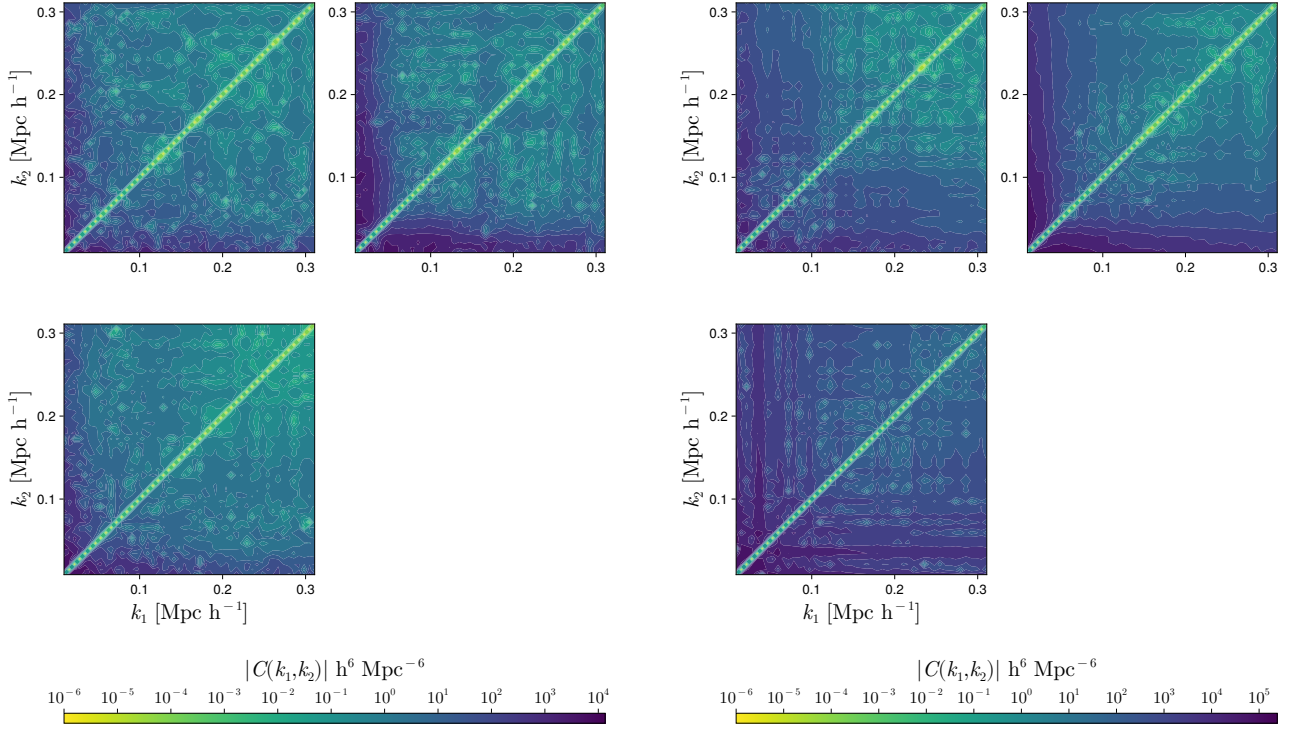


FIG. 27: The asymmetry matrix as given in Eq. (25) for  $n_s$  in the reduced parameter case, without SSC corrections (left hand pair of columns) and with them (right hand pair of columns). In both cases, the top left panel shows the value with the full response matrix, the top right panel shows the result with the approximate response matrix, and the bottom panel shows the result with the response matrix set to zero.

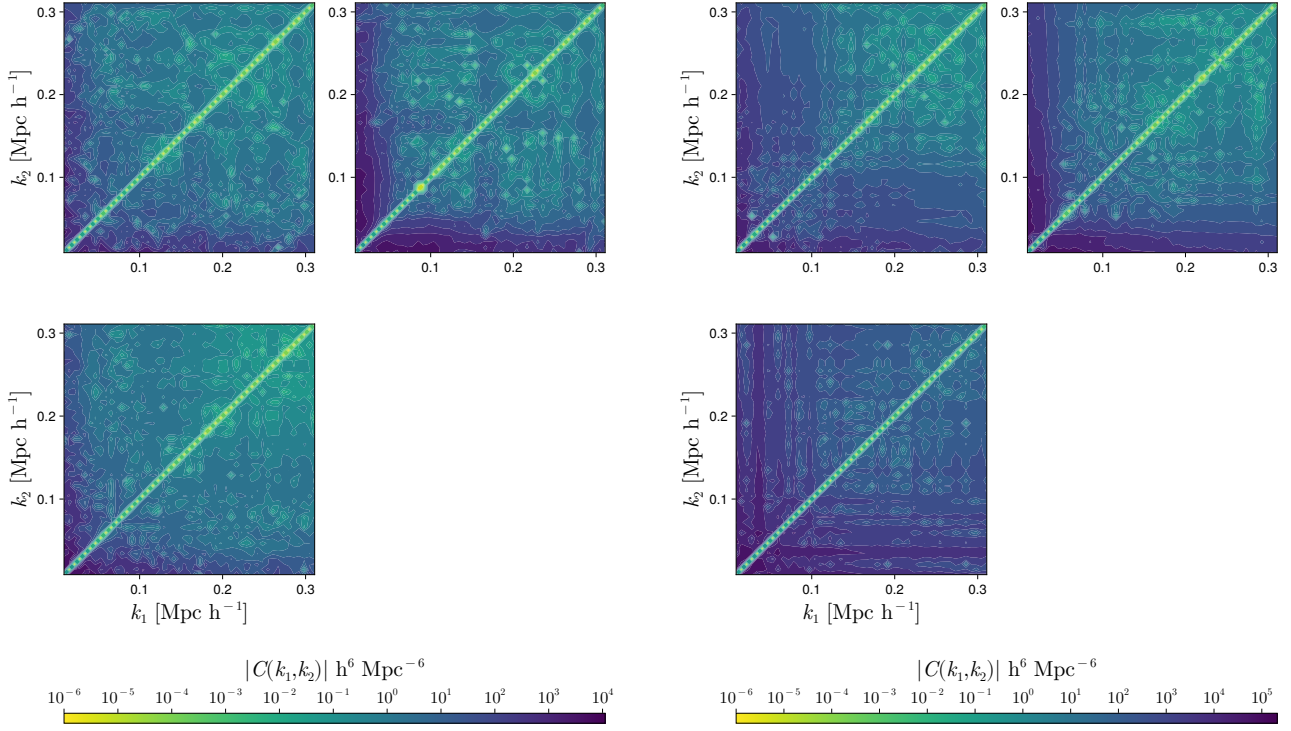


FIG. 28: The asymmetry matrix as given in Eq. (25) for  $n_s$  in the increased parameter case, without SSC corrections (left hand pair of columns) and with them (right hand pair of columns). In both cases, the top left panel shows the value with the full response matrix, the top right panel shows the result with the approximate response matrix, and the bottom panel shows the result with the response matrix set to zero.

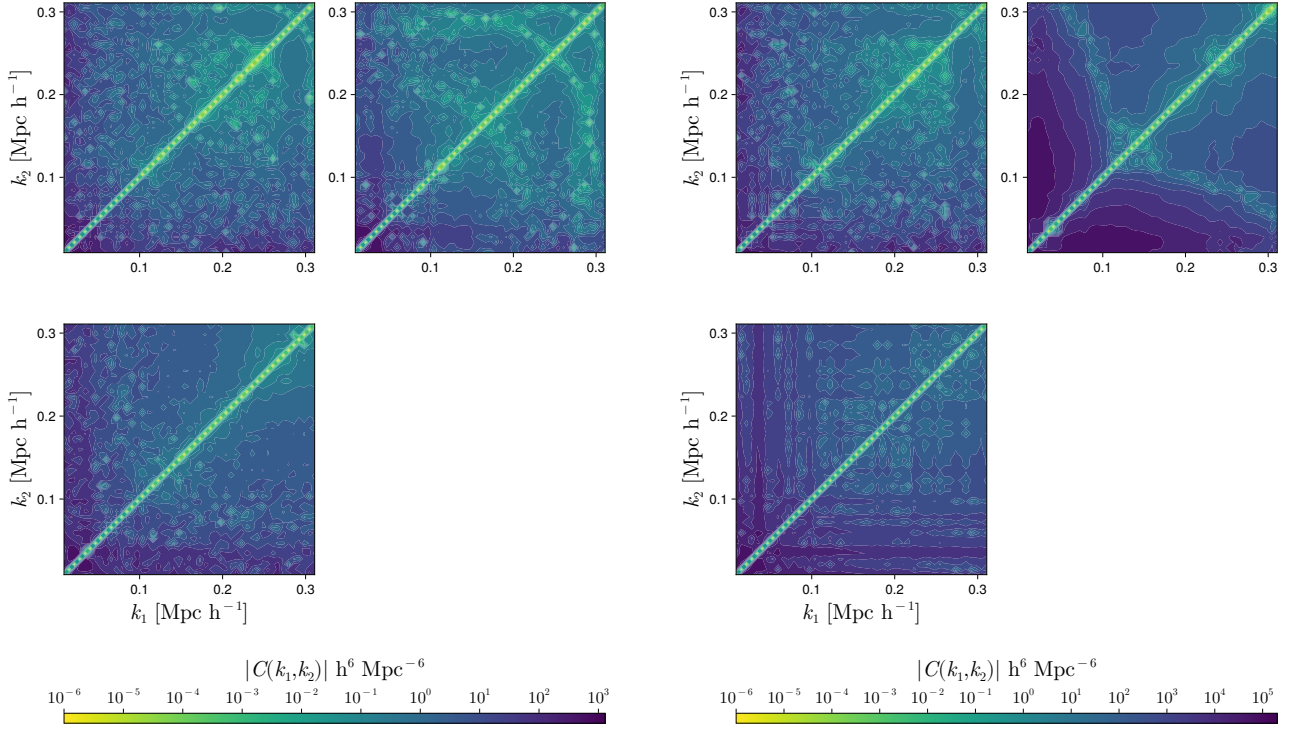


FIG. 29: The asymmetry matrix as given in Eq. (25) for  $\sigma_8$  in the reduced parameter case, without SSC corrections (left hand pair of columns) and with them (right hand pair of columns). In both cases, the top left panel shows the value with the full response matrix, the top right panel shows the result with the approximate response matrix, and the bottom panel shows the result with the response matrix set to zero.

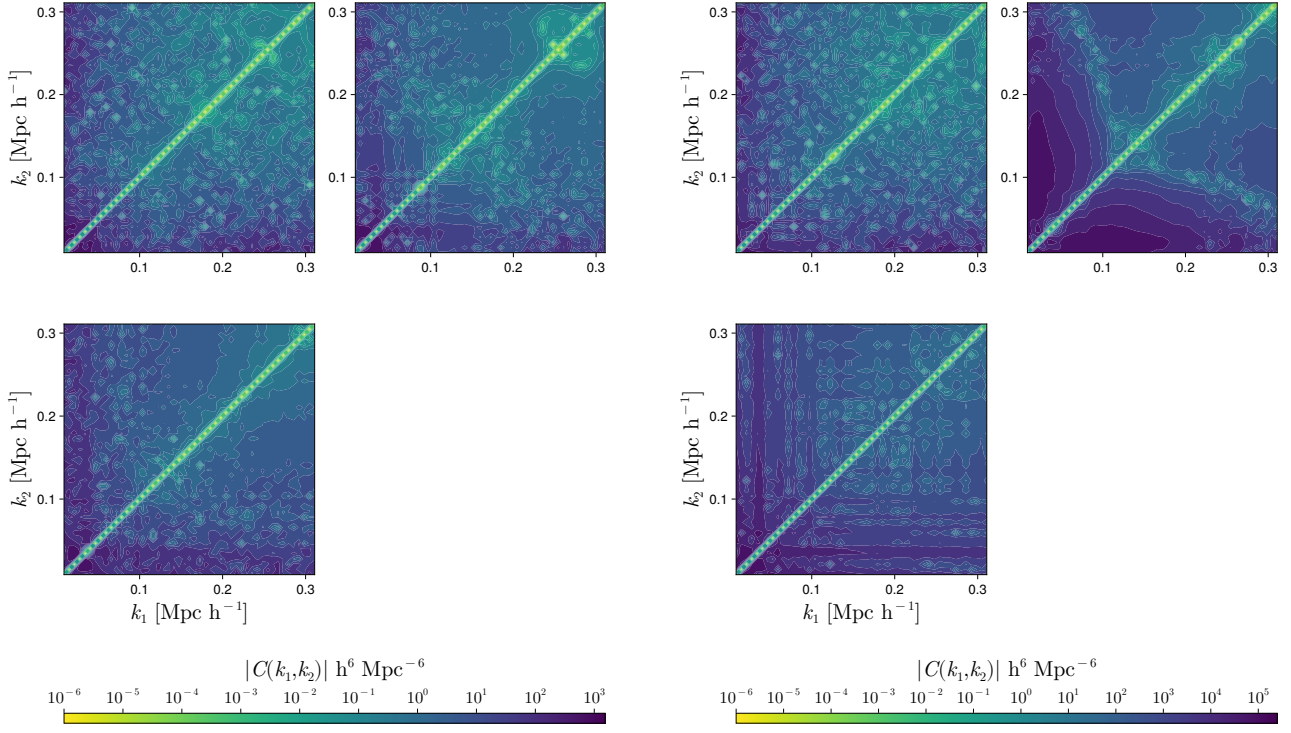


FIG. 30: The asymmetry matrix as given in Eq. (25) for  $\sigma_8$  in the increased parameter case, without SSC corrections (left hand pair of columns) and with them (right hand pair of columns). In both cases, the top left panel shows the value with the full response matrix, the top right panel shows the result with the approximate response matrix, and the bottom panel shows the result with the response matrix set to zero.

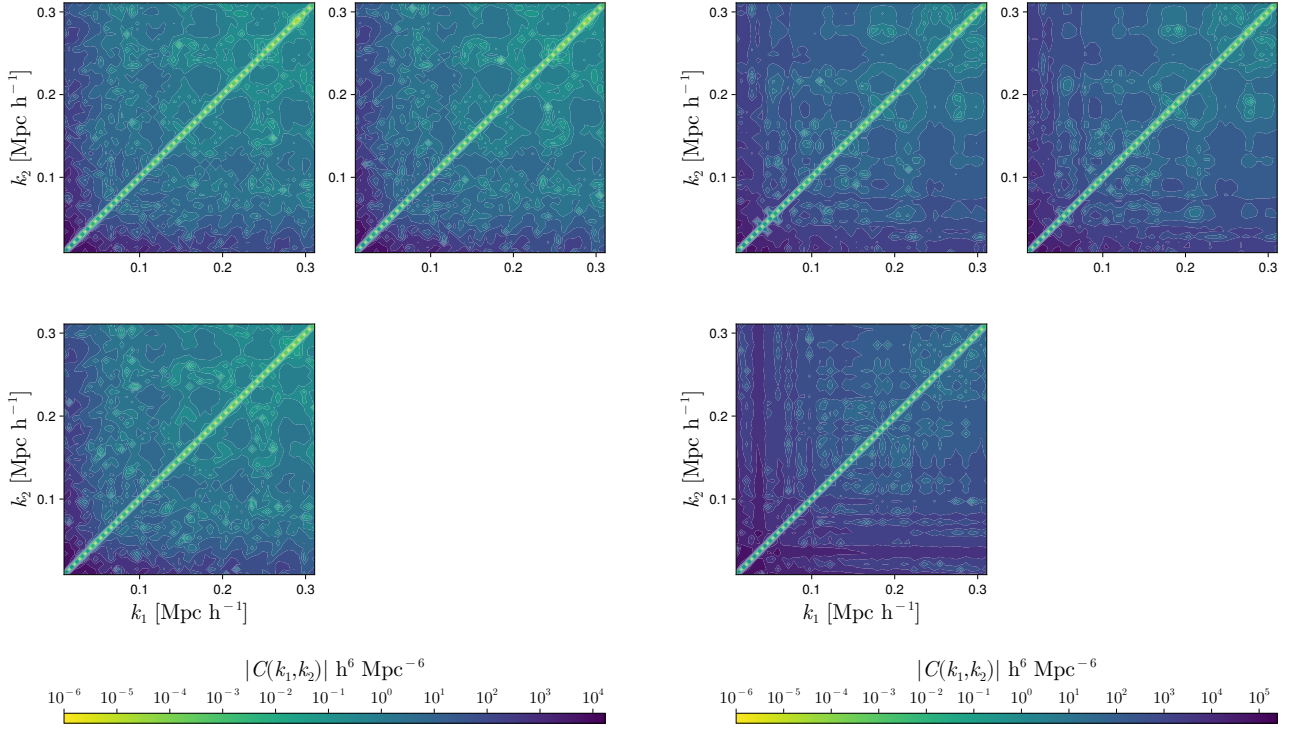


FIG. 31: The asymmetry matrix as given in Eq. (25) for  $h$  in the reduced parameter case, without SSC corrections (left hand pair of columns) and with them (right hand pair of columns). In both cases, the top left panel shows the value with the full response matrix, the top right panel shows the result with the approximate response matrix, and the bottom panel shows the result with the response matrix set to zero.

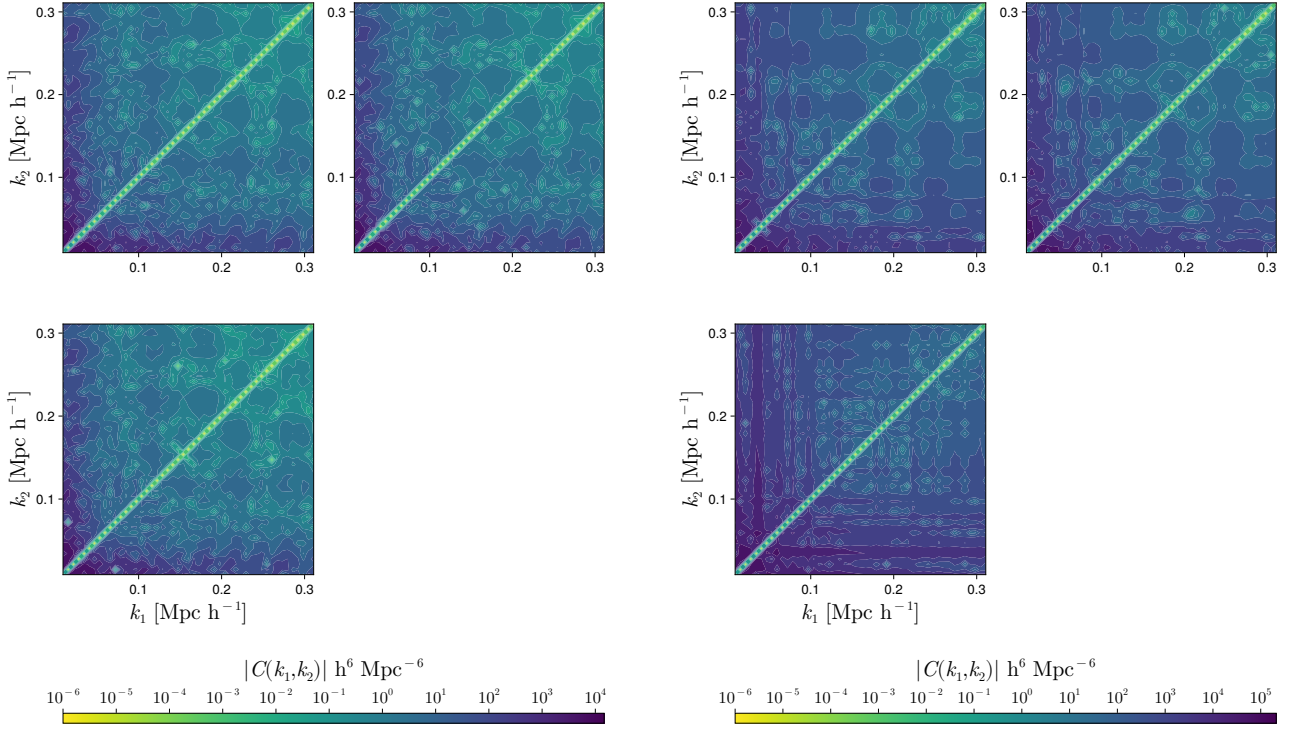


FIG. 32: The asymmetry matrix as given in Eq. (25) for  $h$  in the increased parameter case, without SSC corrections (left hand pair of columns) and with them (right hand pair of columns). In both cases, the top left panel shows the value with the full response matrix, the top right panel shows the result with the approximate response matrix, and the bottom panel shows the result with the response matrix set to zero.

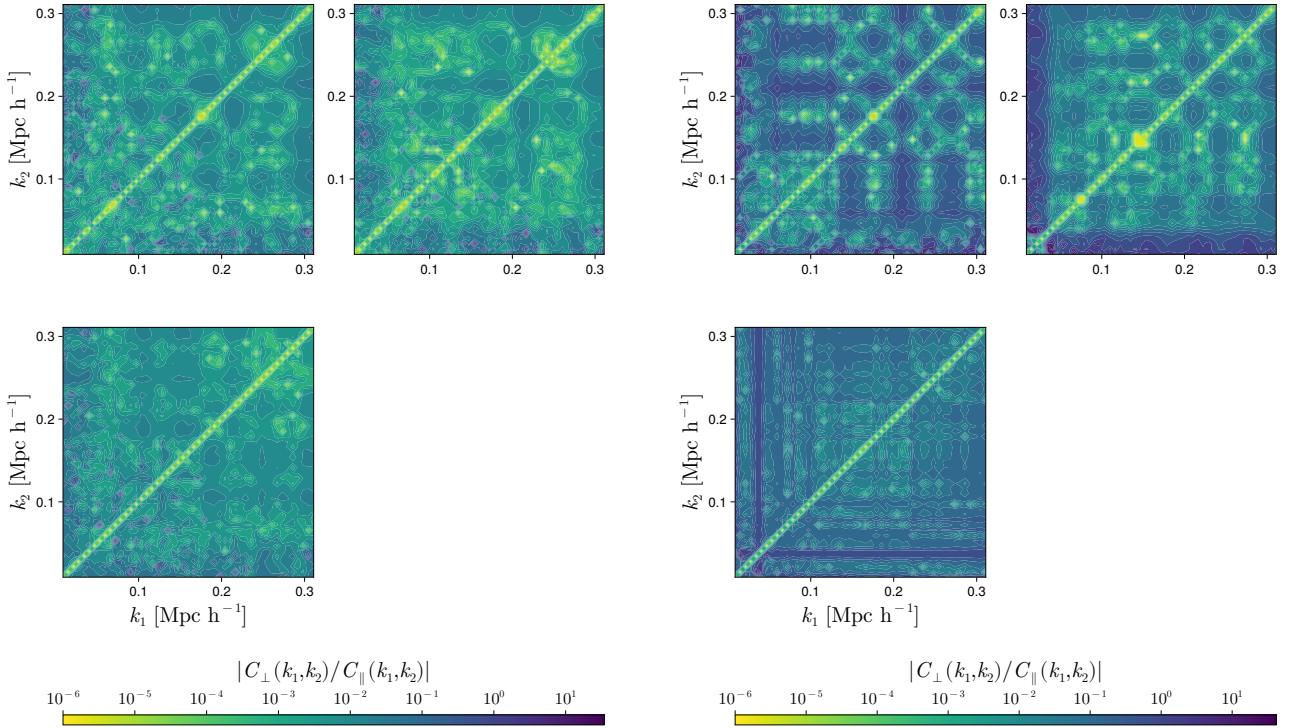
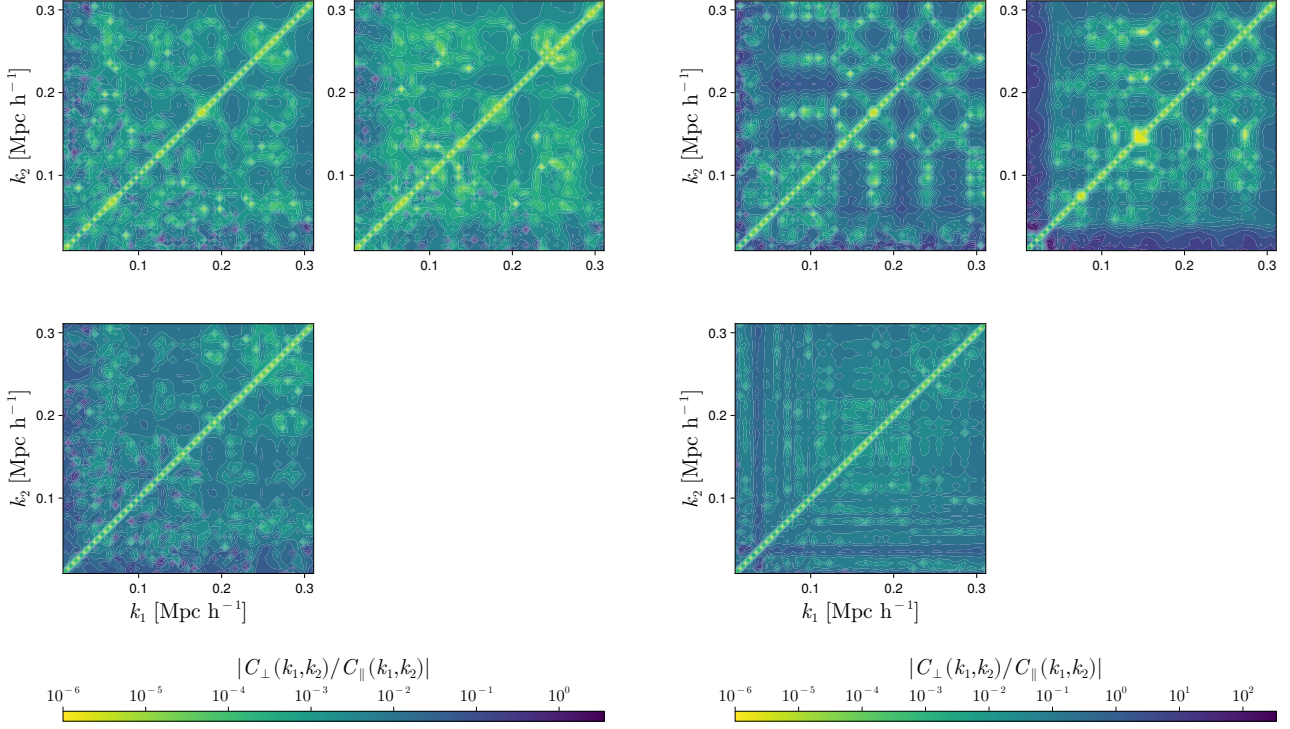
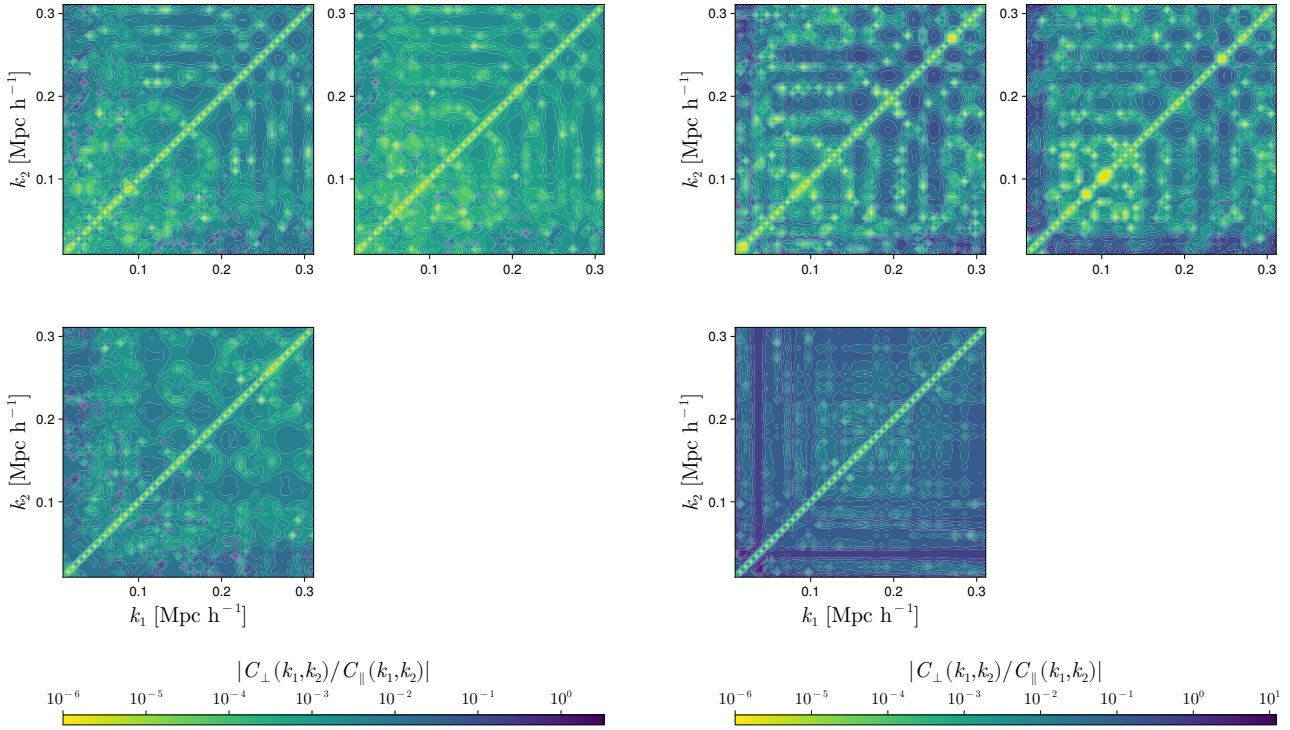


FIG. 33: The elementwise ratios of  $C_{\perp}$  and  $C_{\parallel}$  for the reduced case of  $\Omega_m$ .

FIG. 34: The elementwise ratios of  $C_{\perp}$  and  $C_{\parallel}$  for the increased case of  $\Omega_m$ .FIG. 35: The elementwise ratios of  $C_{\perp}$  and  $C_{\parallel}$  for the reduced case of  $\Omega_m$ .

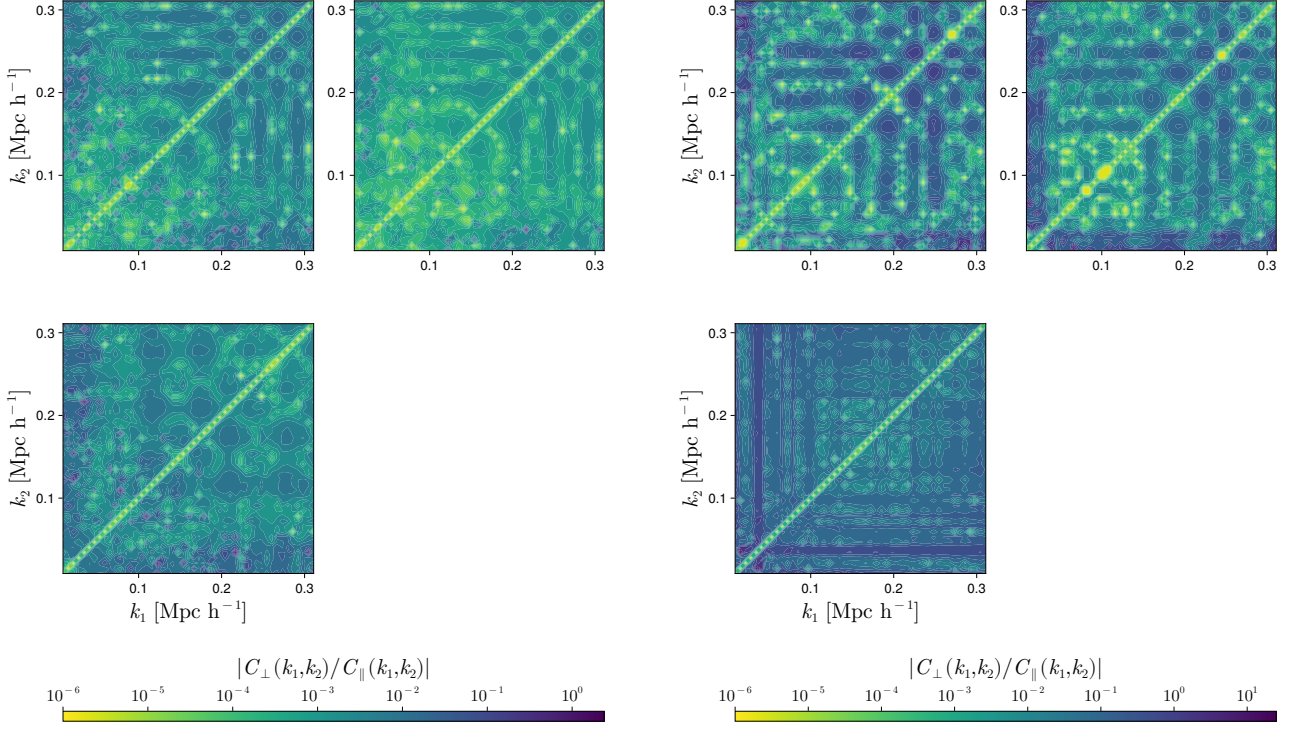


FIG. 36: The elementwise ratios of  $C_{\perp}$  and  $C_{\parallel}$  for the increased case of  $\Omega_b$ .

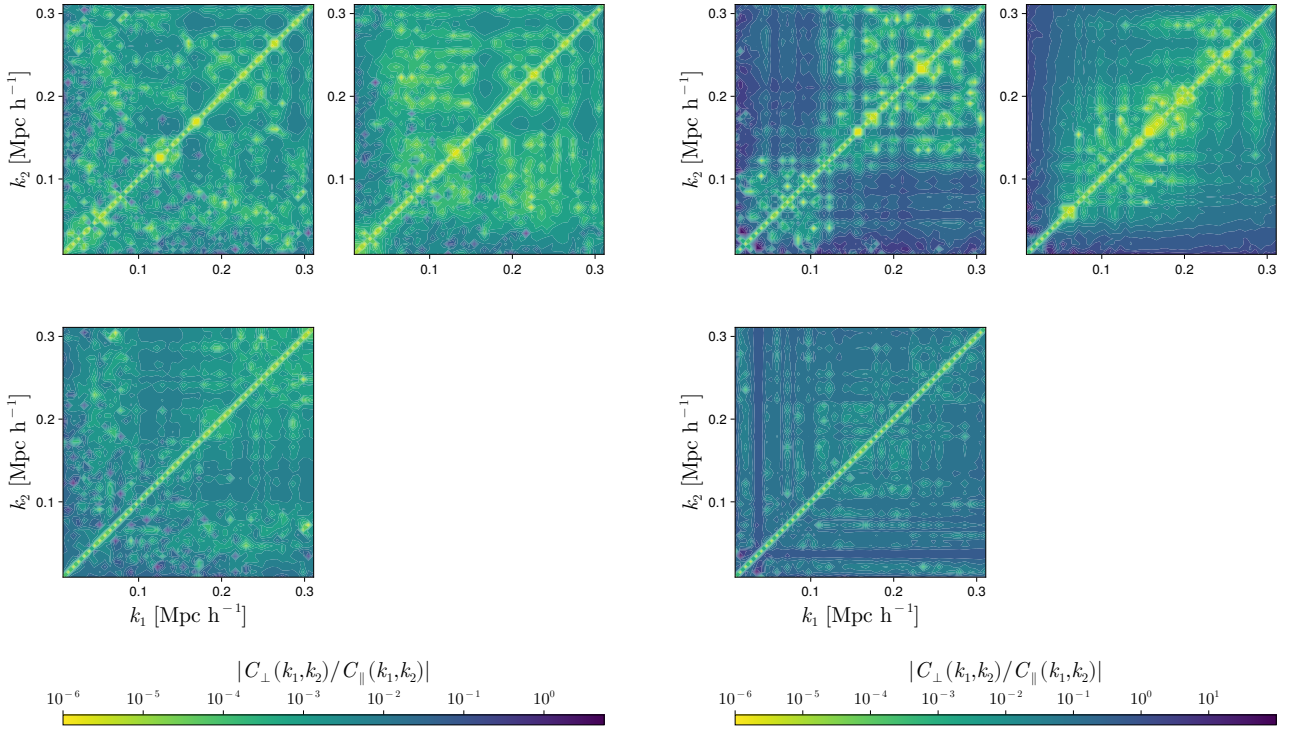
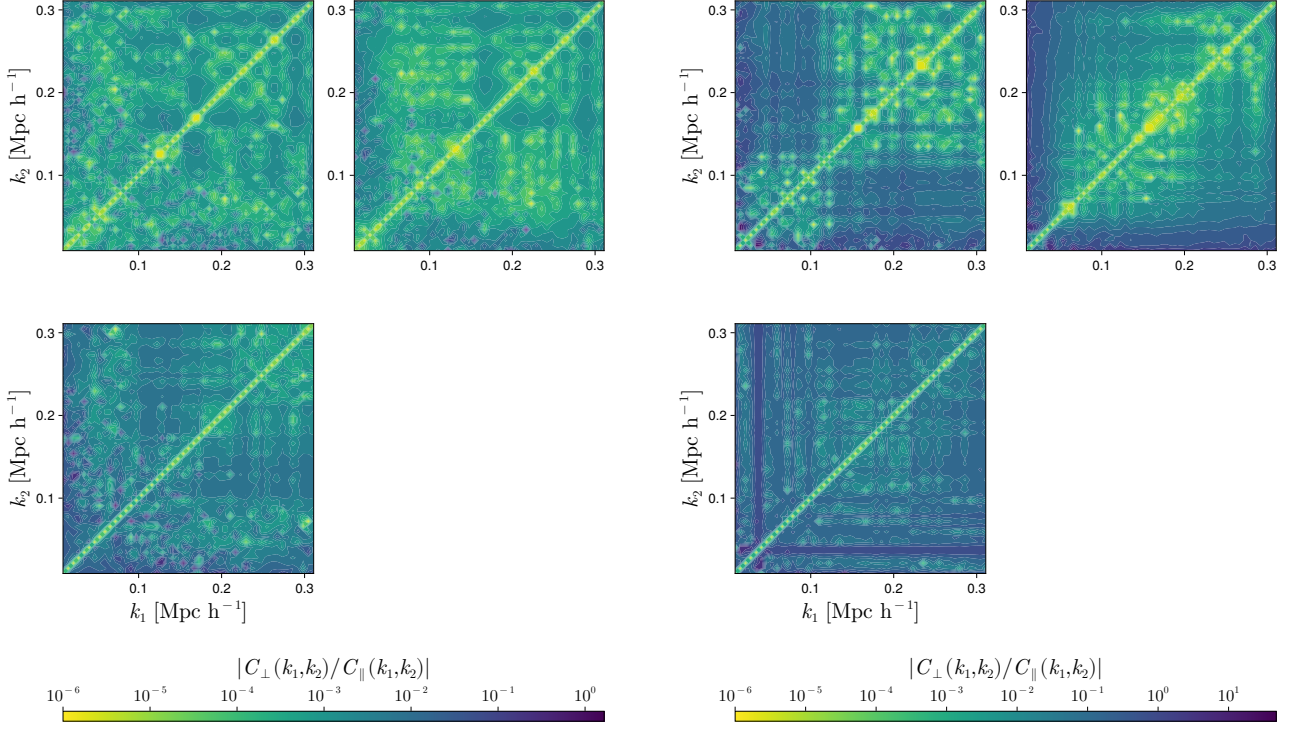
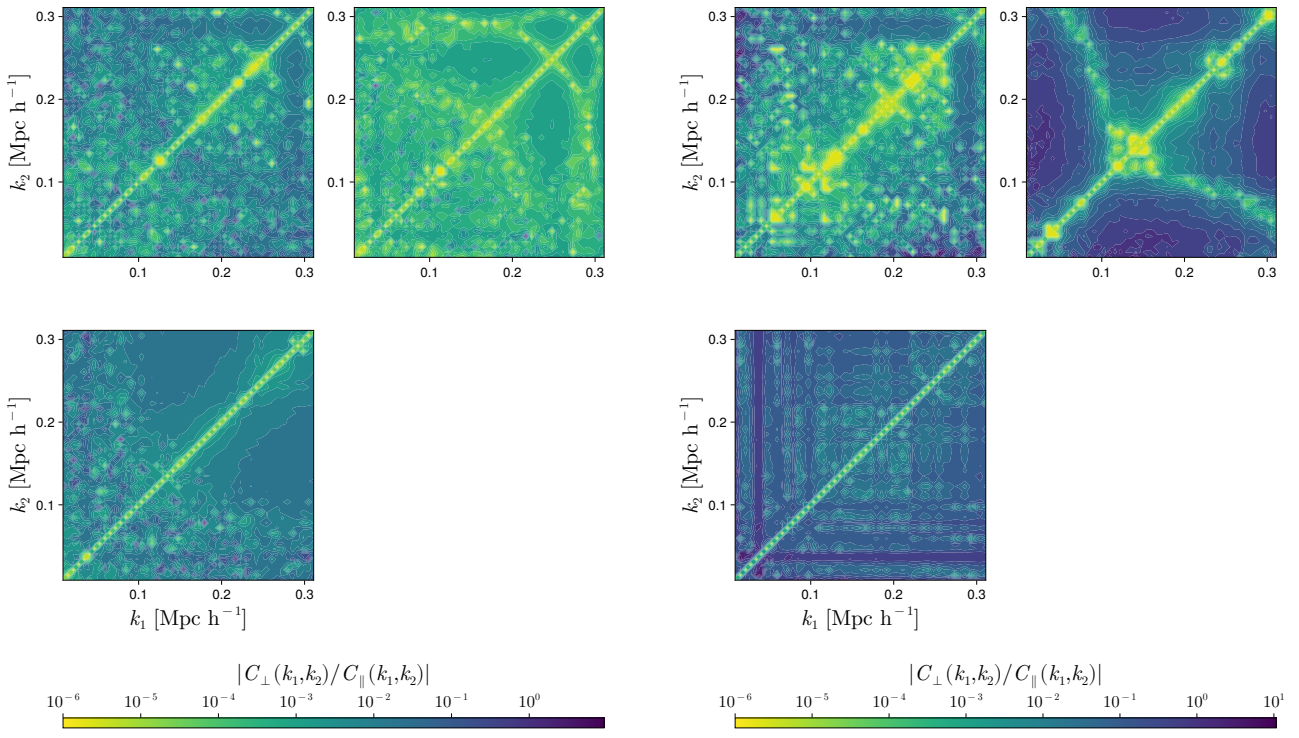
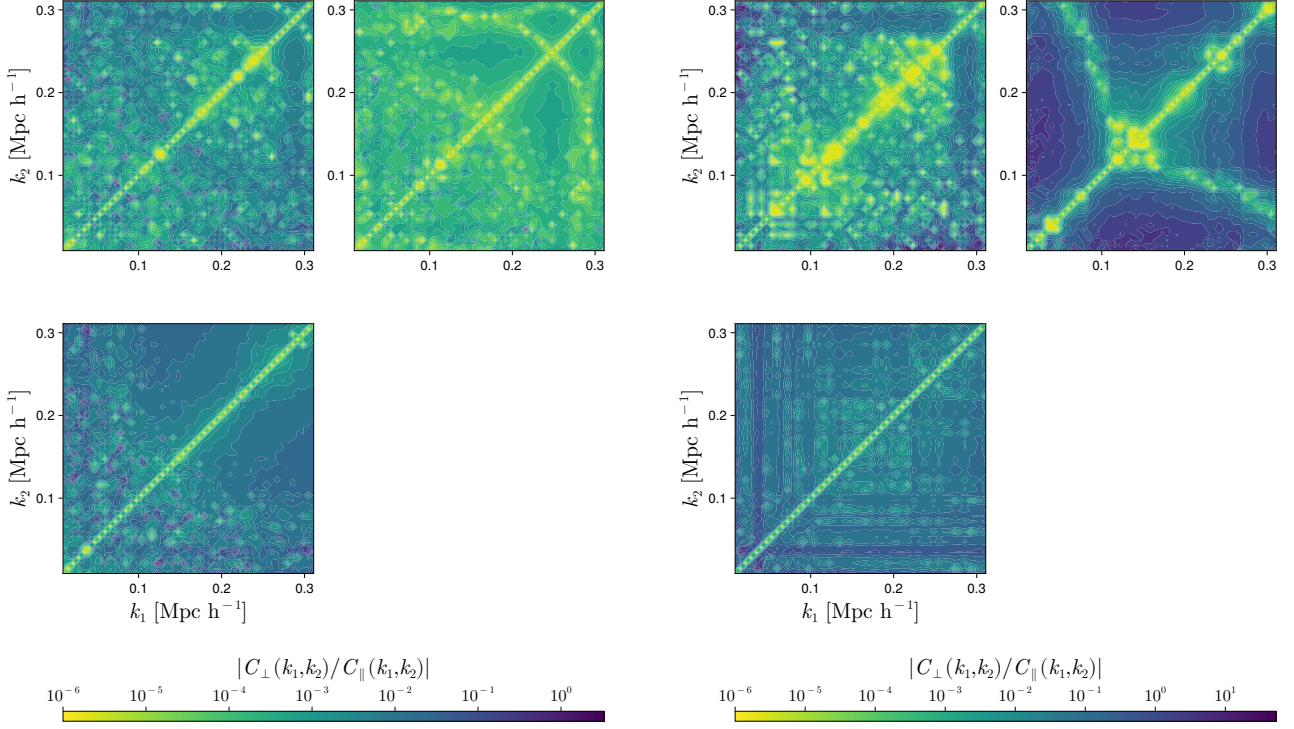
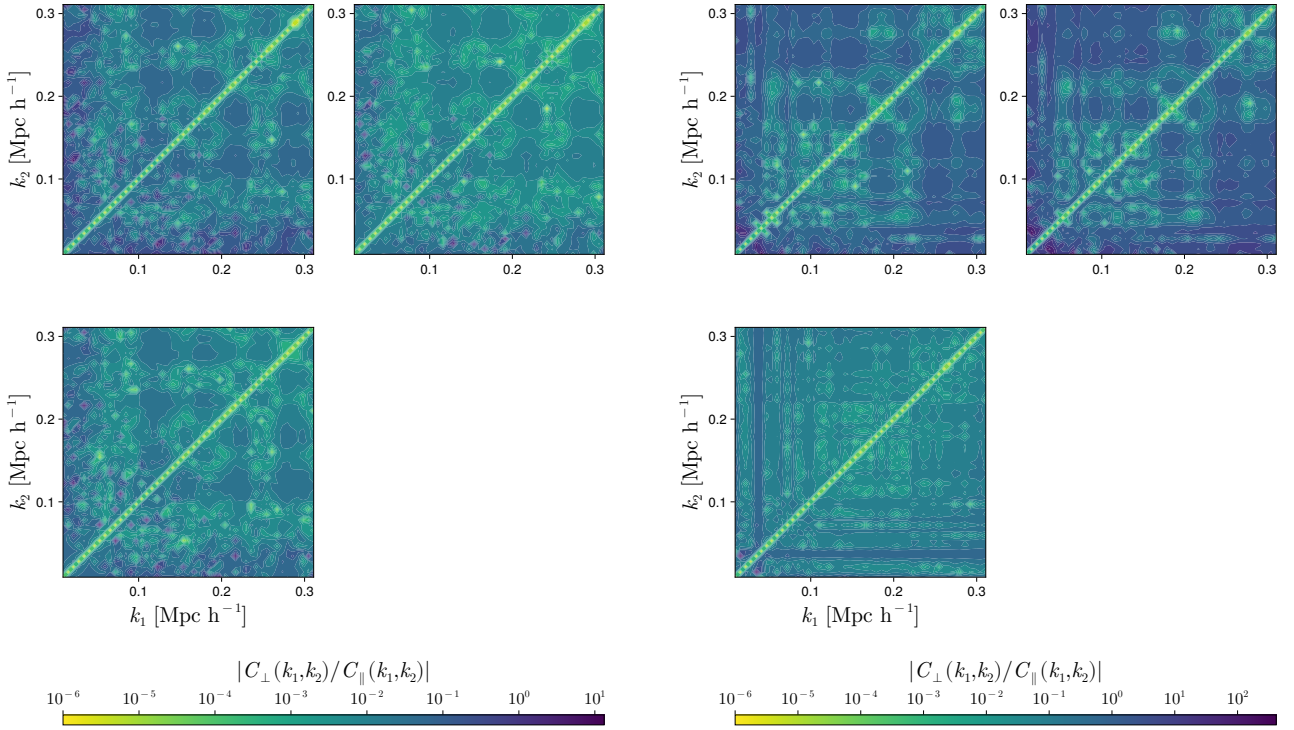


FIG. 37: The elementwise ratios of  $C_{\perp}$  and  $C_{\parallel}$  for the reduced case of  $n_s$ .

FIG. 38: The elementwise ratios of  $C_{\perp}$  and  $C_{\parallel}$  for the increased case of  $n_s$ .FIG. 39: The elementwise ratios of  $C_{\perp}$  and  $C_{\parallel}$  for the reduced case of  $\sigma_8$ .

FIG. 40: The elementwise ratios of  $C_{\perp}$  and  $C_{\parallel}$  for the increased case of  $\sigma_8$ .FIG. 41: The elementwise ratios of  $C_{\perp}$  and  $C_{\parallel}$  for the reduced case of  $h$ .

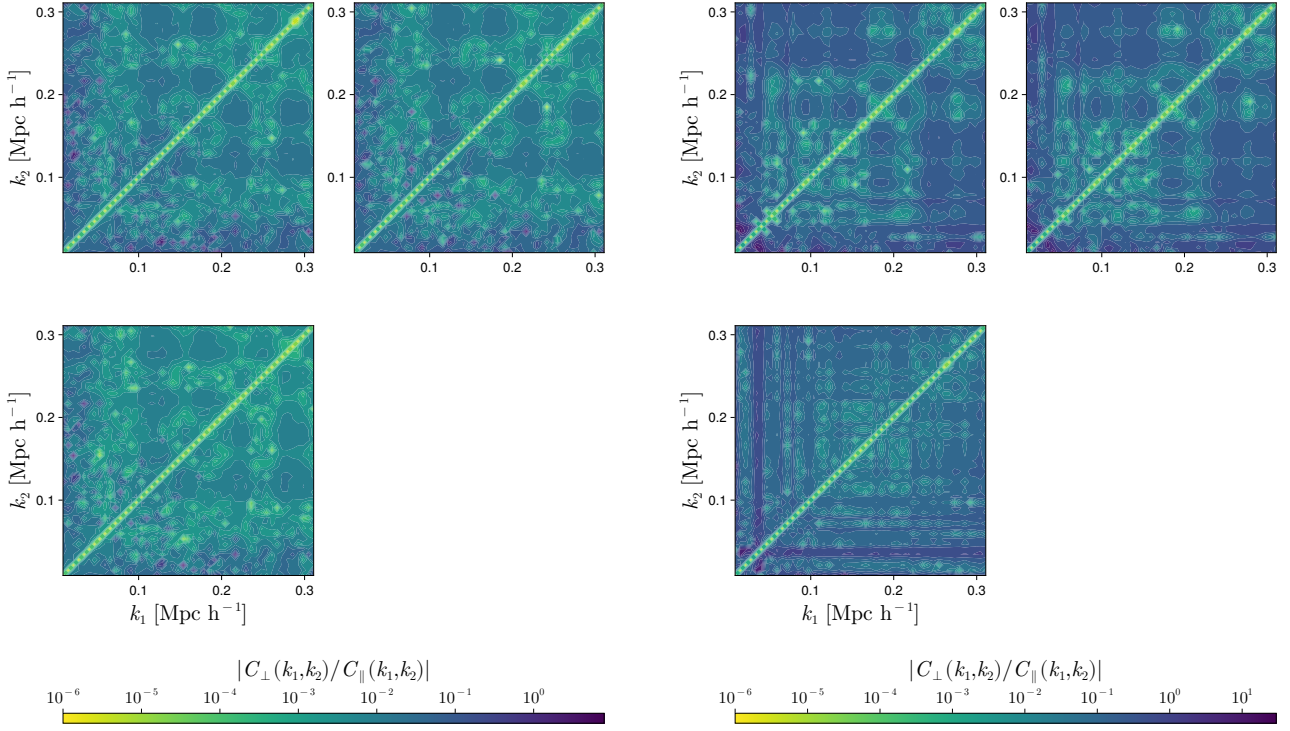


FIG. 42: The elementwise ratios of  $C_{\perp}$  and  $C_{\parallel}$  for the increased case of  $h$ .

### Appendix A: Standard Perturbation Theory

In this appendix, we will briefly review the formalism of SPT.

SPT begins with the assumption that gravitating matter can be treated as a collisionless perfect fluid. This is valid as a description of dark matter but not of baryonic effects, which are accounted for with additional parameters not discussed in this paper, in which a treatment of all matter as purely gravitating was taken. Under this approximation, we can describe matter via the collisionless Boltzmann equation,

$$\frac{Df}{Dt} = \frac{\partial f}{\partial t} + \frac{\mathbf{p}}{ma^2} \cdot \frac{df}{d\mathbf{x}} - m \frac{d\phi}{d\mathbf{x}} \frac{df}{d\mathbf{p}} = 0. \quad (A1)$$

Taking the first two moments of this equation gives us forms for the matter and momentum densities which, inserted back into Eq. (A1), give us our equations of motion for a collisionless perfect fluid:

$$\dot{\rho} + 3H\rho + \frac{1}{a}\partial_i(\rho v^i) = 0, \quad (A2)$$

$$\dot{v}^i + Hv^i + \frac{1}{a}v^j\partial_j v^i + \frac{1}{a}\partial_i\phi = 0. \quad (A3)$$

Defining the density contrast,  $\delta = \rho/\bar{\rho} - 1$ , Eq. (A2) becomes

$$\partial_\eta\delta + \nabla \cdot [(1 + \delta) v^i] = 0 \quad (A4)$$

where the proper time is defined by  $ad\eta = dt$ .

We may now take the derivative of Eq. (A3) and define the velocity divergence field,  $\theta = \partial_i v^i$  to obtain

$$\partial_\eta\theta + \mathcal{H}\theta + v^i\partial_i\theta + \partial_i v^j\partial_j v^i + \delta\phi = 0. \quad (A5)$$

Taking the Fourier transforms of Eqs. (A4) and (A5) gives us

$$\partial_\eta\delta(\mathbf{k}, \eta) + \theta(\mathbf{k}, \eta) = \mathcal{S}_\alpha(\mathbf{k}, \eta), \quad (A6)$$

$$\partial_\eta\theta(\mathbf{k}, \eta) + \mathcal{H}\theta(\mathbf{k}, \eta) + \frac{3}{2}\Omega_m \mathcal{H}^2 \delta(\mathbf{k}, \eta) = \mathcal{S}_\beta(\mathbf{k}, \eta), \quad (A7)$$

where  $\mathcal{S}_\alpha$  and  $\mathcal{S}_\beta$  are the non-linear source terms defined as

$$\mathcal{S}_\alpha(\mathbf{k}, \eta) = - \int \frac{d^3\mathbf{q}}{(2\pi)^3} \alpha(\mathbf{q}, \mathbf{k} - \mathbf{q}) \theta(\mathbf{q}, \eta) \delta(\mathbf{k} - \mathbf{q}, \eta) , \quad (\text{A8})$$

$$\mathcal{S}_\beta(\mathbf{k}, \eta) = - \int \frac{d^3\mathbf{q}}{(2\pi)^3} \beta(\mathbf{q}, \mathbf{k} - \mathbf{q}) \theta(\mathbf{q}, \eta) \theta(\mathbf{k} - \mathbf{q}, \eta) , \quad (\text{A9})$$

where the kernels

$$\alpha(\mathbf{k}_1, \mathbf{k}_2) = \frac{\mathbf{k}_1 \cdot (\mathbf{k}_1 + \mathbf{k}_2)}{k_1^2} , \quad (\text{A10})$$

$$\beta(\mathbf{k}_1, \mathbf{k}_2) = \frac{1}{2} (\mathbf{k}_1 + \mathbf{k}_2)^2 \frac{\mathbf{k}_1 \cdot \mathbf{k}_2}{k_1^2 k_2^2} \quad (\text{A11})$$

capture the coupling between modes of different wavelengths.

We now assume the separability of space and time components,  $\delta_n(\mathbf{k}, a) = D_n(a) \delta_n(\mathbf{k})$ , where we have reparametrised time in terms of the comoving distance. In the simple example of an EdS cosmology, we would have  $D_n(a) = a^n$ , making it a commonly used model for approximate calculations, while growth factors for other cosmologies must be derived order by order.

We may now solve our equations of motion using a power series, yielding the following expression for the  $n$ th order Fourier space density field in terms of the linear field:

$$\delta_n(\mathbf{k}) = \int_{\mathbf{q}_1} \dots \int_{\mathbf{q}_n} \delta^D \left( \mathbf{k} - \sum_{i=1}^n \mathbf{q}_i \right) F_n(\mathbf{q}_1, \dots, \mathbf{q}_n) \prod_{i=1}^n \delta_1(\mathbf{q}_i) , \quad (\text{A12})$$

where  $\int_{\mathbf{q}} = \int \frac{d^3\mathbf{q}}{(2\pi)^3}$  and the gravitational coupling kernels are given by

$$F_n(\mathbf{k}_1, \dots, \mathbf{k}_n) = \sum_{m=1}^{n-1} \frac{G_m(\mathbf{k}_1, \dots, \mathbf{k}_m)}{(2n+3)(n-1)} \left[ (2n+1) \alpha(\kappa_1^m, \kappa_{m+1}^n) F_{n-m}(\mathbf{k}_{m+1}, \dots, \mathbf{k}_n) \right. \quad (\text{A13})$$

$$\left. + 2\beta(\kappa_1^m, \kappa_{m+1}^n) G_{n-m}(\mathbf{k}_{m+1}, \dots, \mathbf{q}_n) \right] , \quad (\text{A14})$$

$$G_n(\mathbf{k}_1, \dots, \mathbf{k}_n) = \sum_{m=1}^{n-1} \frac{G_m(\mathbf{k}_1, \dots, \mathbf{k}_m)}{(2n+3)(n-1)} \left[ 3\alpha(\kappa_1^m, \kappa_{m+1}^n) F_{n-m}(\mathbf{k}_{m+1}, \dots, \mathbf{k}_n) \right] \quad (\text{A15})$$

$$\left. + 2n\beta(\kappa_1^m, \kappa_{m+1}^n) G_{n-m}(\mathbf{k}_{m+1}, \dots, \mathbf{q}_n) \right] , \quad (\text{A16})$$

where  $\kappa_i^j = \sum_{l=1}^j \mathbf{k}_l$  and we in general use the symmetrised forms for these kernels,  $F_n^s$  and  $G_n^s$ .

These perturbative density fields are used to build correlators in momentum space at various orders, which can be represented using a Feynman diagram notation in which loops represent couplings between large scale modes and those of arbitrarily small scales. Thus, we generally refer to the leading order perturbative contributions to correlators as tree-level and higher order contributions as  $n$ -loop terms. Furthermore, we note that when constructing estimators for covariance matrices from SPT correlation functions, we maintain a consistent sum of the orders of all density fields across all correlators. So, when employing a power spectrum (two-point correlator) up to two-loops, where we correlate fields whose orders sum to 6, we will use for the same covariance matrix the one-loop bispectrum (three-point correlator) and tree-level trispectrum (four-point correlator), as these also correlate fields whose orders sum to 6.

## 1. The Power Spectrum

From these power ordered density fields, we can construct correlation functions which relate the probability of finding a perturbation of one form a given distance in momentum space from perturbations of another. The second order correlation function in Fourier space is called the power spectrum and is defined as  $(2\pi)^3 \delta^D(k_1 + k_2) P_{ij}(k_1, k_2) \equiv \langle \delta_i(k_1) \delta_j(k_2) \rangle$  where we note that, due to cosmic symmetries, the power spectrum is dependent only upon the magnitude of its momentum vectors.

The linear power spectrum,  $P_{11}$ , correlates two linear density fields and is the only tree-level power spectrum term. The one-loop contributions to the power spectrum are

$$P_{31}(k) = 3P_{11}(k) \int_{\mathbf{q}} F_3^s(\mathbf{k}, \mathbf{q}, -\mathbf{q}) P_{11}(q) , \quad (\text{A17})$$

$$P_{22}(k) = 2 \int_{\mathbf{q}} F_2^s(\mathbf{k} - \mathbf{q}, \mathbf{q})^2 P_{11}(|\mathbf{k} - \mathbf{q}|) P_{11}(q) \quad (\text{A18})$$

and the two-loop contributions are

$$P_{51}(k) = 30P_{11}(k) \int_{\mathbf{q}_1} \int_{\mathbf{q}_2} F_5^s(\mathbf{k}, \mathbf{q}_1, -\mathbf{q}_1, \mathbf{q}_2, -\mathbf{q}_2) P_{11}(q_1) P_{11}(q_2) , \quad (\text{A19})$$

$$P_{42}(k) = 24 \int_{\mathbf{q}_1} \int_{\mathbf{q}_2} F_4^s(\mathbf{q}_1 - \mathbf{k}, -\mathbf{q}_1, \mathbf{q}_2, -\mathbf{q}_2) F_2^s(\mathbf{k} - \mathbf{q}_1, \mathbf{q}_1) P_{11}(|\mathbf{k} - \mathbf{q}|) P_{11}(q_1) P_{11}(q_2) P_{11}(|\mathbf{k} - \mathbf{q}_1|) \quad (\text{A20})$$

$$P_{33,a}(k) = 6 \int_{\mathbf{q}_1} \int_{\mathbf{q}_2} F_3^s(\mathbf{q}_1, \mathbf{q}_2, \mathbf{k} - \mathbf{q}_1 - \mathbf{q}_2) F_3^s(-\mathbf{q}_1, -\mathbf{q}_2, -\mathbf{k} + \mathbf{q}_1 + \mathbf{q}_2) P_{11}(q_1) P_{11}(q_2) P_{11}(|\mathbf{k} - \mathbf{q}_1 - \mathbf{q}_2|) , \quad (\text{A21})$$

and  $P_{33,b} = P_{31}^2 / P_{11}$ .

The above terms can be summed to give an approximation of the non-linear power spectrum that would be measured in simulations, as  $P_{nn} \approx P_{11} + P_{31} + P_{22} + P_{51} + P_{42} + P_{33,a} + P_{33,b}$ .

## 2. The Bispectrum

The bispectrum is the Fourier space correlation function of three fields [37], defined as  $(2\pi)^3 \delta^D(\mathbf{k}_1 + \mathbf{k}_2 + \mathbf{k}_3) B_{ijl}(\mathbf{k}_1, \mathbf{k}_2, \mathbf{k}_3) = \langle \delta_i(\mathbf{k}_1) \delta_j(\mathbf{k}_2) \delta_l(\mathbf{k}_3) \rangle$ . At tree level, we have

$$B_{211} = 2F_2^s(\mathbf{k}_2, \mathbf{k}_3) P_{11}(k_2), P_{11}(k_3) \quad (\text{A22})$$

and at one-loop, the contributions are

$$B_{411} = 12 \int_{\mathbf{q}} F_4^s(-\mathbf{k}_2, -\mathbf{k}_3, \mathbf{q}, -\mathbf{q}) P_{11}(k_2) P_{11}(k_3) P_{11}(q) , \quad (\text{A23})$$

$$B_{321,a} = 6 \int_{\mathbf{q}} F_3^s(-\mathbf{k}_3, -\mathbf{q}, \mathbf{q} - \mathbf{k}_2) F_2^s(\mathbf{q}, \mathbf{k}_2 - \mathbf{q}) P_{11}(|\mathbf{k}_2 + \mathbf{q}|) P_{11}(k_3) P_{11}(q) , \quad (\text{A24})$$

$$B_{321,b} = 6 \int_{\mathbf{q}} F_3^s(\mathbf{q}, -\mathbf{q}, \mathbf{k}_3) F_2^s(\mathbf{k}_2, \mathbf{k}_3) P_{11}(k_2) P_{11}(k_3) P_{11}(q) , \quad (\text{A25})$$

$$B_{222} = 8 \int_{\mathbf{q}} F_2^s(-\mathbf{q}, \mathbf{k}_3 + \mathbf{q}) F_2^s(\mathbf{k}_3 + \mathbf{q}, \mathbf{k}_2 - \mathbf{q}) F_2^s(\mathbf{k}_2 - \mathbf{q}, \mathbf{q}) P_{11}(|\mathbf{k}_2 - \mathbf{q}|) P_{11}(|\mathbf{k}_3 - \mathbf{q}|) P_{11}(q) . \quad (\text{A26})$$

These sum to give an approximation of the non-linear bispectrum:  $B_{nnn} \approx B_{211} + B_{411} + B_{321} + B_{222}$ . Bispectra must obey the triangle condition that  $\mathbf{k}_1 + \mathbf{k}_2 + \mathbf{k}_3 = 0$ , such that we only need to explicitly specify two momentum vectors in order to be able to fully fit the function.

## 3. The Trispectrum

The trispectrum is the four-point Fourier space correlator [38],  $(2\pi)^3 \delta^D(\mathbf{k}_1 + \mathbf{k}_2 + \mathbf{k}_3 + \mathbf{k}_4) T_{ijlm}(\mathbf{k}_1, \mathbf{k}_2, \mathbf{k}_3, \mathbf{k}_4) = \langle \delta_i(\mathbf{k}_1) \delta_j(\mathbf{k}_2) \delta_l(\mathbf{k}_3) \delta_m(\mathbf{k}_4) \rangle$ . The tree-level contributions are given by

$$T_{3111} = 6F_3^s(\mathbf{k}_2, \mathbf{k}_3, \mathbf{k}_4) P_{11}(k_2) P_{11}(k_3) P_{11}(k_4) , \quad (\text{A27})$$

$$T_{2211} = 4F_2^s(\mathbf{k}_4, -\mathbf{k}_3 - \mathbf{k}_4) F_2^s(\mathbf{k}_2, \mathbf{k}_3 + \mathbf{k}_4) P_{11}(k_2) P_{11}(k_3) P_{11}(|\mathbf{k}_3 + \mathbf{k}_4|) , \quad (\text{A28})$$

which sum to give a first order approximation of the non-linear trispectrum:  $T_{nnnn} \approx T_{3111} + T_{2211}$ .

In general cases, trispectra can occupy a wide range of configurations as all four external momentum vectors can vary freely. However, in the case of the covariance matrix of the power spectrum, we are only interested in trispectra with  $\mathbf{k}_3 = -\mathbf{k}_1$  and  $\mathbf{k}_4 = -\mathbf{k}_2$ , simplifying calculations substantially.

## Appendix B: Simulation Parameters

For this work, we used the publicly available QUIJOTE simulation results. In these simulations,  $\omega = -1$ ,  $M_\nu = 0$ , and  $\Omega_k = 0$ , while the following parameters were permuted; in the fiducial case, every parameter has its central value, while a separate pair of simulations for each parameter ran with that parameter in its higher and lower value while keeping the other parameters fixed at their fiducial values:

$$\begin{aligned}\Omega_m &\in \{0.3075, 0.3175, 0.3275\} \\ \Omega_b &\in \{0.047, 0.049, 0.051\} \\ n_s &\in \{0.9424, 0.9624, 0.9824\} \\ \sigma_8 &\in \{0.819, 0.834, 0.849\} \\ h &\in \{0.6511, 0.6711, 0.6911\}\end{aligned}$$

## Appendix C: Response Matrices

In this appendix, we collect the full and approximate response and reduced response matrices for all of our cosmological permutations.

## Appendix D: Reconstructed Matrix Accuracy

In this appendix we compile the ratios of the norms of each of our perpendicular and parallel matrices:  $|C_\perp|/|C_\parallel|$ . All results are shown in Table I. As can be seen, the reconstructed matrices show good accuracy by achieving multiple orders of magnitude greater norms than the accuracy test matrices, which would in a perfect case be zero. In all cases except that of  $h$ , the reconstructions with  $R_0$  yielded less accurate results than those with a response matrix. This indicates that the response matrix is generally an accurate tool for the study of cosmological parameter variations but that due to numerical instabilities the response matrix for  $h$  actually decreased the accuracy of the model compared to setting it to zero.

Cosmology	Full	Approx	$R_0$	Full SSC	Approx SSC	$R_0$ SSC
$\Omega_m^-$	$2.586 \times 10^{-5}$	$2.953 \times 10^{-5}$	$1.33 \times 10^{-3}$	$2.647 \times 10^{-5}$	$8.707 \times 10^{-5}$	$2.199 \times 10^{-2}$
$\Omega_m^+$	$5.464 \times 10^{-5}$	$6.096 \times 10^{-5}$	$1.345 \times 10^{-3}$	$5.816 \times 10^{-5}$	$1.011 \times 10^{-4}$	$2.265 \times 10^{-2}$
$\Omega_b^-$	$7.032 \times 10^{-6}$	$8.397 \times 10^{-6}$	$3.543 \times 10^{-4}$	$5.455 \times 10^{-6}$	$1.347 \times 10^{-5}$	$2.241 \times 10^{-2}$
$\Omega_b^+$	$6.89 \times 10^{-6}$	$8.135 \times 10^{-6}$	$3.423 \times 10^{-4}$	$5.374 \times 10^{-6}$	$1.34 \times 10^{-5}$	$2.215 \times 10^{-2}$
$n_s^-$	$1.028 \times 10^{-5}$	$8.920 \times 10^{-6}$	$8.83 \times 10^{-4}$	$1.933 \times 10^{-5}$	$3.82 \times 10^{-5}$	$2.216 \times 10^{-2}$
$n_s^+$	$7.944 \times 10^{-6}$	$9.436 \times 10^{-6}$	$9.164 \times 10^{-4}$	$1.89 \times 10^{-5}$	$3.686 \times 10^{-5}$	$2.243 \times 10^{-2}$
$\sigma_8^-$	$4.236 \times 10^{-6}$	$5.231 \times 10^{-6}$	$1.309 \times 10^{-4}$	$3.165 \times 10^{-6}$	$8.335 \times 10^{-6}$	$2.14 \times 10^{-2}$
$\sigma_8^+$	$4.747 \times 10^{-6}$	$5.878 \times 10^{-6}$	$1.347 \times 10^{-4}$	$3.636 \times 10^{-6}$	$8.484 \times 10^{-6}$	$2.318 \times 10^{-2}$
$h^-$	$1.198 \times 10^{-3}$	$1.192 \times 10^{-3}$	$8.603 \times 10^{-4}$	$1.312 \times 10^{-3}$	$1.314 \times 10^{-3}$	$2.208 \times 10^{-2}$
$h^+$	$1.258 \times 10^{-3}$	$1.265 \times 10^{-3}$	$8.149 \times 10^{-4}$	$1.375 \times 10^{-3}$	$1.379 \times 10^{-3}$	$2.25 \times 10^{-2}$

TABLE I: A table of the ratios of the norms of the estimated errors  $C_\perp$  and the estimated covariance matrices  $C_\parallel$  for our assorted reconstructed cosmologies.

---

[1] R. Laureijs *et al.*, Euclid Definition Study Report, arXiv e-prints , arXiv:1110.3193 (2011), [arXiv:1110.3193 \[astro-ph.CO\]](https://arxiv.org/abs/1110.3193).  
[2] Željko. Ivezic *et al.*, LSST: From Science Drivers to Reference Design and Anticipated Data Products, *ApJ* **873**, 111 (2019), [arXiv:0805.2366 \[astro-ph\]](https://arxiv.org/abs/0805.2366).  
[3] O. Doré *et al.*, Cosmology with the SPHEREX All-Sky Spectral Survey, (2014), [arXiv:1412.4872 \[astro-ph.CO\]](https://arxiv.org/abs/1412.4872).  
[4] S. Yahya *et al.*, Cosmological performance of SKA Hi galaxy surveys, *Monthly Notices of the Royal Astronomical Society* **450**, 2251 (2015), <https://academic.oup.com/mnras/article-pdf/450/3/2251/18504481/stv695.pdf>.  
[5] Z. Wang *et al.*, The clustering of galaxies in the DESI imaging legacy surveys DR8: I. The luminosity and color dependent intrinsic clustering, *Sci. China Phys. Mech. Astron.* **64**, 289811 (2021), [arXiv:2106.14159 \[astro-ph.GA\]](https://arxiv.org/abs/2106.14159).

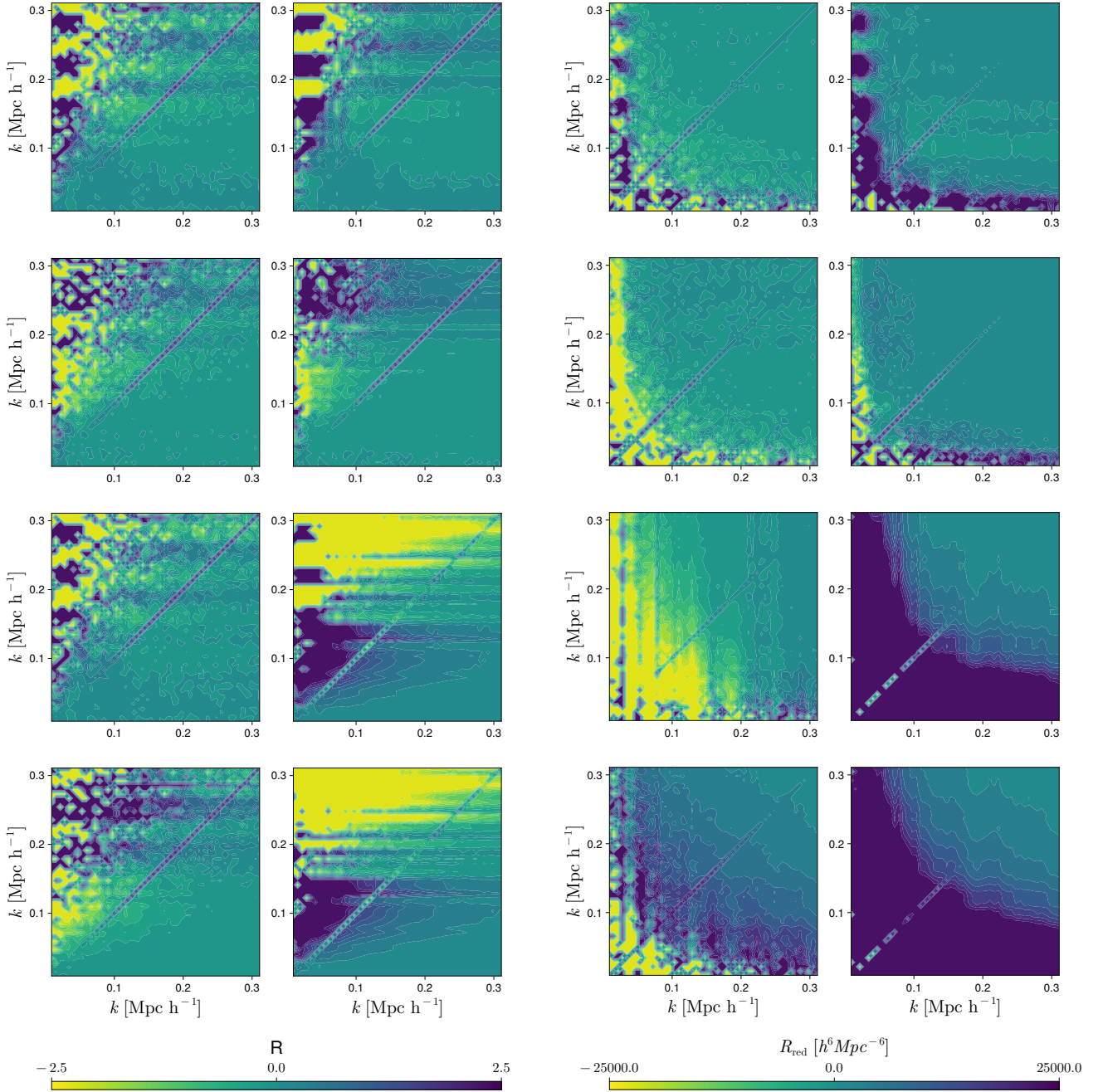


FIG. 43: The response matrices for  $\Omega_m$  (left hand pair of columns) and the corresponding reduced response matrices. In each case, the top row shows the non-Gaussian response matrices without SSC corrections, the second row show the Gaussian response matrices without SSC corrections, the third row show the non-Gaussian response matrices with SSC corrections, and the bottom row shows the Gaussian response matrices with SSC corrections, with the left hand column showing the results obtained with the full response matrix and the right hand column showing the results from the approximate form of the response matrix.

- [6] A. Pullen, C. Hirata, O. Doré, and A. Raccanelli, Interloper bias in future large-scale structure surveys, *Publications of the Astronomical Society of Japan* **68** (2015).
- [7] J. Richard *et al.*, 4MOST Consortium Survey 8: Cosmology Redshift Survey (CRS), *The Messenger* **175**, 50 (2019), [arXiv:1903.02474 \[astro-ph.CO\]](https://arxiv.org/abs/1903.02474).
- [8] M. Takada *et al.*, Extragalactic science, cosmology, and Galactic archaeology with the Subaru Prime Focus Spectrograph, *Publications of the Astronomical Society of Japan* **66**, [10.1093/pasj/pst019](https://doi.org/10.1093/pasj/pst019) (2014), r1,

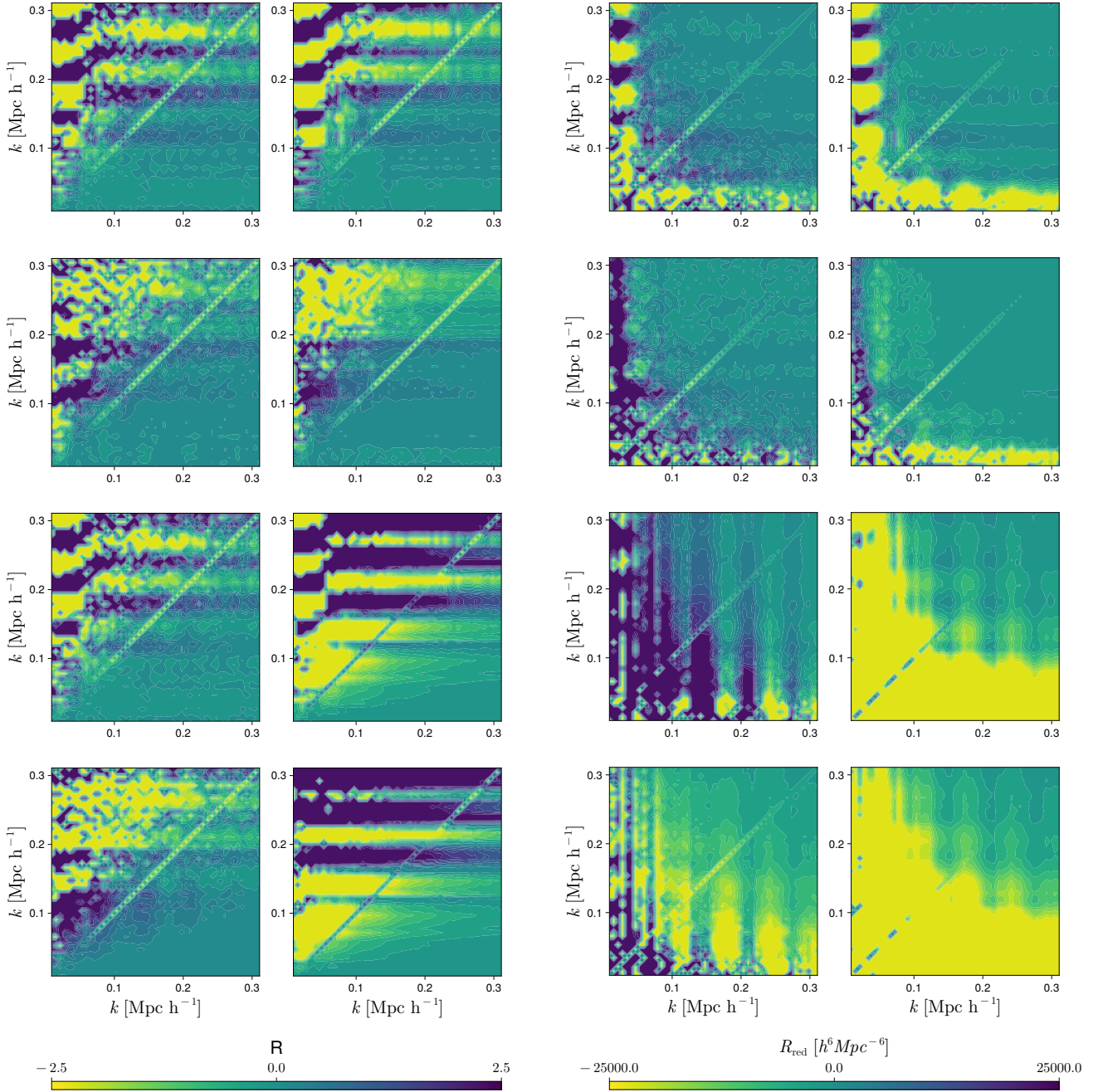


FIG. 44: The response matrices for  $\Omega_m$  (left hand pair of columns) and  $\Omega_b$  (right hand pair of columns). In each case, the top row shows the non-Gaussian response matrices without SSC corrections, the second row show the Gaussian response matrices without SSC corrections, the third row show the non-Gaussian response matrices with SSC corrections, and the bottom row shows the Gaussian response matrices with SSC corrections, with the left hand column showing the results obtained with the full response matrix and the right hand column showing the results from the approximate form of the response matrix.

<https://academic.oup.com/pasj/article-pdf/66/1/R1/4425324/pst019.pdf>.

- [9] H. Hildebrandt *et al.*, KiDS-1000 catalogue: Redshift distributions and their calibration, *Astron. Astrophys.* **647**, A124 (2021), arXiv:2007.15635 [astro-ph.CO].
- [10] K. S. Dawson *et al.*, The Baryon Oscillation Spectroscopic Survey of SDSS-III, *The Astronomical Journal* **145**, 10.1088/0004-6256/145/1/10, arXiv:1208.0022 [astro-ph.CO].
- [11] M. Icaza-Lizaola *et al.*, The clustering of the SDSS-IV extended Baryon Oscillation Spectroscopic Survey DR14 LRG sam-

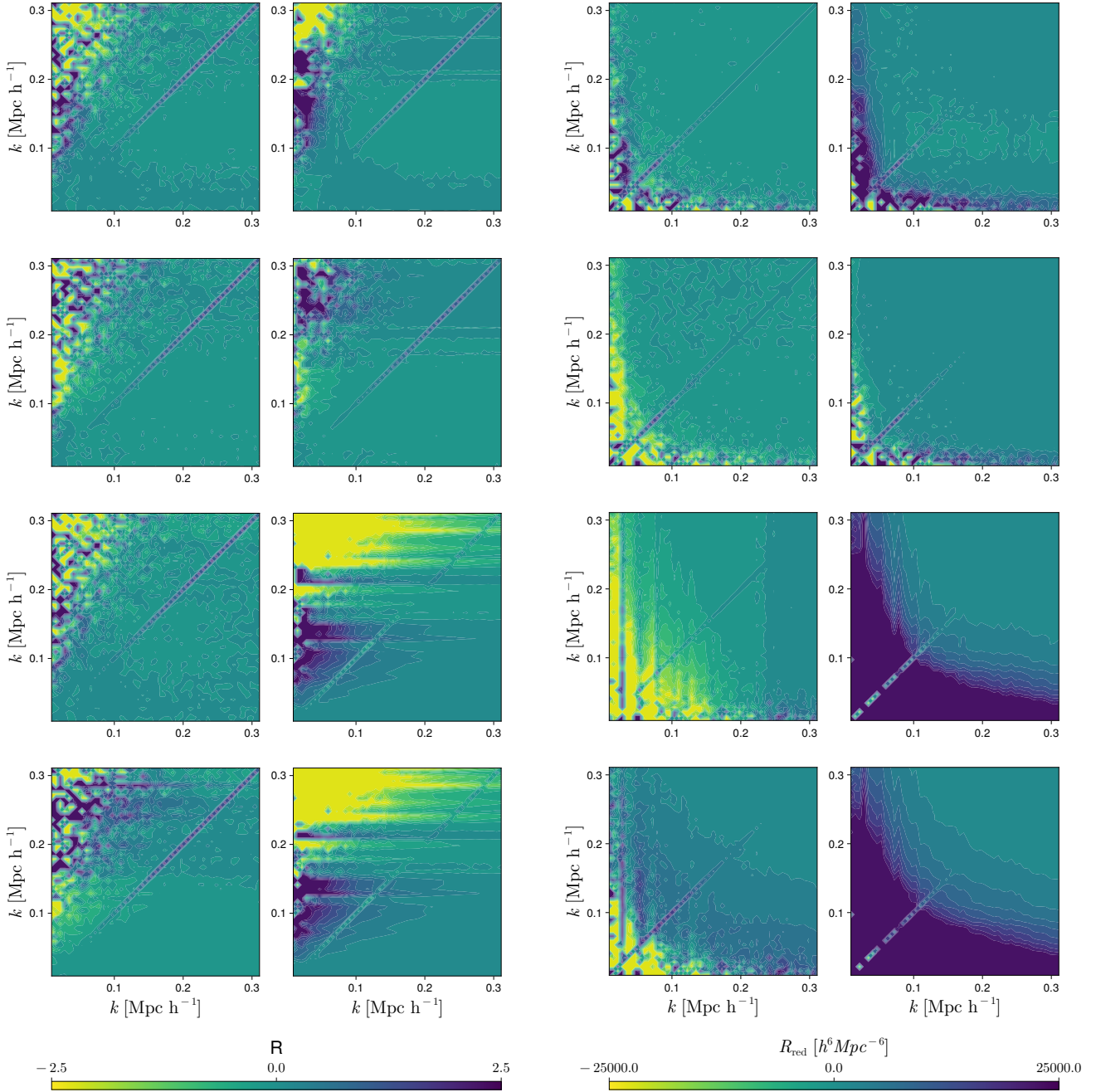


FIG. 45: The response matrices for  $n_s$  (left hand pair of columns) and  $\Omega_b$  (right hand pair of columns). In each case, the top row shows the non-Gaussian response matrices without SSC corrections, the second row show the Gaussian response matrices without SSC corrections, the third row show the non-Gaussian response matrices with SSC corrections, and the bottom row shows the Gaussian response matrices with SSC corrections, with the left hand column showing the results obtained with the full response matrix and the right hand column showing the results from the approximate form of the response matrix.

ple: structure growth rate measurement from the anisotropic LRG correlation function in the redshift range  $0.6 < z < 1.0$ , *Monthly Notices of the Royal Astronomical Society* **492**, 4189 (2019), <https://academic.oup.com/mnras/article-pdf/492/3/4189/32217846/stz3602.pdf>.

- [12] F. Bernardeau, S. Colombi, E. Gaztanaga, and R. Scoccimarro, Large scale structure of the universe and cosmological perturbation theory, *Phys. Rept.* **367**, 1 (2002), [arXiv:astro-ph/0112551](https://arxiv.org/abs/astro-ph/0112551).
- [13] D. Blas, M. Garny, M. M. Ivanov, and S. Sibiryakov, Time-Sliced Perturbation Theory for Large Scale Structure I: General

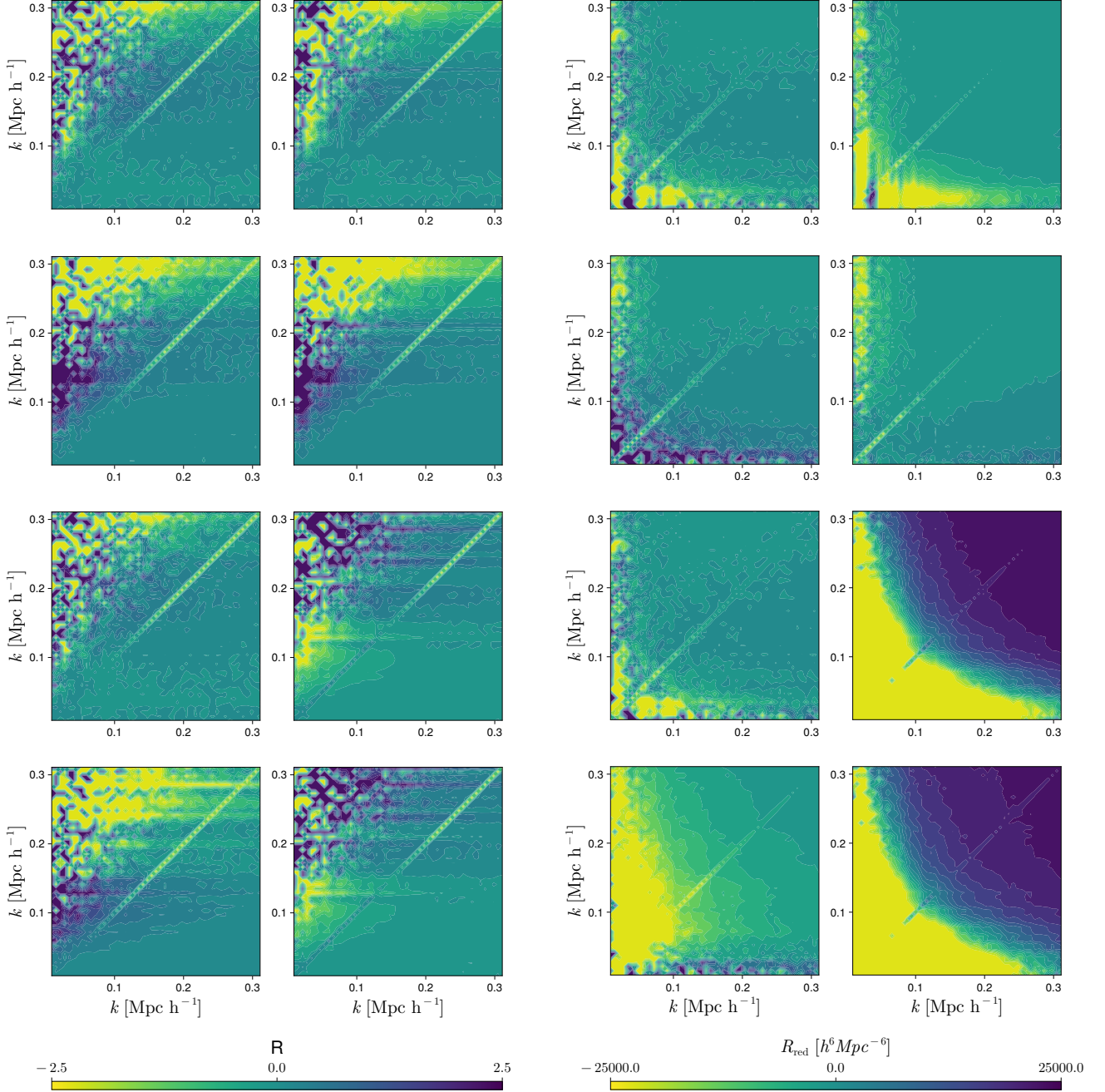


FIG. 46: The response matrices for  $\Omega_m$  (left hand pair of columns) and  $\Omega_b$  (right hand pair of columns). In each case, the top row shows the non-Gaussian response matrices without SSC corrections, the second row show the Gaussian response matrices without SSC corrections, the third row show the non-Gaussian response matrices with SSC corrections, and the bottom row shows the Gaussian response matrices with SSC corrections, with the left hand column showing the results obtained with the full response matrix and the right hand column showing the results from the approximate form of the response matrix.

Formalism, [JCAP 07, 052, arXiv:1512.05807 \[astro-ph.CO\]](#).

- [14] D. Blas, M. Garny, M. M. Ivanov, and S. Sibiryakov, Time-Sliced Perturbation Theory II: Baryon Acoustic Oscillations and Infrared Resummation, [JCAP 07, 028, arXiv:1605.02149 \[astro-ph.CO\]](#).
- [15] D. Blas *et al.*, Large scale structure from viscous dark matter, [JCAP 11, 049, arXiv:1507.06665 \[astro-ph.CO\]](#).
- [16] D. Baumann, A. Nicolis, L. Senatore, and M. Zaldarriaga, Cosmological Non-Linearities as an Effective Fluid, [JCAP 07, 051, arXiv:1004.2488 \[astro-ph.CO\]](#).

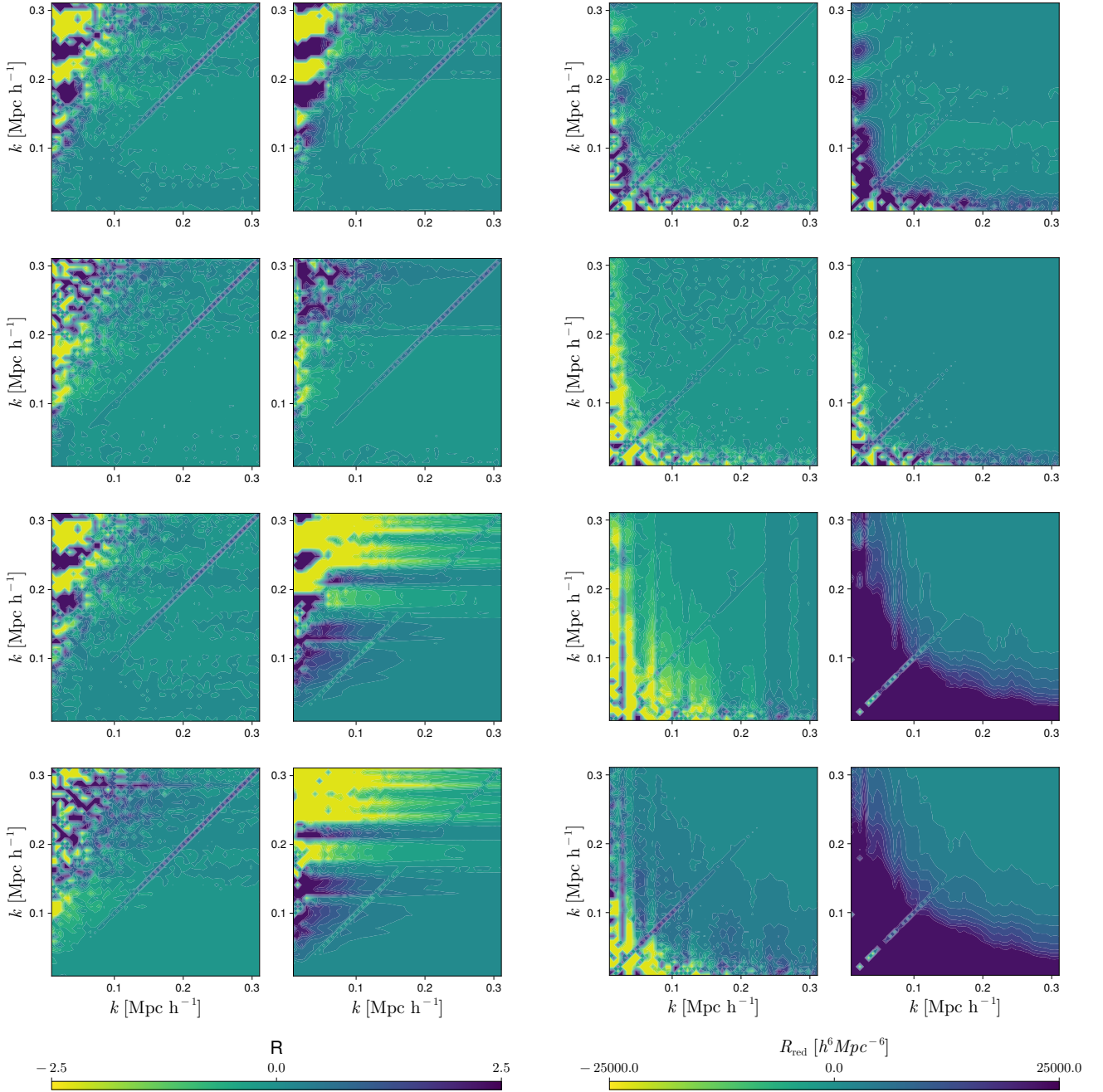


FIG. 47: The response matrices for  $h$  with (left hand pair of columns) and without (right hand pair of columns) the inverse term. In each case, the top row shows the non-Gaussian response matrices without SSC corrections, the second row show the Gaussian response matrices without SSC corrections, the third row show the non-Gaussian response matrices with SSC corrections, and the bottom row shows the Gaussian response matrices with SSC corrections, with the left hand column showing the results obtained with the full response matrix and the right hand column showing the results from the approximate form of the response matrix.

- [17] J. J. M. Carrasco, M. P. Hertzberg, and L. Senatore, The Effective Field Theory of Cosmological Large Scale Structures, [JHEP 09, 082, arXiv:1206.2926 \[astro-ph.CO\]](#).
- [18] G. Aricò, R. E. Angulo, and M. Zennaro, Accelerating Large-Scale-Structure data analyses by emulating Boltzmann solvers and Lagrangian Perturbation Theory [10.12688/openreurope.14310.2](#) (2021), [arXiv:2104.14568 \[astro-ph.CO\]](#).
- [19] G. Cusin, M. Lewandowski, and F. Vernizzi, Dark Energy and Modified Gravity in the Effective Field Theory of Large-Scale Structure, [JCAP 04, 005, arXiv:1712.02783 \[astro-ph.CO\]](#).

- [20] V. Assassi *et al.*, Effective theory of large-scale structure with primordial non-Gaussianity, *JCAP* **11**, 024, arXiv:1505.06668 [astro-ph.CO].
- [21] L. Senatore and M. Zaldarriaga, The Effective Field Theory of Large-Scale Structure in the presence of Massive Neutrinos, (2017), arXiv:1707.04698 [astro-ph.CO].
- [22] A. Chudaykin and M. M. Ivanov, Measuring neutrino masses with large-scale structure: Euclid forecast with controlled theoretical error, *JCAP* **11**, 034, arXiv:1907.06666 [astro-ph.CO].
- [23] A. Vasudevan, M. M. Ivanov, S. Sibiryakov, and J. Lesgourgues, Time-sliced perturbation theory with primordial non-Gaussianity and effects of large bulk flows on inflationary oscillating features, *JCAP* **09**, 037, arXiv:1906.08697 [astro-ph.CO].
- [24] P. Zhang and Y. Cai, BOSS full-shape analysis from the EFTofLSS with exact time dependence, *JCAP* **01** (01), 031, arXiv:2111.05739 [astro-ph.CO].
- [25] M. M. Ivanov, M. Simonović, and M. Zaldarriaga, Cosmological Parameters from the BOSS Galaxy Power Spectrum, *JCAP* **05**, 042, arXiv:1909.05277 [astro-ph.CO].
- [26] P. Carrilho, C. Moretti, and A. Pourtsidou, Cosmology with the EFTofLSS and BOSS: dark energy constraints and a note on priors, *JCAP* **01**, 028, arXiv:2207.14784 [astro-ph.CO].
- [27] A. G. Adame *et al.* (DESI), DESI 2024 VI: Cosmological Constraints from the Measurements of Baryon Acoustic Oscillations, (2024), arXiv:2404.03002 [astro-ph.CO].
- [28] S.-F. Chen *et al.*, Suppression without Thawing: Constraining Structure Formation and Dark Energy with Galaxy Clustering, (2024), arXiv:2406.13388 [astro-ph.CO].
- [29] G. Cabass *et al.*, BOSS Constraints on Massive Particles during Inflation: The Cosmological Collider in Action, (2024), arXiv:2404.01894 [astro-ph.CO].
- [30] N. S. Sugiyama *et al.*, New constraints on cosmological modified gravity theories from anisotropic three-point correlation functions of BOSS DR12 galaxies 10.1093/mnras/stad1505 (2023), arXiv:2302.06808 [astro-ph.CO].
- [31] M. Takada and W. Hu, Power Spectrum Super-Sample Covariance, *Phys. Rev. D* **87**, 123504 (2013), arXiv:1302.6994 [astro-ph.CO].
- [32] Y. Li, W. Hu, and M. Takada, Super-Sample Covariance in Simulations, *Phys. Rev. D* **89**, 083519 (2014), arXiv:1401.0385 [astro-ph.CO].
- [33] F. Villaescusa-Navarro *et al.*, The Quijote simulations, *Astrophys. J. Suppl.* **250**, 2 (2020), arXiv:1909.05273 [astro-ph.CO].
- [34] H. A. Feldman, N. Kaiser, and J. A. Peacock, Power spectrum analysis of three-dimensional redshift surveys, *Astrophys. J.* **426**, 23 (1994), arXiv:astro-ph/9304022.
- [35] I. Mohammed, U. Seljak, and Z. Vlah, Perturbative approach to covariance matrix of the matter power spectrum, *Mon. Not. Roy. Astron. Soc.* **466**, 780 (2017), arXiv:1607.00043 [astro-ph.CO].
- [36] H. A. Feldman, N. Kaiser, and J. A. Peacock, Power-Spectrum Analysis of Three-dimensional Redshift Surveys, *ApJ* **426**, 23 (1994), arXiv:astro-ph/9304022 [astro-ph].
- [37] T. Steele and T. Baldauf, Precise Calibration of the One-Loop Bispectrum in the Effective Field Theory of Large Scale Structure, *Phys. Rev. D* **103**, 023520 (2021), arXiv:2009.01200 [astro-ph.CO].
- [38] T. Steele and T. Baldauf, Precise Calibration of the One-Loop Trispectrum in the Effective Field Theory of Large Scale Structure, *Phys. Rev. D* **103**, 103518 (2021), arXiv:2101.10289 [astro-ph.CO].